AD-773 844

MANUAL CONTROL PERFORMANCE AND DYNAMIC RESPONSE DURING SINUSOIDAL VIBRATION

R. Wade Allen, et al

Systems Technology, Incorporated

Prepared for:

Aerospace Medical Research Laboratory

October 1973

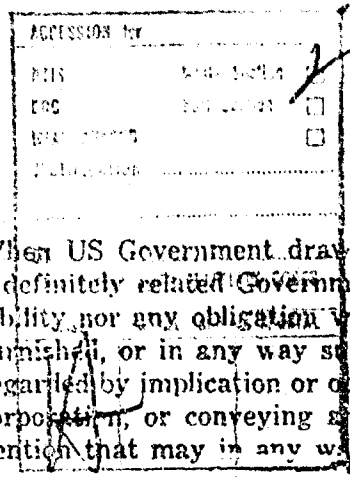

NOTICES

When US Government drawings, specifications, or other data are used for any purpose other than a definitely related Government procurement operation, the Government thereby incurs no responsibility nor any obligation whatsoever, and the fact that the Government may have formulated, furnished, or in any way supplied the said drawings, specifications, or other data, is not to be regarded by implication or otherwise, as in any manner licensing the holder or any other person or corporation, or conveying any rights or permission to manufacture, use, or sell any patented invention that may in any way be related thereto.

Organizations and individuals receiving announcements or reports via the Aerospace Medical Research Laboratory automatic mailing lists should submit the addressograph plate stamp on the report envelope or refer to the code number when corresponding about change of address or cancellation.

Do not return this copy. Retain or destroy.

Please do not request copies of this report from Aerospace Medical Research Laboratory. Additional copies may be purchased from:

National Technical Information Service
5285 Port Royal Road
Springfield, Virginia 22151

The voluntary informed consent of the subjects used in this research was obtained as required by Air Force Regulation 80–33.

This report has been reviewed and cleared for open publication and/or public release by the appropriate Office of Information (OI) in accordance with AFR 190–17 and DODD 5230.0. There is no objection to unlimited distribution of this report to the public at large or by DDC to the National Technical Information Service (NTIS).

This technical report has been reviewed and is approved for publication.

FOR THE COMMANDER

H. E. G. von Gierke

HENNING E. G. von GIERKE, DR ING
Director
Biodynamics and Bionics Division
Aerospace Medical Research Laboratory

AIR FORCE/56780/3 January 1974 — 100

Unclassified
Security Classification

AD-773844

DOCUMENT CONTROL DATA - R & D

(Security classification of title, body of abstract and indexing annotation must be entered when the overall report is classified)

1. ORIGINATING ACTIVITY (Corporate author)	2a. REPORT SECURITY CLASSIFICATION
Systems Technology, Inc. 13766 South Hawthorne Boulevard Hawthorne, California 90250	Unclassified 2b. GROUP

3. REPORT TITLE

MANUAL CONTROL PERFORMANCE AND DYNAMIC RESPONSE DURING SINUSOIDAL VIBRATION

4. DESCRIPTIVE NOTES (Type of report and inclusive dates)
Final Report, July 1971 to June 1972

5. AUTHOR(S) (First name, middle initial, last name)
R. Wade Allen
Henry R. Jex
Raymond E. Magdaleno

6. REPORT DATE	7a. TOTAL NO. OF PAGES	7b. NO. OF REFS
October 1973	~~157~~ 165	57

8a. CONTRACT OR GRANT NO	9a. ORIGINATOR'S REPORT NUMBER(S)
F33615-71-C-1487 b. PROJECT NO.	STI TR-1013-2
c. d.	9b. OTHER REPORT NO(S) (Any other numbers that may be assigned this report) AMRL-TR-73-78

10. DISTRIBUTION STATEMENT

Approved for public release: distribution unlimited

11. SUPPLEMENTARY NOTES	12. SPONSORING MILITARY ACTIVITY
	Aerospace Medical Research Laboratory Aerospace Medical Division, Air Force Systems Command, Wright-Patterson AFB, OH

13. ABSTRACT

A variety of dynamic response and performance measurements are presented for compensatory manual control tasks performed under both vertical, lateral, and fore-aft sinusoidal vibration. Special, on-line measurement techniques allowed the partitioning of error and control response variances into portions correlated with the tracking task and vibration inputs, and an uncorrelated or remnant portion. Vibration effects on visual-motor response were generally subtle, and the most sensitive effects occurred in error remnant and "vibration-induced" feedthrough to the control response. Dramatic increases in remnant were obtained under low-frequency lateral vibration with a low spring gradient displacement stick, while an isometric control showed little effect.

As part of the study, body motion and control response measurements were used to develop biomechanical models of the vibration-to-control "feedthrough" process. Under vertical vibration a simplified model, based on the operator's seat-to-shoulder transmissibility and a quasi-rigid arm linkage, was found to give an adequate description of vibration feedthrough. Under lateral vibration body motion effects were found to be secondary, while inertial forces on the arm and control stick masses ("bobweight" effects) proved to be the primary cause of vibration-induced control response. During fore-aft vibration, measurements show that body motions are a relatively important factor in the feedthrough process. Models for vertical, lateral, and fore-aft vibration control feedthrough are presented, and implications on the closed-loop performance of manual control systems are discussed.

DD FORM 1 NOV 68 1473

Unclassified
Security Classification

14 KEY WORDS	LINK A		LINK B		LINK C	
	ROLE	WT	ROLE	WT	ROLE	WT
Manual Control Human Dynamic Response Vibration						

SUMMARY

Section I — Introduction

The basic objective of this research was to investigate the underlying causes of vibration interference with the performance of manual control tasks. This section defines the biodynamic elements and interfaces involved, and notes that the signals circulating in manual control systems under vibration can be associated with three sources:

- Command or disturbance inputs.
- Vibration feedthrough to the human operator's control.
- Noise (remnant) effects due to the operator's signal processing activities.

Section II — Background

Previous vibration research pertinent to this study is reviewed, and the basic measurement and analysis approach used here is discussed. Techniques based on manual control theory are employed to determine the effect of vibration on each of the above three signal components and, more fundamentally, to determine which aspects of human operator behavior (including visual-motor and biomechanical response) are responsible for the various effects.

Section III — Experimental Setup

Measurement techniques are described that were developed to partition error and control signals into system input correlated, vibration acceleration correlated, and uncorrelated or remnant components, and to identify the human operator's dynamic response behavior. The frequency domain dynamic response measurements which were employed included visual-motor describing functions (measures of the human operator's dynamic response to visually displayed tracking errors) and transmissibility and control feedthrough dynamics (measures of human operator biomechanical response and control stick response to the vibration input). More conventional performance measures, such as mean-square tracking error and control activity, were also taken.

The experimental setup consisted of a single-axis, simulated aircraft attitude control task, using a CRT display and centerstick controller manipulated with an outstretched arm. Two different control sticks, one with normal spring gradient, the other very stiff (nearly isometric) were tested to demonstrate the effects of control "feel" characteristics on vibration feedthrough to control response. Sinusoidal vibration was administered via the AMRL Western Gear Shaker over the frequency range from 1.3-10 Hz, in individual runs. The major axes of vibration (fore-aft, G_x; lateral, G_y; and vertical, G_z) were studied in separate experiments employing the single control axis most likely to be affected in each. The major findings for each experiment were as follows.

Section IV — Vertical Vibration, G_z (Pitch Control Task)

This was a "pilot" experiment, intended mainly for technique development. Tracking performance degraded most under higher-frequency vibration ($f_v > 6$ Hz), with increases in both input-correlated and remnant error components. Vertical vibration in the region of 10 Hz seems to have a subjectively adverse effect

on the visual and motor processes, objectively manifested as increased phase lags. This effect consequently leads to lower closed-loop bandwidth and higher input-correlated tracking errors. The interference with the motor process may also lead to increased remnant. Vertical torso compliance was responsible for vibration feedthrough to the control responses, and the stiff control stick gave relatively more high-frequency vibration control feedthrough.

Section V — Lateral Vibration, G_Y (Roll Control Task)

With a lightly-sprung stick, the input-correlated behavior and tracking errors were not much affected but error remnant increased by an order of magnitude under low-frequency vibration ($f_V < 5$ Hz). Low-frequency lateral vibration induces large control stick movements mainly through limb-stick "bobweight" effects, which lead to subjectively reported uncertainty in control position, and thereby to increased remnant. This effect was absent for the stiff control stick. Low-frequency G_Y vibration led to the greatest body motion and vibration-correlated control response, and the stiff stick yielded the most high-frequency vibration control feedthrough on a relative basis.

Section VI — Fore-Aft Vibration, G_X (Pitch Control Task)

A moderate general increase in tracking error at all frequencies was found under fore-aft vibration. More idiosyncratic behavior between subjects was noted, compared with the G_Z and G_Y experiments, apparently due to the greater role of restraint and posture in this case. Large differences in performance results apparently stem from the idiosyncrasies in G_X biodynamic response between subjects. Adverse vibration interference with the motor process, as found under G_Z vibration, was also noted here. A resonant peak in vibration-correlated control response was found in the 3-5 Hz region, with the stiff stick giving relatively more high-frequency vibration control feedthrough as in the G_Z and G_Y experiments.

Section VII — Vibration Feedthrough Models

The biomechanical nature of vibration control feedthrough was analyzed with preliminary models developed in Appendices A and B and is summarized in Section VII. Linearized perturbation models appear adequate to describe the control feedthrough phenomenon. These models account for effects of vibration transmissibility of the human operator, the limb-control interface complicance, and the mechanical properties of the control stick, as shown by comparing the model predictions with data.

Section VIII — Conclusions and Recommendations

The key findings of this investigation are summarized, and recommendations for future research are included. With further development, the models and data base started here will be useful for describing changes in feedthrough effects due to changes in control stick properties and factors affecting transmissibility such as: seat cushions, restraints, and vibration isolation seats. The results are directly applicable to such problems as centerstick control interference from the elastic mode vibrations of large bombers, effects of buffeting at high angles of attack on fighter gunnery, and pilot-induced oscillations due to biodynamic feedthrough (e.g., bobweight effects).

PREFACE

This study was initiated by the Biodynamics and Bionics Division of the Aerospace Medical Research Laboratories, Wright-Patterson Air Force Base. The research was performed by Systems Technology, Inc., of Hawthorne, California, under Contract F33615-71-C-1487. Mr. Henry R. Jex was the principal investigator and Mr. R. Wade Allen the project engineer for Systems Technology, Inc. Capt. Darrell Wilburn was the Contract Technical Monitor for AMRL during the initial phases of this research, with John B. Carmichael acting in this capacity during the final stages of work.

The authors are indebted to a large number of people who made this study and report possible. Thanks go to AMRL/BBV personnel who assisted in the use of Wright Field facilities, particularly Lou Muhic for help on instrumentation in the Western Gear vibration lab, Darrell Wilburn for assistance with the digital computer facilities, and Jack Carmichael for coordinating the use of facilities, equipment, and subjects. Thanks are also due Darrell Wilburn, Dick Shoenberger, and Phil Houck for thought-provoking discussions of the work and results and review of the final report. Finally, our deepest appreciation to the STI production staff for preparing this document.

TABLE OF CONTENTS

LIST OF FIGURES

LIST OF TABLES

SECTION I

INTRODUCTION

A. BACKGROUND AND MOTIVATION FOR RESEARCH

Degradation of human performance in biodynamic environments* is a continuing problem in the man-machine systems area. Current operational problems include:

- Controlling large elastic aircraft through strong convective turbulence and maneuvering fighters under transonic buffet conditions.
- Piloting and manual fire control operations in out-of-balance rotor craft.
- Control of high-speed vehicles over rough terrain or waves.

The design and development of these systems would be considerably aided if the effects of the biodynamic environment on the pilot/vehicle system could be quantitatively assessed. This is currently not possible, however, because of the general lack of applicable dynamic models and data, particularly in regard to the performance of complex manual control tasks.

A great deal of effort has been expended over the years on measuring the effects of vibration on man, and the body of this research is summarized in Refs. 1-10. Human tolerance and subjective comfort levels of vibration have been investigated (Refs. 11-17), and models for the biomechanical response of the body (transmissibility) to vertical motion inputs (vibration and shock) are available (e.g., Ref. 12). Biodynamic response to lateral and longitudinal vibration is less well understood, however, and knowledge of psychomotor performance effects is mainly empirical, although some attempts have been made to coalesce and extrapolate the present data base (Refs. 8-10).

*A "biodynamic environment" is defined as a varying acceleration applied to a structural frame containing the human subject, thereby producing varying forces on the body.

The lack of performance quantification for tasks involving human control of a vehicle in a biodynamic environment is mainly due to the absence, until fairly recently, of either a well developed theoretical basis or efficient measurement techniques for the complex properties of manual control systems. A set of reasonably well validated manual control system models are now available (Refs. 18-20, 23) which can be used to guide the measurement and analysis of vibration effects on manual control. Furthermore, efficient test techniques and equipment have been recently developed for measuring both dynamic response behavior and performance in manual control systems (Refs. 21 and 22).

B. GENERAL APPROACH

The effects of vibration on the human operator involved in a control task are quite complicated. An overall conceptual model of the various means by which a biodynamic environment interferes with man-machine performance is illustrated in Fig. 1 (originally presented in Ref. 20). The human operator is assumed to be performing a precision closed-loop control task with emphasis on accuracy in following the command inputs (on the left) while rejecting various disturbances within the loop. Meanwhile, the biodynamic environment interferes with this effort at various interfaces with the man:

- Display and head motions can distort visual information (e.g., degraded acuity).
- Motions induced into the operator's limb and control stick can cause extraneous control actions.
- Body and head motions may cause unwanted disturbances to the CNS (e.g., nystagmus) and interfere with the actuation dynamics of the neuromuscular system.
- The general stress effect of vibration may induce changes in the operator's psychophysiological state in terms of rather ill-defined variables such as motivation, arousal, and fatigue.

The approach used in the present research is to employ control-theory-based techniques that allow partitioning of the man-machine performance into basic components:

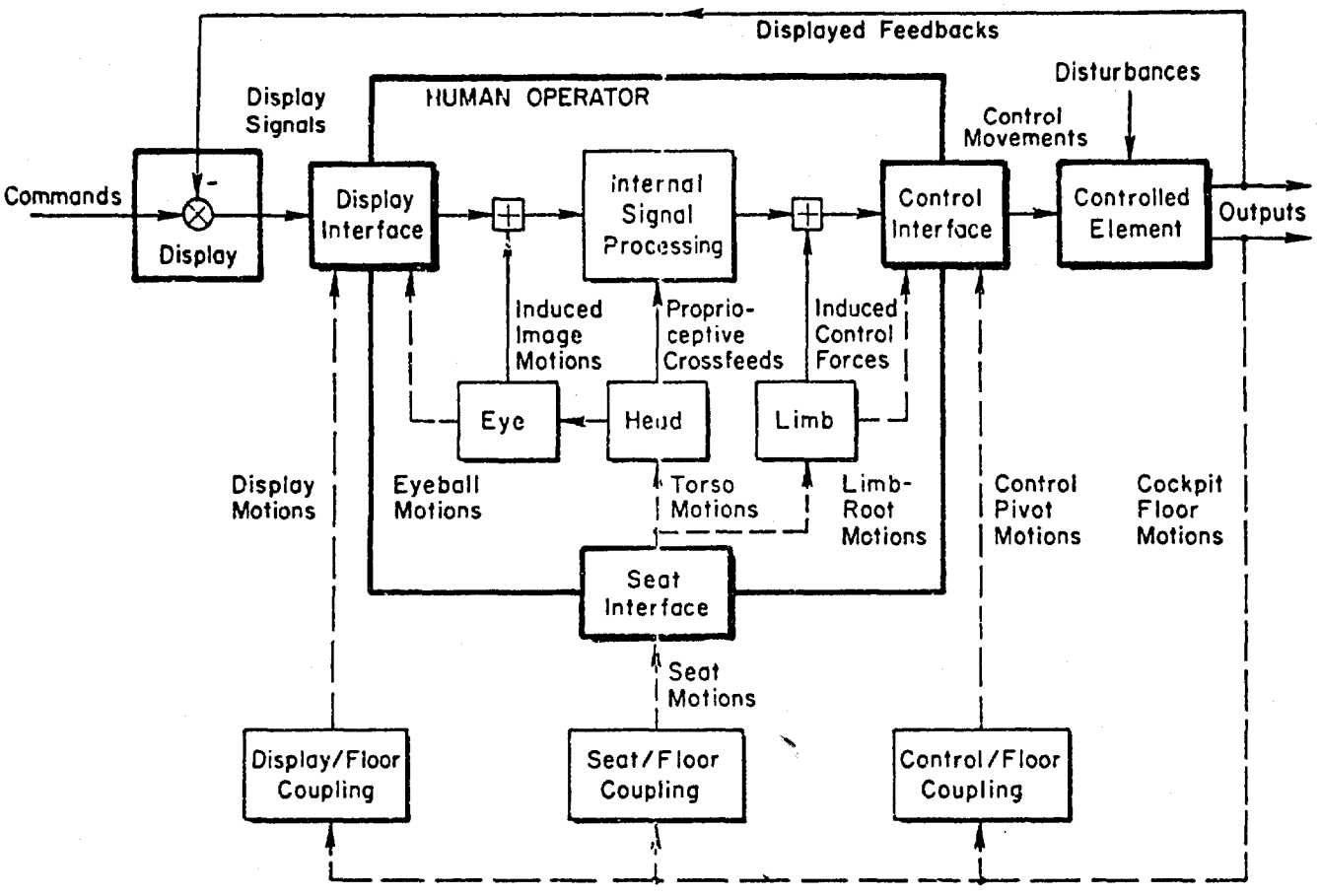

Figure 1. Overall Block Diagram for Pilot/Vehicle System, Including Biodynamic Influences

1. A portion of the operator's visual-motor response associated (coherent) with the command input.

2. A "feedthrough" portion directly induced by the vibration input.

3. A remaining portion or "remnant" that is uncorrelated with either the command or vibration inputs.

These techniques also allow the identification and modeling of dynamic response properties of both the visual-motor behavior and vibration feed-through process that result in the measured performance. It is the trends in these dynamic models and their empirically-derived parameters that allow one to draw meaningful conclusions about the effects of vibration, in a given case, and to extrapolate these findings to new situations.

C. REPORT OUTLINE

The background for this research study is reviewed in Section II, covering relevant literature, measurement techniques, and models. Details of the experimental approach and setup are discussed in Section III. Three separate experiments were performed in this research, and Sections IV-VI present the results for vertical, lateral, and fore-aft vibration, respectively. The results are somewhat detailed so that each section is concluded with a separate summary of results.

Biomechanical modeling results are summarized in Section VII, with a more complete development given in Appendices A and B. Finally, conclusions based on the overall results are given in Section VIII along with recommendations for application of the present results and recommendations for further research.

SECTION II

BACKGROUND

A. PREVIOUS RESEARCH ON MANUAL CONTROL PERFORMANCE UNDER VIBRATION

The authors' assessment of published vibration research indicates that while many of the fundamental biodynamic effects of vibration are well understood, the more complex effects associated with manual control performance are not firmly established. Some investigators of biodynamic response have used mechanical impedance concepts for measurements and modeling, and this approach has accounted for many biomechanical effects (e.g., Refs. 11-12). The subjective response to vibration (e.g., comfort, pain) seems to have been extensively investigated with some attempts at quantification (e.g., Refs. 13-17). Visual problems have been studied (e.g., Refs. 33-39); however, the basis for these effects is still not well understood. Visual-motor and vehicle control performance under vibration has been widely investigated (e.g., Refs. 40-47); most of the results are task- or simulation-specific, however, making generalization difficult. Finally, there are several summaries and bibliographies of vibration research available (e.g., Refs. 1-10), including two notably comprehensive works, one by Guignard (Ref. 4) and another by Roth (Ref. 6). The remainder of this section summarizes key vibration research results which are most pertinent to the technical approach of this research.

1. Biodynamic Response

Modeling the biodynamic response of the human operator is an important aspect of the vibration feedthrough models presented here. Biodynamic response to vertical* (G_z) vibration is roughly accounted for by a complex spring-mass-damper mechanical system (e.g., Ref. 6). The thorax-abdomen torso system is

*We use the following nomenclature for axes of vibration, as referenced to a normally seated person (Ref. 6):

"Fore-aft vibration": G_x is positive forward.
"Lateral vibration": G_y is positive rightward.
"Vertical vibration": G_z is positive downward.

very elastic with various parts resonating in the frequency range 3-11 Hz. Movements of visceral organs are a limiting factor in human tolerance in the 4-8 Hz range. Head-to-shoulder resonance occurs between 20 and 30 Hz and interferes with visual acuity. Overall head-to-seat resonance for a seated subject occurs in the 4-6 Hz range, with the detailed impedance effects depending on subject size and posture (Ref. 6).

Biodynamic response in the horizontal plane (G_y and G_x) is quite different from vertical vibration due to articulation of the hip joint and bending of the spine. Lateral resonances at low frequencies in the region of 1-3 Hz are reported (Refs. 4 and 6). Fore-aft vibration (G_x) also leads to vertical head motions (Ref. 6) which may induce visual blurring at high frequencies. No detailed biodynamic models for horizontal vibration seem to be available, so a lateral transmissibility model was developed in the course of the present research (Appendix B). Reference 26 was of considerable help in this regard in determining the mass and moments of inertia of various model elements.

2. Performance and Dynamic Response Measurements

Vibration effects on the performance of complex visual-motor tasks arise from a combination of the effects mentioned above. However, very few studies have included measures of each component effect (visual, motor, vibration feedthrough, etc.). Therefore, results such as tracking error are difficult to extrapolate to new situations or between studies. It is generally conceded that fine visual-motor control (such as required for threading a needle) is highly disturbed by vibration, while tasks with high impedance controls that can be firmly gripped (e.g., handwheels) are resistant to vibrational disturbance (Refs. 4 and 6). Rosenberg and Segal (Ref. 47) performed a rather complete investigation of fire control tracking in a helicopter simulation. They measured tracking error spectra and were able to partition out the portion correlated with cockpit vibration. Although describing functions weren't measured, per se, they were able to explain many of the measured effects through closed-loop analysis of the control system dynamics, including an appropriate human operator model. Finally, a study performed by Shoenberger (Ref. 31) is quite pertinent to the research reported here, since it concerns tracking performance under G_x, G_y, and G_z sinusoidal vibration over the

frequency range 1-11 Hz. Vertical vibration was found to cause a general increase in tracking error with little sensitivity to vibration frequency. The story was much different for lateral vibration, however, where a dramatic increase in tracking error was found for low vibration frequencies. Low-frequency fore-aft vibration also induced performance degradation, although not to the same extent as in the lateral case.

B. MODEL AND MEASURES FOR TRACKING PERFORMANCE AND DYNAMIC RESPONSE

The control tasks used in this research comprise simple linear systems simulating the key aspects of operational situations. The measurement and analysis techniques are based on a large body of quasi-linear pilot/vehicle response studies accumulated over the years (Refs. 18-25). We are not assuming here that the human operator (visual-motor and biomechanical response) is necessarily linear, but rather that the quasi-linear "describing function" measurement and analysis techniques will adequately and most efficiently describe the phenomena of interest (see Ref. 54). Analysis of manual control under vibration from a measurement and modeling point of view follows.

1. Model Structure for Measurements

The man-machine system structure shown earlier in Fig. 1 is simplified for measurement purposes as shown in Fig. 2. In this "compensatory" control system the human operator (represented by the characteristics in the dashed box) operates on a displayed error signal (e) to produce control stick inputs (c) to the controlled element dynamics, $Y_c(j\omega)$. The subject's objective is to produce a system motion output signal (m) similar to the tracking input (i) resulting in small tracking errors. In a vibration environment there is an additional input which enters the control loop, however. Through biomechanical motions and inertial forces acting directly on the control stick, the vibration input (v) is transmitted into the tracking loop and appears as a component in the control stick signal (c_v). Because of the separate (and presumed uncorrelated) tracking commands and vibration disturbances, the human operator's dynamic behavior must be accounted for by two describing functions:

- $Y_p(j\omega)$, the traditional visual-motor response function that operates on the perceived error signal (e.g., Refs. 18 and 19).

- $Y_v(j\omega)$, a vibration feedthrough process that causes control activity correlated with the vibration disturbance (Ref. 20).

The human operator's stick activity is not totally accounted for by the above describing functions, and the remaining uncorrelated portion is accounted for by:

- $\Phi_{nn_e}(\omega)$, the now routinely-accepted perceptual (visual) noise process (Refs. 23 and 24).

- $\Phi_{nn_c}(\omega)$, an output (motor) noise process which the present research indicates to be significant under certain biodynamic circumstances.

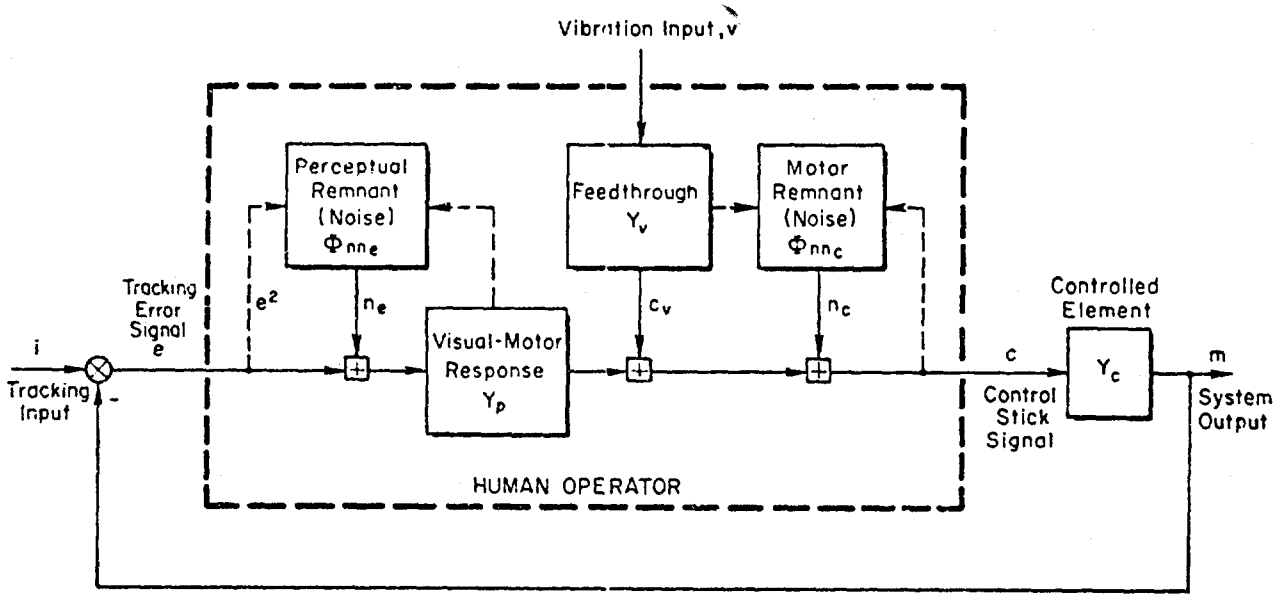

Figure 2. Measurement Model Structure

It is desirable to measure each of the elements of human operator behavior shown in Fig. 2 if we are to understand the complex and often confounding effects caused by a stress such as vibration. Some possible biodynamic environment effects are as follows:

- Visual Motor Dynamics (Y_p)*. Both voluntary and involuntary effects may occur here. For controlled elements requiring lead generation (anticipation), vibration may interfere with the rate perception process, thereby reducing lead capabilities. Vibration may also mechanically interfere with the neuromuscular system, thus affecting the high-frequency portion of the human operator's response (i.e., increasing high-frequency phase lags). Finally, the operator may voluntarily control the amount of lead (prediction) and gain he employs in order to mediate the effect of factors such as increased lags, remnant, and vibration feedthrough.

- Vibration Feedthrough Dynamics (Y_v). Vibration feedthrough will appear in the control response, and depending on frequency content and magnitude as determined by Y_v and the environment, recirculate around the tracking loop and become a significant factor in the system error. Also, in an operational situation such as piloting, the induced high-frequency control activity can cause adverse effects on a flight control system and/or excite high-frequency structural modes, which would further aggravate the vibration environment.

- Perceptual Remnant (Φ_{nn_e}). Differential motion between the display and eye (due to eye, head, and torso resonance effects) can cause visual blurring which might increase remnant generation at this point. "Threshold" and "saturation" nonlinearities in the perceptual processes can also contribute to remnant (Ref. 24).

- Motor Remnant (Φ_{nn_c}). This source may be due to a variety of effects including vibration interference with the neuromuscular actuation process and proprioceptive feedbacks.

It should be noted that with only one control output from the man we can measure but one uncorrelated noise spectrum, so implicit techniques will be required in order to differentiate between the perceptual and motor sources of the circulating (closed-loop) remnant spectrum.

In order to gain some insight into the complex relationships between the dynamic response and performance of the system in Fig. 2, let us now consider the relationships describing the spectral properties of the various signals. Assuming quasi-linear dynamic processes (or linear estimate

*Henceforth, the complex frequency arguments ($j\omega$) are often omitted from Y_p, Y_v, etc., and the frequency argument (ω) is omitted from Φ_{nn_e}, Φ_{nn_c}, etc., once the terms are introduced.

measurements) we can partition the error and control signals into a linear sum of components associated with the tracking input, vibration input, and the visual and motor noise processes:

Total	=	Components from:							
		Tracking Input		Vibration Input		Perceptual Noise		Motor (Output) Noise	
$e(t)$	=	$e_i(t)$	+	$e_v(t)$	+	$e_{n_e}(t)$	+	$e_{n_c}(t)$	(1)
$c(t)$	=	$c_i(t)$	+	$c_v(t)$	+	$c_{n_e}(t)$	+	$c_{n_c}(t)$	

Noting that the various inputs are assumed to be linearly uncorrelated (e.g., see Ref. 54 for the specific details), the analogous frequency domain equations for the power spectral density components of each signal are as follows:

$$\begin{aligned} \Phi_{ee}(\omega) &= \Phi_{ee_i}(\omega) + \Phi_{ee_v}(\omega) + \Phi_{ee_{n_e}}(\omega) + \Phi_{ee_{n_c}}(\omega) \\ \Phi_{cc}(\omega) &= \Phi_{cc_i}(\omega) + \Phi_{cc_v}(\omega) + \Phi_{cc_{n_e}}(\omega) + \Phi_{cc_{n_c}}(\omega) \end{aligned} \tag{2}$$

The mean (offset) values are assumed to be zero or negligible compared with the oscillatory components, which is usually true for trimmed flight situations. Integrating these equations over the frequency range then gives the variance components for each of the signals:

$$\begin{aligned} \sigma_e^2 &= \sigma_{e_i}^2 + \sigma_{e_v}^2 + \sigma_{e_{n_e}}^2 + \sigma_{e_{n_c}}^2 \\ \sigma_c^2 &= \sigma_{c_i}^2 + \sigma_{c_v}^2 + \sigma_{c_{n_e}}^2 + \sigma_{c_{n_c}}^2 \end{aligned} \tag{3}$$

The components of the power spectrum equation (2) can be derived from the various input signals through transfer functions (Ref. 54), e.g.:

$$\Phi_{ee_i}(\omega) = |G_{ie}(j\omega)|^2 \Phi_{ii}(\omega) \tag{4}$$

where $G_{ie}(j\omega)$ is a closed-loop transfer function between the tracking input and error signal and $\Phi_{ii}(\omega)$ is the tracking input power spectrum.

The closed-loop transfer function, G_{ie}, is derived as follows. The correlated error signal is the vector difference between the tracking input and correlated system output:

$$E_i(j\omega) = I(j\omega) - M_i(j\omega) \tag{5}$$

where capital letters refer to the Fourier transform of the respective time signals. The correlated system output is equal to the correlated error operated on by the human operator and controlled element transfer functions:

$$M_i(j\omega) = E_i(j\omega)[Y_p(j\omega) \cdot Y_c(j\omega)] \tag{6}$$

Finally, $G_{ie}(j\omega)$ is the ratio of Fourier transforms between the error and input signals so in combining Eqs. 5 and 6 we obtain:

$$G_{ie}(j\omega) = \frac{E_i(j\omega)}{I(j\omega)} = \frac{1}{1 + Y_p Y_c(j\omega)} \tag{7}$$

Through a similar process a transfer function for each of the remaining components in Eq. 2 can be derived, thus giving expressions in terms of the input power spectra:

$$\Phi_{ee} = \left|\frac{1}{1 + Y_p Y_c}\right|^2 \Phi_{ii} + \left|\frac{Y_v Y_c}{1 + Y_p Y_c}\right|^2 \Phi_{vv} + \left|\frac{Y_p Y_c}{1 + Y_p Y_c}\right|^2 \Phi_{nn_e} + \left|\frac{Y_c}{1 + Y_p Y_c}\right|^2 \Phi_{nn_c} \tag{8}$$

"Coherent" Components | "Remnant" Components

$$\Phi_{ee} = \left|\frac{Y_p}{1 + Y_p Y_c}\right|^2 \Phi_{ii} + \left|\frac{Y_v}{1 + Y_p Y_c}\right|^2 \Phi_{vv} + \left|\frac{Y_p}{1 + Y_p Y_c}\right|^2 \Phi_{nn_e} + \left|\frac{1}{1 + Y_p Y_c}\right|^2 \Phi_{nn_c} \tag{9}$$

Some insight into the effect of vibration on manual control performance can be gained from Eqs. 8 and 9. For instance, these equations show that the operator has some control over the vibration feedthrough term if he can influence the feedthrough dynamics, Y_v. Also, if vibration power is within the bandwidth of the tracking loop (< 1 Hz typically), then the operator can adjust the system closed-loop dynamics $[1/(1 + Y_p Y_c)]$ in order to avoid undue amplification of the feedthrough. Furthermore, any vibration input, Φ_{vv}, is filtered by the controlled element dynamics, Y_c, before reaching the error point, so that the error variance will have a relatively small contribution from vibration feedthrough compared to the control stick output.

Equations 8 and 9 also show that the remnant processes have different effects on the error and control signal spectra. If the controlled element dynamics, Y_c, include a pure integration, as is the case for this research, the dynamic functions multiplying the remnant spectra in the error, Eq. 8, approach a finite value at low frequency, while the corresponding functions in the control output, Eq. 9, approach zero. Consequently, the net error variance is affected mainly by low-frequency remnant, while the control variance is affected mainly by high-frequency remnant. These theoretical implications are important for interpreting the large difference between error and control remnant reported in Section V.

C. VIBRATION FEEDTHROUGH CONCEPTUAL MODEL AND MEASURES

One of the long-range objectives of this research is to understand the fundamentals of the vibration feedthrough process so that data obtained here can be extended to new situations. The approach is to develop simple biomechanical models which capture the key features of the measured phenomenon. It is not our purpose, here, to develop definitively detailed models of all effects, since neither the nature of the measurements nor utility of the results justify that degree of complexity. Nonetheless, an adequate understanding of the process does deserve some attempt at modeling, in terms of dominant physical properties of the man-machine system (masses, lengths, moments of inertia, etc.). We will review the background of some preliminary efforts in this direction with details to be found in Appendices A and B.

Our conceptual model of the feedthrough process is shown in Fig. 3. Basically, the human operator and control are assumed mounted on the same structural platform which is driven with the motion, x_p. At low frequencies, (< 0.1 Hz), the operator and control move in unison with the platform with no relative control motion. As frequency increases this state of affairs changes, however. The dynamic response properties (transmissibility) of the body mass cause it to move at a different amplitude and phase than the platform, so that the torso undergoes differential motion with respect to the platform. Because the limb is attached to the moving torso, the torso motions are coupled through the limb to the control dynamics to induce vibration "feedthrough" (motion-correlated control responses).

Vibration feedthrough can also be caused by inertial forces that act directly on the mass of the arm and control stick. This situation arises in operational aircraft control situations (Ref. 28) and is referred to as the "bobweight" effect.

Coupling the body transmissibility model to the dynamics of the limb/control stick system results in a model for quantifying the vibration feedthrough process. The details of the best model for a given vibration axis will differ greatly. The dynamics of the arm and control stick were not important factors in the vertical vibration configuration studied here, so a very simple feedthrough model resulted, as will be summarized later in Section VII and detailed in Appendix A. The lateral vibration data were somewhat more complex, and the resulting model reflects this, as also summarized in Section VII and derived in Appendix B. The lateral transmissibility model requires more elements, and bobweight effects become important. Even so, a fairly tractable model resulted. Thus, we believe that the conceptual model of Fig. 3 can lead to a fairly comprehensive understanding of the feedthrough process and its ramifications on manual control system performance.

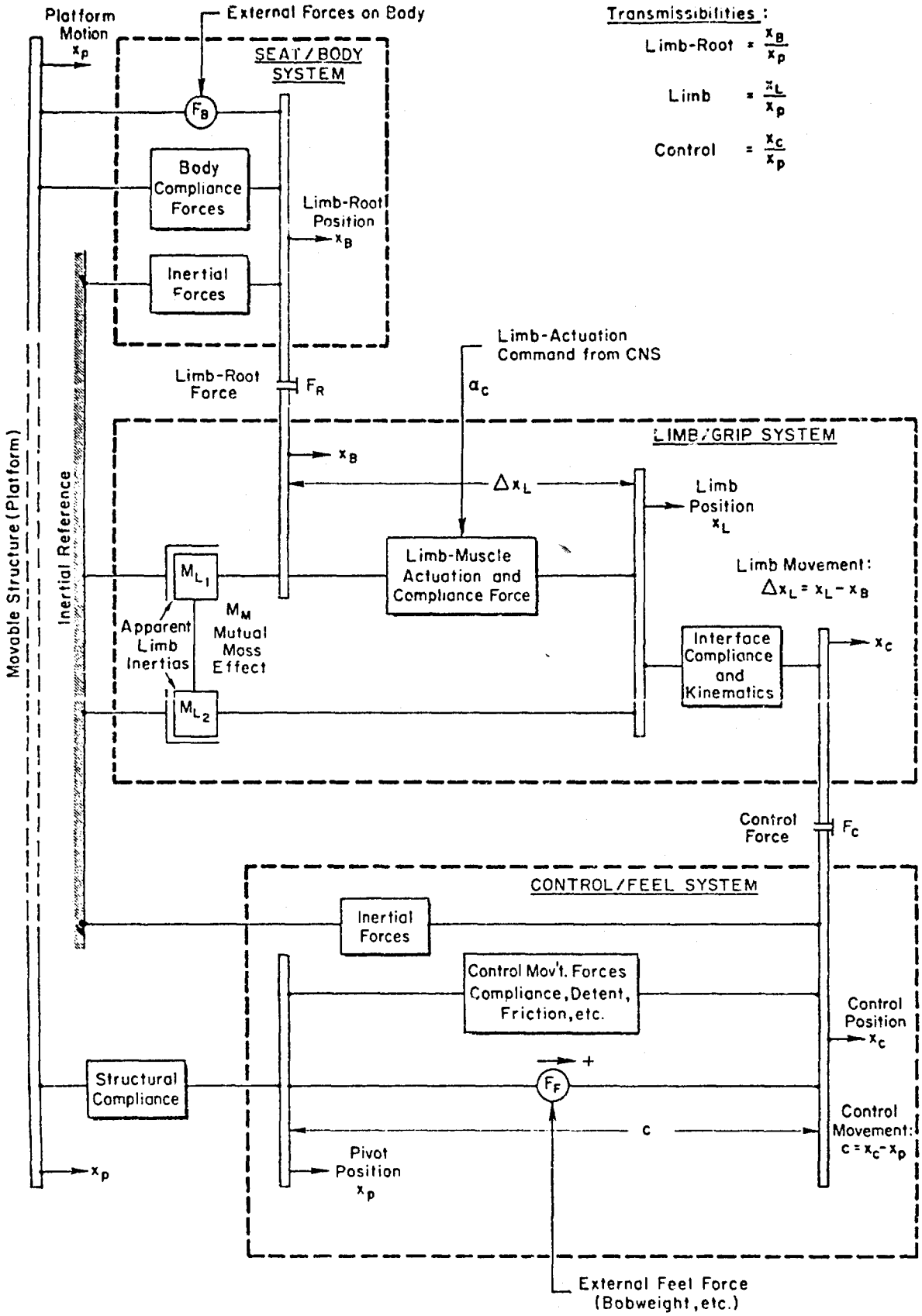

Figure 5. Simplified Mobility Diagram for Conceptual Feedthrough Model

D. SPECIFIC OBJECTIVES

The measurements and experiments herein were designed to provide answers to a number of questions which have been raised in the previous discussions. These are summarized and restated here, against which the overall results are compared in the conclusions of Section VIII:

1. Visual-Motor Behavior

- Does vibration lead to involuntary effects such as changes in neuromuscular dynamics (high-frequency phase lags) and remnant (noise) processes?
- What effect does vibration have on voluntary control behavior such as gain or lead (anticipation)?
- If present, do voluntary changes relate to attempts to control vibration-induced remnant or vibration feedthrough, or do they reflect a stress reaction?

2. Vibration Transmissibility and Control Feedthrough

- Under what conditions is transmissibility a significant factor in manual control performance?
- Under what conditions is vibration control feedthrough a significant effect?
- To what extent can the feedthrough process be modeled?
- Can simple biodynamic feedthrough models give any insight into the phenomenon or allow extrapolation to new situations?

3. Performance

- Can all the underlying causes of performance effects be accounted for?
- What changes in visual-motor behavior and vibration control feedthrough underlie vibration effects on performance measures of tracking error and control activity?

SECTION III

EXPERIMENTAL SETUP

A. SCOPE

The general approach taken in the experimental phases of this program was to make as comprehensive a set of measurements as feasible, in order to define vibration effects on both man-machine performance and on the visual-motor and biodynamic response properties of the human operator. Pre-experimental analysis was employed to define likely operator behavior for the selected control tasks and to define the likely vibration frequency range over which it was important to identify transmissibility and vibration feedthrough response dynamics.

The experimental program was divided into three phases, a pilot study and two formal experiments. Vertical vibration (G_Z) was selected for the pilot study, and (as it turned out) a complete experiment was accomplished on three subjects, albeit with a limited set of measurements. Having established a satisfactory measurement technique at this stage and determined some of the general effects of vibration, we then turned to lateral (G_Y) and fore-aft (G_X) vibration for the formal experiments, with the complete set of desired measurements. Previous research (Refs. 6 and 31) has shown lateral and fore-aft effects to be more dramatic and complex than vertical cases, and the additional measurements utilized in these latter experimental rounds were helpful in explaining the observed phenomena.

B. PHYSICAL SETUP

In Fig. 4 a subject is shown performing the control task on the AMRL-BBV Lab's Western Gear shaker facility located at Wright-Patterson Air Force Base, Ohio. A Tektronix Model 601 CRT, having a view area of 8 × 10 cm, was used as the visual display for the compensatory tracking task. The subject controlled the task with a joystick, as shown in Fig. 4. Details of the tracking task and joystick characteristics are given in Section III-C. The seat was rigidly constructed of aluminum, and the control stick and display were

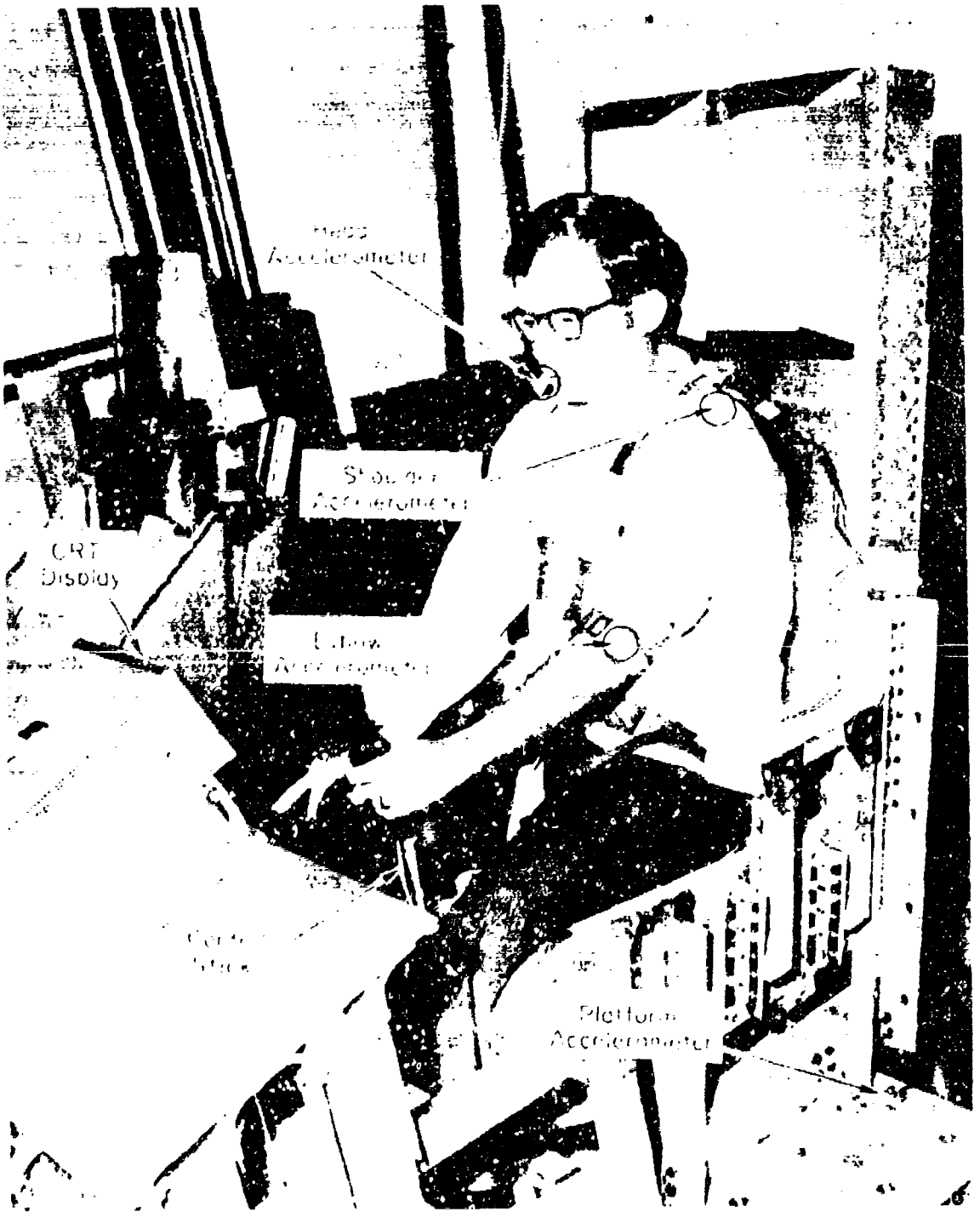

Figure 4. Instrumented Subject Performing Tracking Task Under Vibration

rigidly attached, so that there were no resonances or other distortions to the platform motion as transmitted to the subject, control or display unit, within the frequency range of interest in these studies.

The subject was seated on a standard F-105 parachute container and insulation pad. This setup provided a stiff, yet comfortable, coupling between the seat and subject, without adding significant dynamic effects to the transmissibility measurements. A standard fighter aircraft shoulder strap and seat belt arrangement was also employed. The belts were adjusted to a comfortable tension, but the shoulders were not pinned to the back of the seat. The setup roughly simulated the arrangements in a typical military aircraft.

In order to define the transmissibility and control feedthrough properties of the subjects, accelerometers were used to measure the motion of the platform, and key points on the subject's body. The subject's accelerometers were lightweight (< 0.2 oz) Endevco Model 2222B units, with flat response over the range 1-200 Hz. For the vertical and lateral studies the accelerometer locations were as shown in Fig. 4 with the accelerometer axes oriented in the appropriate direction. The shoulder accelerometer was securely taped to the bony point of the shoulder (acromian), and the elbow unit was strapped around the arm (against the proximal extremity of the ulna). The head accelerometer was affixed to the skull via a small, lightweight bite rod that was gripped in the teeth like a pipestem. Each subject had his own bite bar with an individualized dental impression formed from a thermosetting plastic.

Previous studies (Ref. 6) had reported significant vertical head motions during fore-aft vibration, which could lead to visual blurring effects. Thus, for the G_X study, vertical shoulder and head accelerations were measured as above in addition to fore-aft torso acceleration which was obtained with an accelerometer mounted on the sternum. Fore-aft head and elbow measurements were considered of minor importance since fore-aft head motion would not lead to significant visual blurring and elbow motions would be very close to control stick motions in this case. Consequently, these measurements were dropped for efficiency in the x-axis experiment.

The vibration platform itself was the Western Gear Corporation Model 4010 High Amplitude Vibration Machine operated by the AMRL-BBV laboratory at

Wright-Patterson Air Force Base. Driven via adjustable Scotch yoke mechanisms by a variable speed electric motor, this machine gave reasonably good sinusoidal waveforms over the range from 1-10 Hz. Its characteristics have been described in detail elsewhere (Ref. 30).

The arrangement of the instrumentation and recording equipment situated adjacent to the vibration apparatus is shown in Fig. 5. The control task and some data processing were provided by an EAI 380 analog computer. An STI Mk II Describing Function Analyzer (DFA) provided the input forcing function for the control task in addition to on-line Fourier analysis of control task signals during the tracking runs, as described in Section III-C (also see Ref. 22a). The printed-tape data logger was used to record measurements accumulated during each run. Accelerometer response (via compensated accelerometer amplifiers) was recorded on the strip chart recorder, and these records were then used to determine the subject's transmissibility as described in Section III-C-2.

C. TRACKING TASKS

The tracking tasks were selected to be commensurate with the axis of vibration in each of the studies. A pitch attitude control task was selected for the z- and x-axis vibration experiments as being appropriate to an aircraft environment with vertical and fore-aft cockpit motions. Similarly, for the lateral vibration study, roll attitude tracking was chosen as the appropriate pilot control task. In addition to being pertinent to the vibrating aircraft scenario, the tasks also involved different types of vibration feedthrough to the control stick output:

- For the vertical case, the vibration inputs were perpendicular to the pitch control motions, thereby minimizing direct vibration-induced control action. Only the secondary vibrational motions, transmitted by the operator's arm from his torso, appeared in the control response.

- For the lateral and fore-aft cases, direct control responses are caused by inertial forces acting on the combined arm/stick mass due to platform motion (the "bobweight" effect noted earlier) as well as relative shoulder motions due to torso transmissibility.

The details of the tracking tasks were as follows.

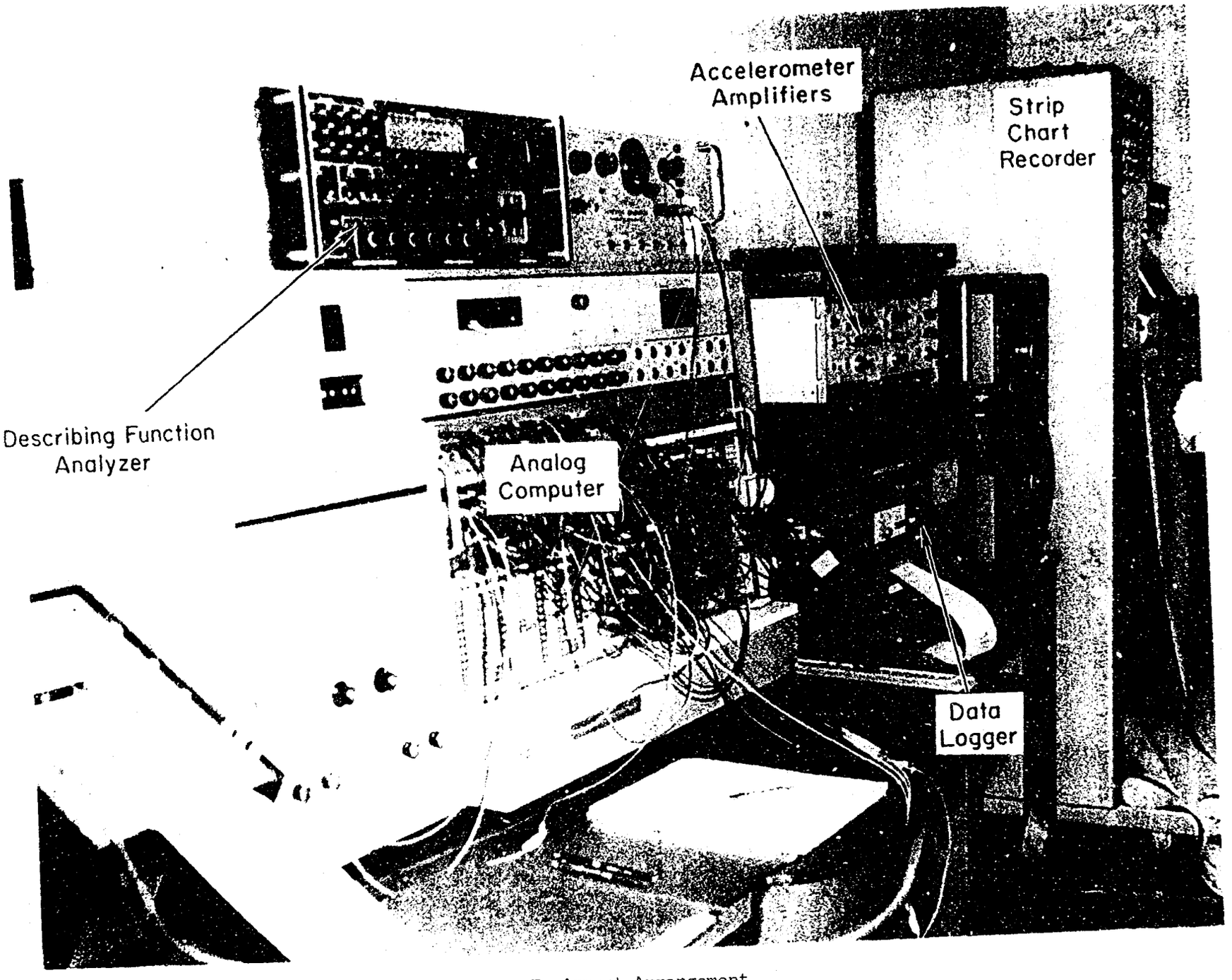

Figure 5. Equipment Arrangement

1. Pitch Control Task (G_z and G_x Studies)

In this task the fore-aft movement of the joystick controlled the vertical motion of a horizontal CRT line. This luminous line and the illuminated reference line were very bright and could easily be perceived under all conditions. In the G_z study three different sets of control dynamics were employed, in order to elicit a range of tracking workload from the subjects. The simplest controlled element was a first-order instability (Ref. 21) which allowed the subject to act as a pure gain (i.e., control outputs proportional to displayed error) in addition to his inherent time delay and neuromuscular properties. A second controlled element had dynamics approximating the short-period response of a large bomber (similar to the XB-70) and required some lead generation by the pilot ($T_L \doteq 0.5$ sec). A third controlled element was composed of a slight instability at 0.5 rad/sec and a first-order lag at 1.92 rad/sec. This controlled element proved to be only slightly more sluggish than the short-period dynamics, and was used only in the training phase of the G_z study. In the G_x experiment, only the short-period dynamics were employed. The controlled element dynamics and appropriate human operator response behavior are given in Table 1. The controlled element gains (K_c) given in Table 1 were adjusted for subject acceptance, and a common gain was selected for all subjects that was on the low side of the preferred level for each task. This is consistent with aircraft practice for large vehicles, and it also minimized the possibility of feedthrough effects dominating task performance.

Two different control sticks were employed with widely different spring restraints in order to investigate the effects of arm/control stick coupling. The "spring" stick had a very light spring gradient with no damping other than ballbearing friction. This control stick provided minimal restriction to arm movement and stick output was proportional to stick deflection. The "stiff" stick was essentially an isometric (force stick) control, having a strain gauge transducer whose output was proportional to applied grip force. In this case arm motion at the hand was constrained to move with the platform motion, and actually provided another anchor point for the body in addition to the seat and feet. The control stick properties are listed in Table 1b.

a. Controlled Element Dynamics

TASK		CONTROLLED ELEMENT DYNAMICS, $Y_c(s)$	CONTROLLED ELEMENT GAIN, K_c		APPROPRIATE HUMAN OPERATOR BEHAVIOR, $Y_p(s)$
			SPRING STICK	STIFF STICK	
Pitch Attitude Tracking (G_z and G_x Studies)	First Order (G_z only)	$\frac{K_c}{s-1}$	1.92 $\frac{\text{display cm/sec}}{\text{stick cm}}$	NA	$K_p e^{-\tau} e^{j\omega}$
	Short Period	$\frac{K_c(s+1.42)}{s[s^2+2(.56)(1.71)s+1.71^2]}$	2.56 $\frac{\text{display cm/sec}^2}{\text{stick cm}}$	0.27 $\frac{\text{display cm/sec}^2}{\text{Newton (stick force)}}$	$K_p(T_L s+1)e^{-\tau} e^{j\omega}$ $T_L \doteq 0.5$ sec
	Second Order (G_z training only)	$\frac{K_c}{(s-0.5)(s+1.92)}$	5.76 $\frac{\text{display cm/sec}^2}{\text{stick cm}}$	NA	$K_p(T_L s+1)e^{-\tau} e^{j\omega}$ $T_L \doteq 0.5$ sec
Roll Attitude Tracking (G_y Study)		$\frac{K_c}{s(s+3)}$	105 $\frac{\text{display deg/sec}^2}{\text{stick cm}}$	17.5 $\frac{\text{display deg/sec}^2}{\text{Newton (stick force)}}$	$K_p(T_L s+1)e^{-\tau} e^{j\omega}$ $T_L \doteq 0.3$ sec

b. Control Stick Properties

STICK	FORCE GRADIENT (Newtons/meter)	NATURAL FREQUENCY (rad/sec)	DAMPING RATIO
Spring	164	23	0.3
Stiff	13,900	207	0.014

c. Tracking Command Input

FREQUENCY, ω_K		AMPLITUDE, A_K	
(Hz)	(rad sec)	Pitch Task (cm on CRT)	Roll Task (deg on CRT)
0.08	0.503	0.646	12.9
0.20	1.26	0.258	5.16
0.48	3.04	0.107	2.16
1.00	6.28	0.0516	1.04
1.67	10.23	0.0309	0.062
Displayed rms, σ_1		0.5 cm	10 deg

A sum of five non-simple-harmonic sinusoids with random initial phasing was used as the input forcing function for the tracking task. The frequencies were roughly logarithmically spaced to most efficiently cover the range of interest for visual-motor response measurements, and the amplitudes were set inversely proportional to frequency (Table 1 c) in order to yield adequate power in the error spectrum for measurement purposes. On the basis of previous research (Refs. 21, 22, 24, and 25), this type of input with power concentrated in a small number of components has proved to be both acceptable from the subject's point of view (random-appearing error signal with a moderate bandwidth) while yielding high signal/noise measurements due to the concentration of signal power at only five frequencies. This scheme yields very low measurement variability despite short run lengths. The measurement technique is described in Section III-D.

2. Roll Control Task (G_y Study)

In this task left or right movement of the joystick controlled the rotation of the luminous horizon line on the CRT display. Based on the findings of the G_z study, the controlled element configuration *per se* did not appear to have a large interaction on the vibration feedthrough effects, so a single set of moderate-difficulty dynamics were selected for the lateral case. The controlled element form approximates the roll response of a stability-augmented aircraft. The controlled element gain was again set to an acceptable level on the less sensitive side of subject preference. The controlled element properties are summarized in Table 1.

The two control sticks employed in the vertical vibration study were again used here. The same input forcing function was used as well, except that the amplitude is now characterized in terms of the angular rotation of the horizon line as given in Table 1. The amplitude was set such that vertical displacements at each edge of the horizon line were comparable to the amplitude used in the G_z and G_x studies, in an attempt to achieve some equivalence in display motions between the pitch and roll tasks.

D. MEASUREMENTS

As indicated in Section II, one of the major measurement objectives in these studies was to partition the error performance and control stick response into components correlated with the tracking task input and vibration feedthrough, and a remaining uncorrelated component due to operator noise or remnant (as derived in Section II):

	Total Variance	=	Tracking Input-Correlated Variance	+	Vibration Feedthrough Correlated Variance	+	Uncorrelated Noise (Remnant)
Error	σ_e^2	=	$\sigma_{e_i}^2$	+	$\sigma_{e_v}^2$	+	$\sigma_{e_n}^2$
Stick	σ_c^2	=	$\sigma_{c_i}^2$	+	$\sigma_{c_v}^2$	+	$\sigma_{c_n}^2$

(10)

Furthermore, in order to understand the cause of the effects shown by the partitioning, we also measured the visual-motor dynamic response properties of the operator responsible for the input-correlated variance, and the biomechanical response properties responsible for the vibration feedthrough components. The measurement procedures were as follows.

1. Performance and Describing Function Measurements

The actual data processing was divided up into two stages:

- Procedures most efficiently done on-line during the tracking runs, consisting of various time integrals.
- Off-Line processing of these time integrals to yield the various signal variance components dynamic response functions and fitted model parameters.

As shown in Fig. 6, the STI Mk II Describing Function Analyzer (DFA) was used to generate the input forcing function for the tracking task as well as perform on-line computations during the tracking runs, including:

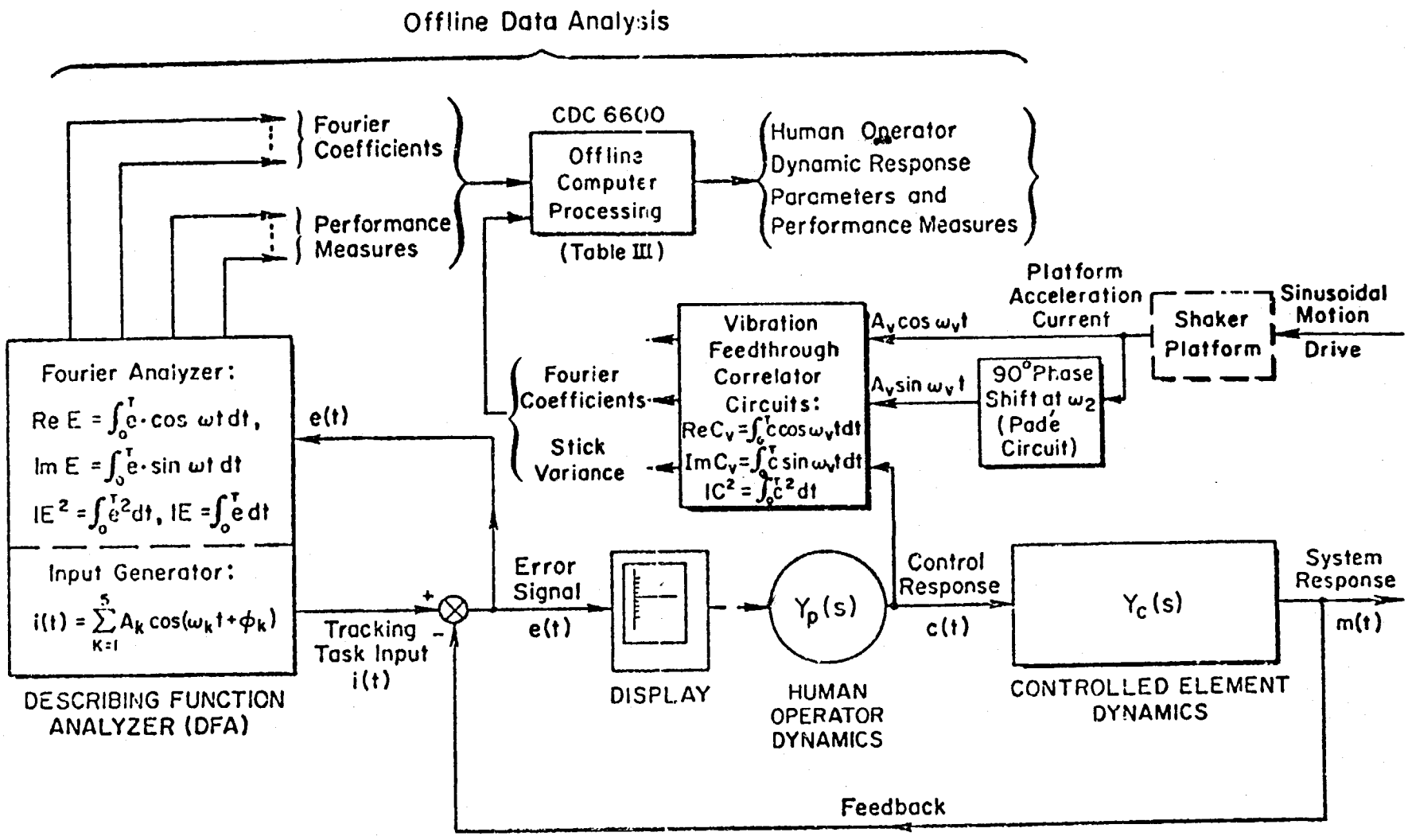

Figure 6. Data Measurements and Analysis

- The Fourier sine and cosine integrals of the tracking error signal at each of the forcing function frequencies.
- The mean and mean square integrals of the error signal and the mean square control response.

References 21 and 22 describe the DFA and the measurement scheme. Similar computations were also performed on the analog computer, as shown in Fig. 7, in order to obtain the Fourier sine and cosine integrals of the control response relative to platform acceleration at the vibration frequency. The above data were then processed off-line on a digital computer, as shown in the flow chart in Table 2, to yield the various variance components, dynamic response functions, and describing function parameters of interest.

Typical describing function data under no vibration is shown in Fig. 8, in order to summarize the various dynamic response and performance measures employed in this research. The detailed human operator describing function (Y_p) is useful in indicating the subject's lead generation (rate perception) ability and neuromuscular properties which occur at high frequencies ($\omega > 6$ rad/sec). The rise in $|Y_p|$ beyond $\omega = 3$ rad/sec shown in Fig. 8a verifies that the subject is generating the appropriate lead to cancel the lag in the controlled element dynamics. This behavior is very consistent over the three repeated runs at this static condition.

In keeping with past manual control measurement practice, the overall dynamic response effects will mainly be presented in terms of $Y_{OL}(j\omega)$, the open-loop describing function (output/error) as shown in Fig. 8b. The relevant parameters characterizing the open-loop response and their importance are explained below (e.g., see Ref. 18 for basic background):

- Gain Crossover Frequency (ω_c), the unity amplitude (0 dB) frequency of Y_{OL} which is proportional to the operator's gain and determines the bandwidth of the manual control loop. This parameter often decreases when the operator is attempting to minimize the influence of noise sources within the loop (such as remnant and possibly vibration feedthrough), while accurate following of the tracking input requires as maximum a bandwidth as possible (see Ref. 24 for a thorough discussion of the tradeoffs involved).

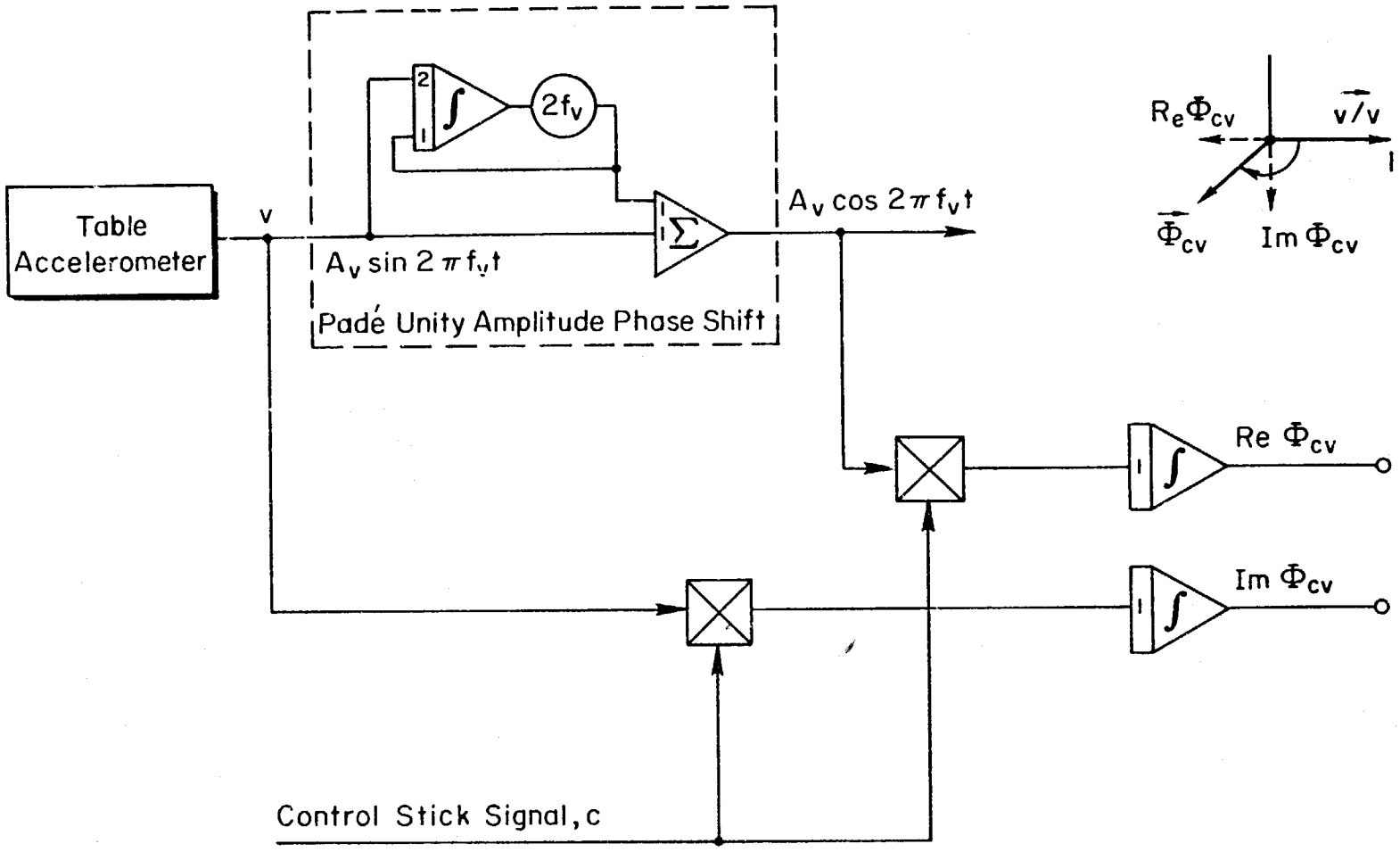

Figure 7. Fourier Cross Correlation Method for Measuring Vibration Feedthrough to Control Stick

TABLE 2

OFF-LINE DATA PROCESSING

Program Operations	Output
Input mean, mean square and Fourier sine and cosine integrals at frequency k	[Note 5 input frequencies; k = 1-5]
Compute error and control output variances	σ_e^2,† σ_c^2†
Compute error components at forcing function frequencies and total input correlated error variance and error coherence (ρ_e^2)	$\Phi_{ee}(\omega_k)$† $\sigma_{e_i}^2 = \sum_{k=1}^{5} \Phi_{ee}(\omega_k)$ $\rho_e^2 = \sigma_{e_i}^2/\sigma_e^2$
Compute error to input describing function and transform to give open-loop describing function	$\frac{E(j\omega_k)}{I(j\omega_k)}$† $= \frac{1}{1 + Y_{OL}(j\omega_k)}$ $Y_{OL}(j\omega_k) = \left[\frac{E(j\omega_k)}{I(j\omega_k)}\right]^{-1} - 1$
Interpolate gain and phase crossover frequencies (ω_c, ω_u) and phase margin (φ_M) from Y_{OL}	ω_c, ω_u, φ_M
Compute pilot describing function given known controlled element $Y_c(j\omega_k)$	$Y_p(j\omega_k) = Y_{OL}(j\omega_k)[Y_c(j\omega_k)]^{-1}$
Compute control stick components at forcing function frequencies and total input correlated control variance	$\Phi_{cc}(\omega_k) = \lvert Y_p(j\omega_k)\rvert^2 \Phi_{ee}(\omega_k)$ $\sigma_{c_i}^2 = \sum_{k=1}^{5} \Phi_{cc}(\omega_k)$
Compute control response and error components correlated with vibration frequency	$\sigma_{c_v}^2 = \Phi_{cc}(\omega_v)$† $\sigma_{e_v}^2 = \lvert Y_c(j\omega_v)\rvert^2 \Phi_{cc}(\omega_v)$
Compute closed-loop vibration feedthrough describing function	$\frac{C(j\omega_v)}{V(j\omega_v)}$† $= \frac{Y_v(j\omega_v)}{1 + Y_p Y_c(j\omega_v)}$

†Computed directly from input data

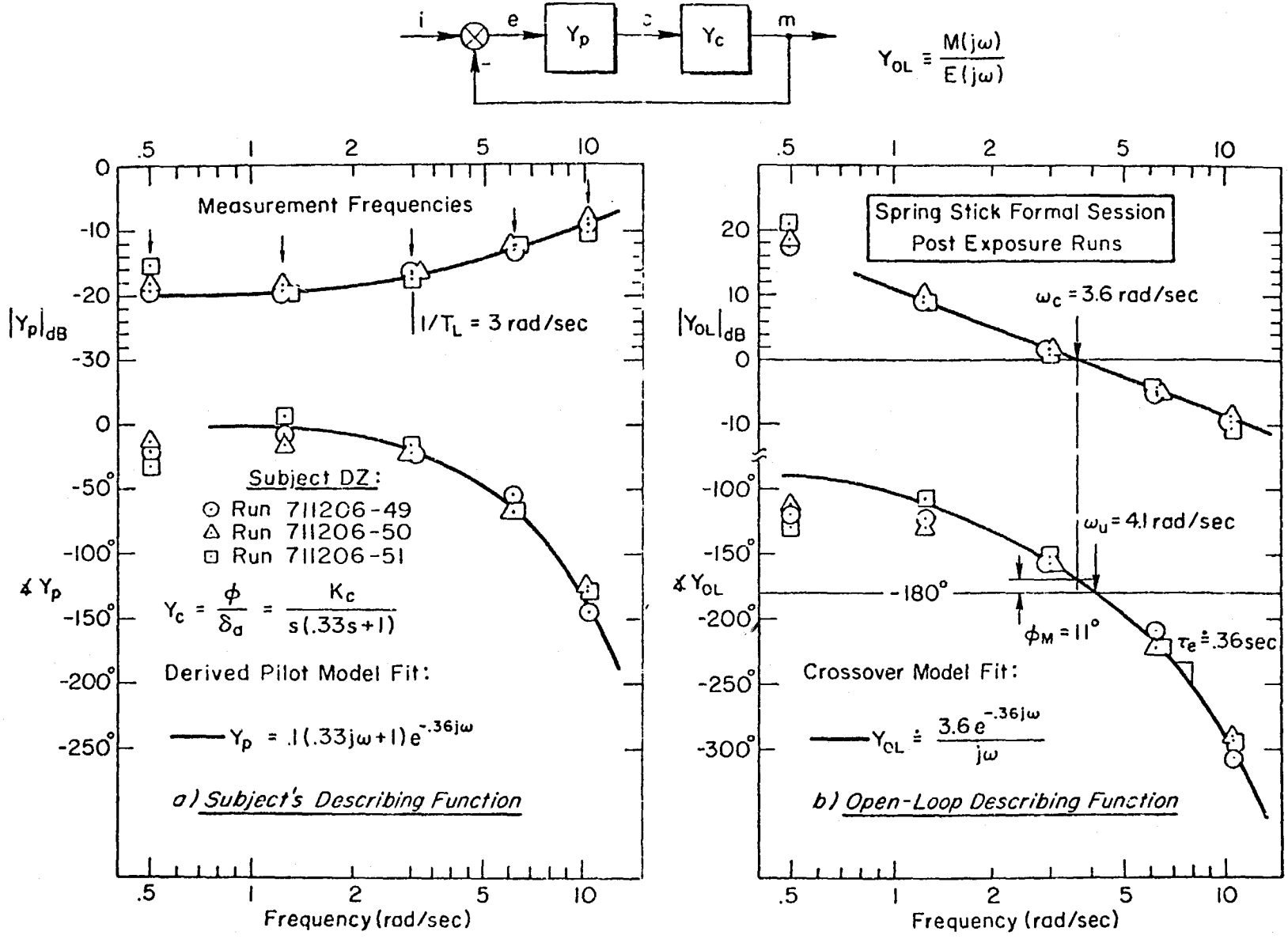

Figure 8. Typical Describing Function Measurements and Parameters: Three Repeat Runs on Subject DZ Measured under Static Conditions during the G_y Vibration Study

- Phase Margin (ϕ_M), a system stability margin, measured at ω_c. As ϕ_M approaches zero the closed-loop damping ratio vanishes, i.e., the manual control system approaches an unstable condition. When under stress or involved in complex tasks (high task workload), the operator will generally adopt generous margins; however, accurate tracking of the system input requires high ω_c's which tend to reduce ϕ_M.

- Phase-Crossover Frequency (ω_u), a high-frequency measure of phase properties with contributions from lead generation, neuromuscular and limb/manipulator dynamics. ω_c could, theoretically, be increased to this frequency if the closed-loop damping were allowed to vanish, so ω_u provides an absolute upper limit on the closed-loop bandwidth. Because the slope of $|Y_{OL}|$ vs. frequency has a slope of about -1.0, ω_c is also a measure of loop gain, and ω_u represents the unstable gain, so the ratio of $|\omega_u/\omega_c|_{dB}$ provides another measure of stability margin, closely approximating the gain margin.

The summary performance parameters to be presented include:

- Error and Stick Variances (σ_e^2, σ_c^2), the average mean square dynamic power in various signals, after removing dc offsets. These variances are also portioned into two correlated and one uncorrelated components, as discussed previously (Eq. 3).

- Error and Stick Coherence (ρ_e^2, ρ_c^2), the fraction of the total signal variance linearly correlated with the describing function measurements. The remaining power ($1 - \rho_i^2 - \rho_v^2$) is due to noise sources internal to the human operator (remnant) fraction.

2. Transmissibility and Vibration Feedthrough Measurements

Transmissibility measurements (response of various points of the subject's body relative to platform motion) were obtained from strip chart recordings of the various accelerometers shown in Fig. 4. Since the vibration wave forms were sinusoidal, it was fairly easy to read amplitudes and relative phase shifts from the recordings (examples are given in Appendix A). The lightweight body-mounted accelerometers were calibrated relative to the accurate platform-mounted strain gauge unit in order to minimize transmissibility measurement errors. This was accomplished by mounting all the accelerometers on the platform which was run at ± 0.4 g throughout the frequency range

1.3-10 Hz. Within the accuracy of strip chart trace reading, no appreciable differences in amplitude or phase were found among the accelerometers. The average measurement error of the subsequent transmissibility measurements is judged to be less than 5 percent.

In the first (G_Z) study strip chart recordings were also used to identify the control feedthrough dynamics as described in Appendix A. In this situation the subjects were asked to stabilize the short-period dynamics with no input forcing function to the control task. In this case it was easy to identify the control response component corresponding to the vibration frequency appearing in the accelerometer traces. In the G_y and G_x experiments vibration correlated control response was computed during each run (as described in the previous section), and these measurements were verified as agreeing with the components visually apparent in the strip chart recordings.

E. VIBRATION CONDITIONS

Because of the exploratory nature of this research we tried to select conditions that would give clear effects. The vibration amplitude of ±0.4 g (zero to peak amplitude) was selected as large enough to produce effects without undue discomfort and allow tie-in with the previous research of Ref. 31. All vibration conditions were administered at this level.

Frequency conditions were selected to elicit a variety of effects including maximum whole-body resonance and visual blurring. In the first (G_Z) study different controlled elements as well as control sticks had to be tested as experimental variables, so that the number of frequencies was limited accordingly. Based on previous transmissibility data, plus experience during shakedown training runs under vibration, three frequencies were selected: 2, 6, and 10 Hz. The 2 Hz condition was selected as being well below whole-body resonance, the 6 Hz condition as a body resonance condition; and 10 Hz as beyond whole-body resonance with subjectively reported visual blurring.

In the G_y and G_x experiments only one controlled element was employed so that additional vibration frequencies could be run. Previous research (Ref. 31) and our own pre-experimental analysis had indicated that low frequencies (1-3 Hz) were likely to cause the largest effects under G_y and G_x,

so that a low vibration frequency of 1.3 Hz was selected that fell in between the two highest control task input frequencies of ω_i = 1.00 and 1.67 Hz (see Table 1). The remaining frequencies were selected to roughly logarithmically span the range between 1.3 and 10 Hz and included 2, 3, 4.5, 7, and 10 Hz. It was anticipated that the lowest frequencies would interact most strongly with the control task and thereby cause large changes in the operator's tracking responses.

F. SUBJECTS

Members of the AMRL-BBV Hazardous Duty Panel were employed as subjects. These Panel members had undergone physical examinations in order to qualify them for participation in hazardous experimental environments. Background and physical data on the subjects are given in Table 3. As noted, most of the subjects had previous experience under vibration and on tracking tasks.

TABLE 3

SUBJECT BACKGROUND

SUBJECT	STUDY	HEIGHT (in.)	WEIGHT (lb)	AGE (yr)	PRIOR EXPERIENCE	
					VIBRATION	TRACKING
PA	G_x	69	146	24	Some	None
BB	G_x, G_z	67	145	30	None	Minimal
BC	G_x, G_y	67	165	34	Appreciable	Extensive
SR	G_y	66	165	25	Appreciable	Appreciable
JS	G_x, G_y, G_z	72	185	25	Extensive	Extensive
DZ	G_y, G_z	72	185	42	Extensive	Extensive

G. EXPERIMENTAL DESIGNS AND PROCEDURES

1. G_z Experiment

a. Training

The subjects were given three 1-hour training sessions on the tracking tasks under static conditions. Two 2-minute trials per controlled element were administered each session, with an additional trial or two on the short-period and second-order controlled elements during the final training session. All training was conducted with the spring stick control, which was the most difficult to use. Training results showed the manual control behavior elicited by the second-order and short-period dynamics to be similar, so the second-order controlled element was eliminated for convenience in the formal test sessions.

b. Vibration Training Session

The purpose of this test session was twofold: 1) to give the subjects an initial encounter at performing the tracking task under vibration; and 2) to obtain body transmissibility and control feedthrough data throughout the frequency range 2-10 Hz. The runs were started at 2 Hz and repeated at 1 Hz increments up to 10 Hz at 0.4 g. A run at a particular frequency lasted about 2 min. During each transmissibility run the subject stabilized the CRT line with the short-period dynamics and spring stick control but with no input forcing function. Thus, the only component in the control output, other than a small amount of remnant, was the vibration feedthrough term.

The measurements in these tests were recorded as strip chart tracings of the stick output and accelerometer response. Vibration and control response amplitude and phase were read from the traces. These data were used to define each subject's transmissibility and feedthrough properties, and to validate our feedthrough model, developed in Appendix A.

At the end of the session the short-period tracking task with input was administered both at 6 Hz vibration (the main torso resonance frequency) and with no vibration as final training runs.

c. Formal Data Sessions

Two formal data sessions were conducted, the first with the spring stick and the second with the stiff stick. At the beginning of each session the subject was instrumented with the accelerometers and given a warmup tracking run under static conditions.

During the first session with the spring stick, the first-order task was administered during the first half of the session, and the short-period dynamics during the second half. The vibration conditions were presented in a semi-random order for each subject as shown in Table 4.

During the second session with the stiff stick control, only the short-period dynamics were employed. Two tracking runs were conducted at each experimental condition, and the conditions were presented in the order shown in Table 4. In addition to the tracking runs, transmissibility and control feedthrough data were obtained at 2, 4, 6, 8, and 10 Hz in the same manner employed in the vibration training session with the moving stick control.

TABLE 4

ORDER OF PRESENTATION OF EXPERIMENTAL CONDITIONS

SESSION	CONTROLLED ELEMENT	SUBJECT		
		BB	JS	DZ
FIRST "Spring" Stick	First Order	Static	10 Hz	6 Hz
		2 Hz	6 Hz	2 Hz
		10 Hz	2 Hz	Static
		6 Hz	Static	10 Hz
	Short Period	6 Hz	Static	10 Hz
		10 Hz	2 Hz	Static
		2 Hz	6 Hz	2 Hz
		Static	10 Hz	6 Hz
SECOND "Stiff" Stick	Short Period	6 Hz	Static	10 Hz
		2 Hz	2 Hz	6 Hz
		Static	10 Hz	2 Hz
		10 Hz	6 Hz	Static

2. G_y and G_x Experiments

a. Training

Training was much less critical for the lateral and fore-aft experiments, because only one controlled element was used. Initial half-hour training sessions (two for G_y and one for G_x) without vibration were conducted with the spring stick control. During each session six 1-minute tracking trials were administered. An additional 1-hour session was conducted with the spring stick to give the subject an initial encounter with 0.4 G_y vibration at each of the test frequencies. Two tracking runs were administered at each vibration frequency. Following the spring stick formal test session, another training session was given with the stiff stick control.

b. Formal Data Sessions

During the formal data session, tracking trials were administered at each vibration frequency, and under "static" test conditions both at the beginning and end of each session. It was not practical to randomize the order of vibration frequencies; so, to balance out order-of-presentation effects, the vibration frequencies were administered in order from low-to-high for two of the subjects and high-to low for the remaining two. The order of presentation was reversed for each subject between the spring and stiff stick sessions.

In order to obtain more data on run-to-run variability in the G_y experiment, three tracking trials with 50 sec measurement period were used, as opposed to the two runs with 100 sec measurement period used in the G_z tests. Previous research (Ref. 32) has shown that reliable describing function estimates can be obtained with the DFA in 50 sec, and this shorter run length was employed in order to avoid excessively long periods of vibration that might unduly fatigue the subjects. In the fore-aft experiment the number of replications was reduced to two, because of the good run-to-run repeatability measured in the G_y tests.

SECTION IV

VERTICAL VIBRATION EXPERIMENT RESULTS AND DISCUSSION

This section contains the basic results from both training and formal runs of the vertical (G_Z) experiment. Because the study included the initial shakedown of the apparatus and measurement techniques, only three subjects were tested, and some desirable conditions had to be foregone due to time limitations. Thus the results should be viewed as somewhat tentative and deserving of further verification. Models for, and implications of, the results are given in later sections.

A. TRAINING

The training session data given in Figs. 9 (performance) and 10 (dynamic response properties) are compared with data obtained under static conditions during the formal experimental sessions. Tracking error (σ_e) was quite stable for all subjects between training and the formal sessions, as shown in Fig. 9. There is a slight improvement in error performance for the final session with the stiff stick and short-period dynamics. This is probably due to the improved dynamic response allowed with the stiff stick rather than a learning effect. The error coherence (ρ_e^2) was fairly stable between the third training session and formal sessions. Note that the short-period dynamics gave greater coherence (a lower remnant fraction) than the second-order subcritical task, because the latter required greater lead equalization. The second-order task was dropped after the training sessions in order to minimize the number of experimental conditions to be run.

Dynamic response parameters obtained from the describing function measurements are shown in Fig. 10. For the first-order task the gain and phase crossover frequencies (ω_c, ω_u) and phase margin (φ_M) are relatively constant between the training and formal sessions.* For the short-period case the data are reasonably stable between the final training session and the first formal session. For the last formal session with the stiff stick, both ω_u and ω_c increase; however, this is most likely due to decreased

*See Section III-D for explanation of these terms.

limb/manipulator phase lags as a consequence of minimal stick motion (Refs. 51 - 53) rather than training effects.

Overall, these shakedown test data indicate that the subjects were reasonably well trained, that learning effects were not a significant factor in the formal session results, and that test-retest reliability is likely to be good.

B. TRANSMISSIBILITY AND CONTROL FEEDTHROUGH DATA

Because of the limitations discussed in Section III, vertical vibration transmissibility and vibration feedthrough data were obtained during special runs, rather than the formal tracking trials, and the data were reduced from strip chart recordings, rather than the on-line cross-correlation. Vertical shoulder acceleration data obtained for each subject with both the moving and force stick controls are plotted in Fig. 11, and compared with Coerman's model for whole body impedance response fitted over eight seated subjects (Ref. 29). Although all subjects exhibited a typically low damped resonance, it is obvious that the response of each of our three subjects is somewhat different in character. Subject JS has a rather sharp resonant peak which trails off quite rapidly. Subject DZ has a very broad resonance, while Subject BB falls somewhere in between. All three subjects have a greater resonance region than that of Coerman's "average." Nevertheless, the match is surprisingly good when taking into account that Coerman's data are based on whole body mechanical impedance (i.e., force vs. velocity) and not the motion of any particular body part.

Each subject was asked for his subjective estimate of the point of maximum whole body resonance. Subjects JS and DZ felt their resonant point was just below 6 Hz, while BB thought his resonance was closer to 5 Hz. On this basis we selected 6 Hz as the near-resonant-frequency condition for the formal experiment. Judging from the subsequent shoulder transmissibility results given in Fig. 11, 5 Hz would probably have been closer to motion resonance for the three subjects. The shoulder acceleration averaged among subjects for the spring and stiff stick cases are compared in Fig. 12. Unfortunately, no stiff stick transmissibility runs were made at 5 Hz, so its resonance peak could not be defined precisely. It is observed that,

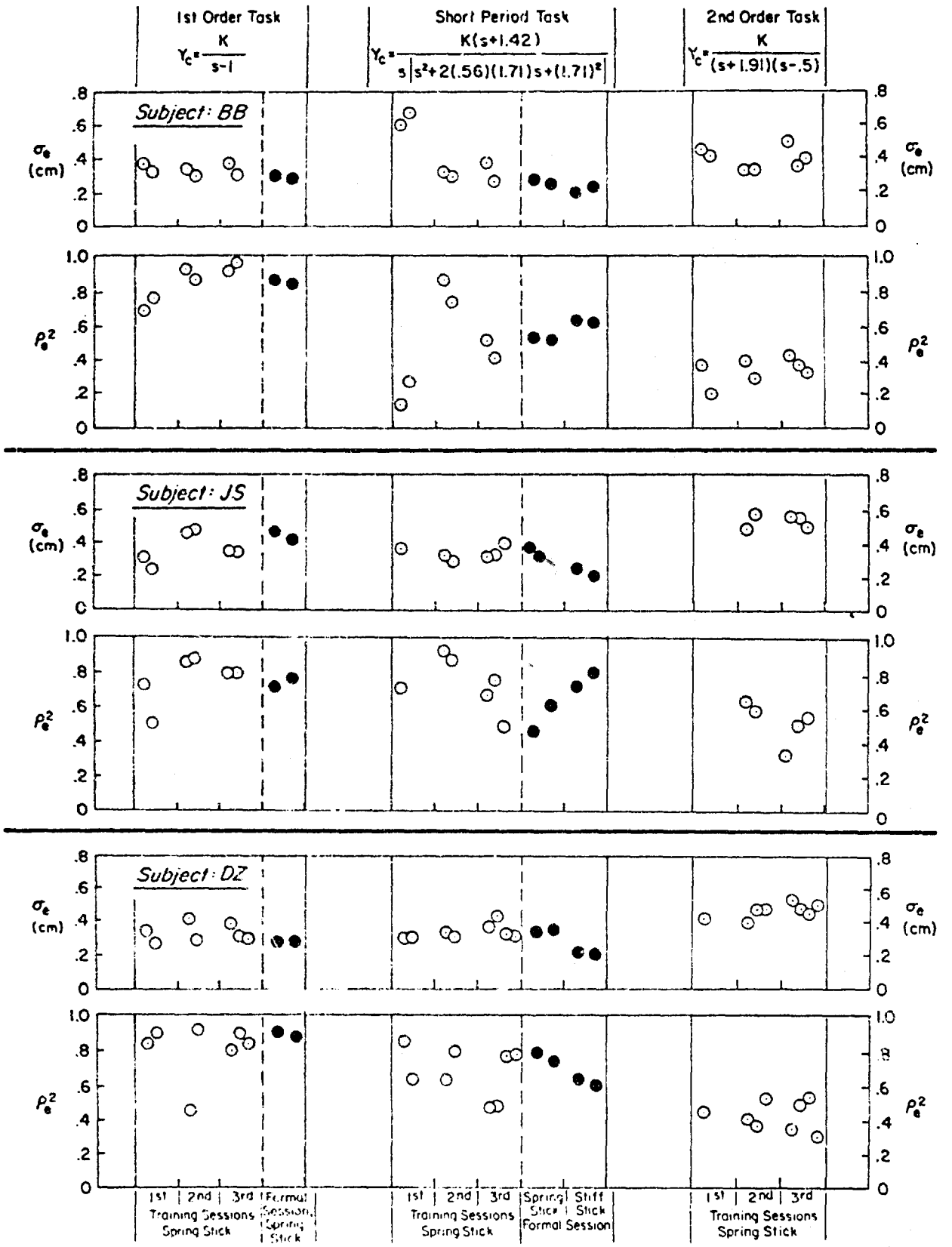

Figure 9. Comparison of Performance During Training and Formal Sessions of G_Z Experiment

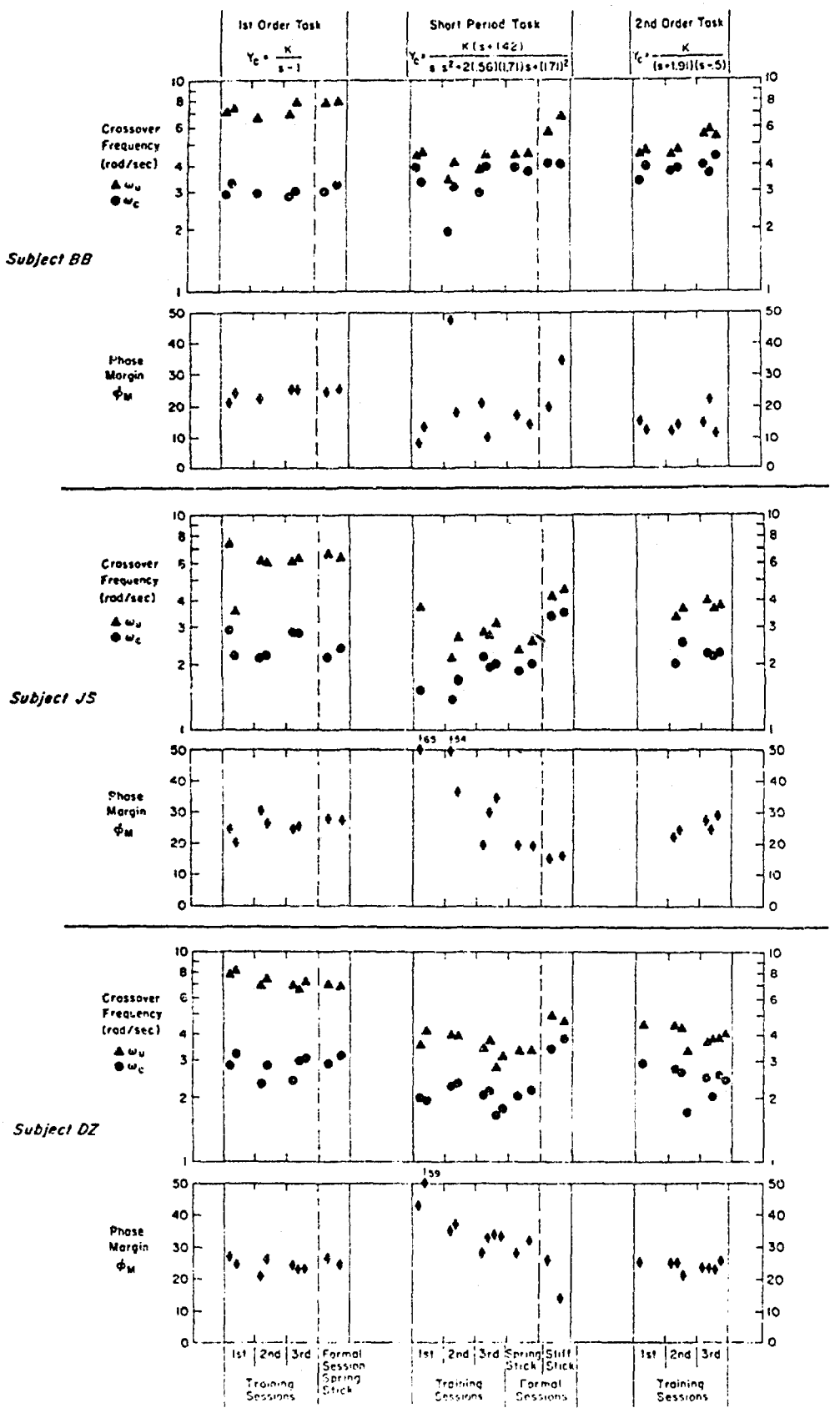

Figure 10. Comparison of Dynamic Response Measurements During Training and Formal Sessions of G_z Experiment

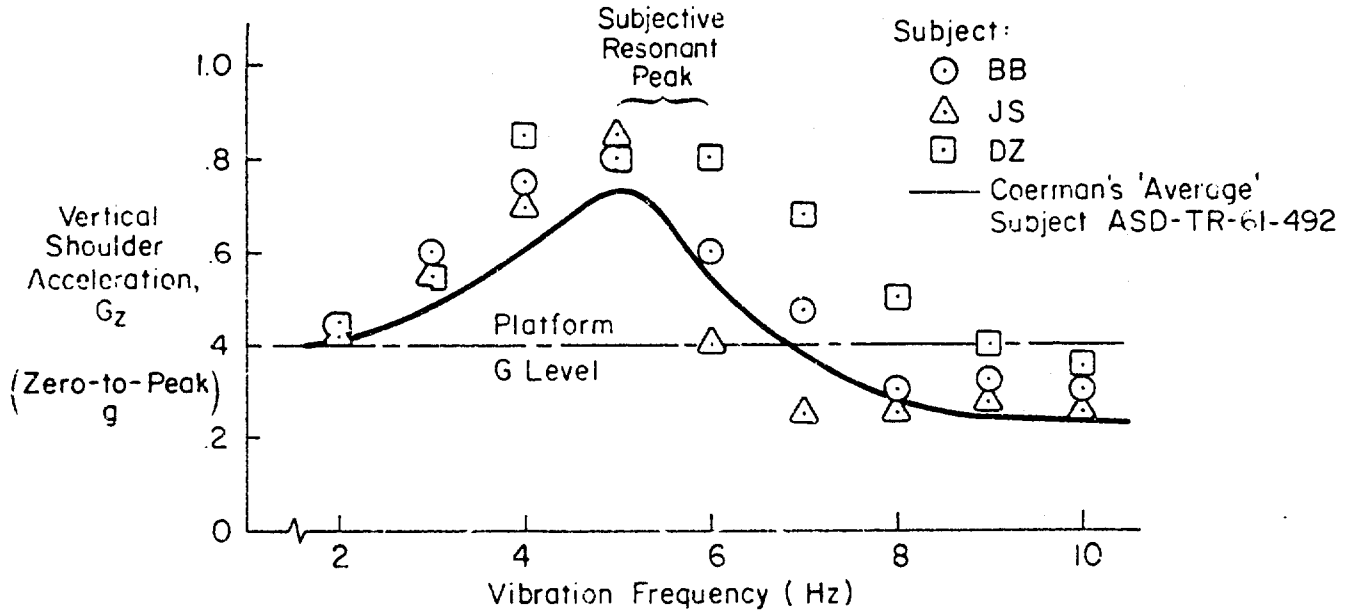

a) With Spring Stick

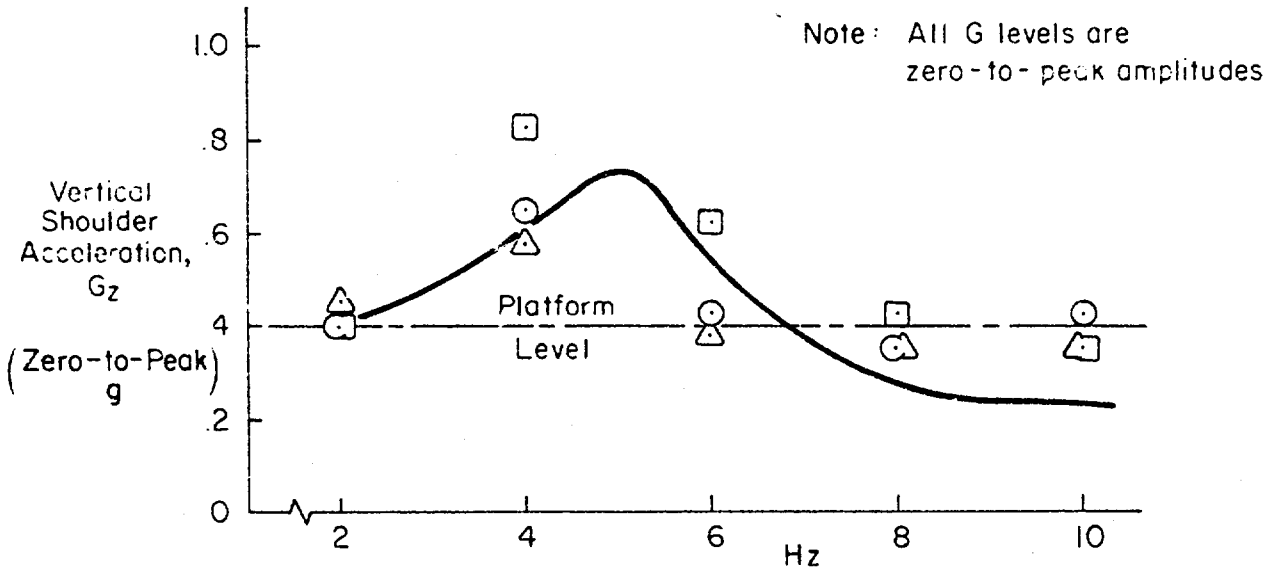

b) With Stiff Stick

Figure 11. Vertical Shoulder Vibration for Three Subjects

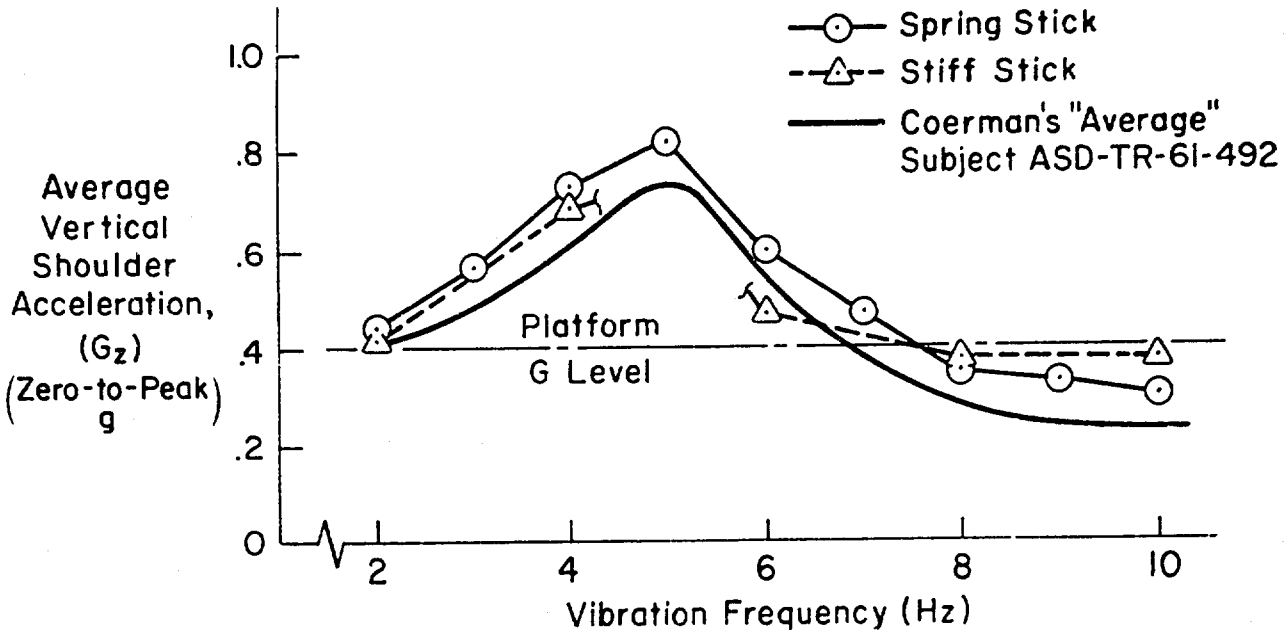

Figure 12. Vertical Shoulder Vibration Averaged Over Subjects

relative to the spring stick, the stiff stick attenuates the shoulder motion around the region of resonance, but actually helps to drive the shoulder motion at 8 Hz and above.

Vertical acceleration measured at the operator's elbow and averaged over the three subjects is shown in Fig. 13. The response is very similar to that measured at the shoulder, so we do not suspect any elbow "flapping" modes, etc., that might complicate the vibration feedthrough effects. Thus, it appears that, under the tested conditions, shoulder motions are directly transmitted through the arm. This provides the basis for "rigid link" assumption used in the vertical feedthrough model development in Appendix A.

Head acceleration (as measured by the bite-mounted accelerometer) is shown in Fig. 14. Comparing this data with shoulder response, we note some departures. Although head acceleration exhibits peak amplitude in the same region of torso resonance as the shoulder, the peak is much sharper with little amplification developed in the region below 4 Hz. At frequencies beyond torso resonance the head amplitude does not attenuate as rapidly as the shoulder, this being due to the second head-on-shoulders biomechanical mode identified by previous investigators (Ref. 6).

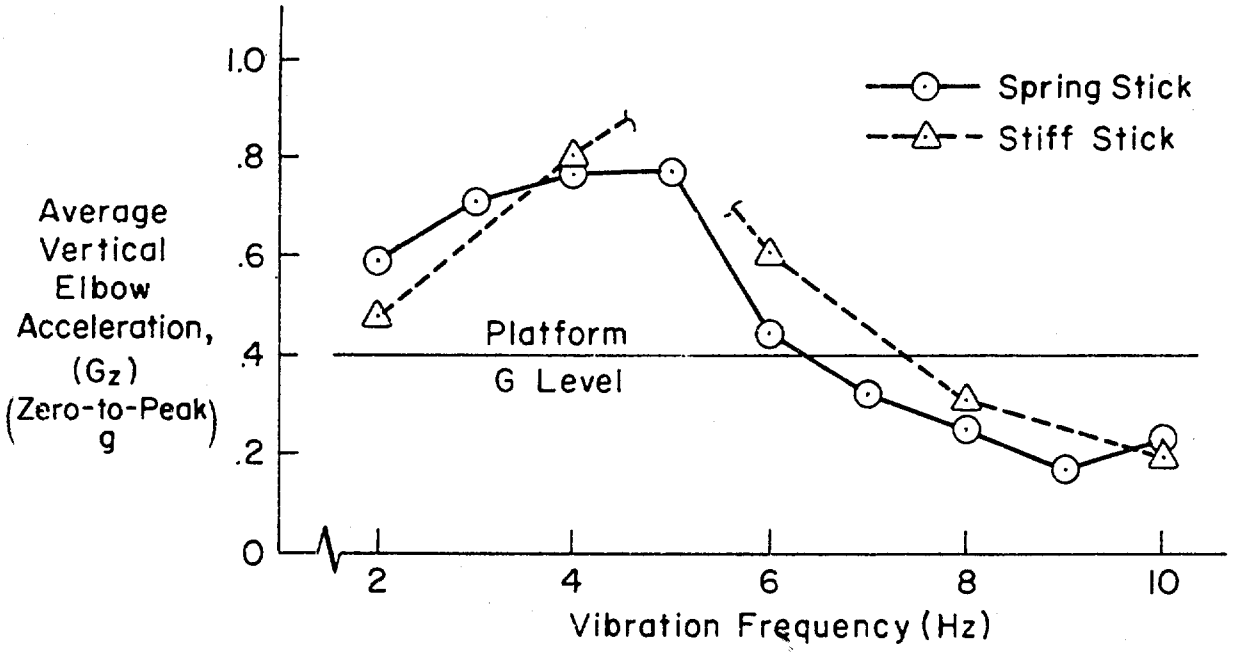

Figure 13. Vertical Elbow Vibration Averaged Over Subjects

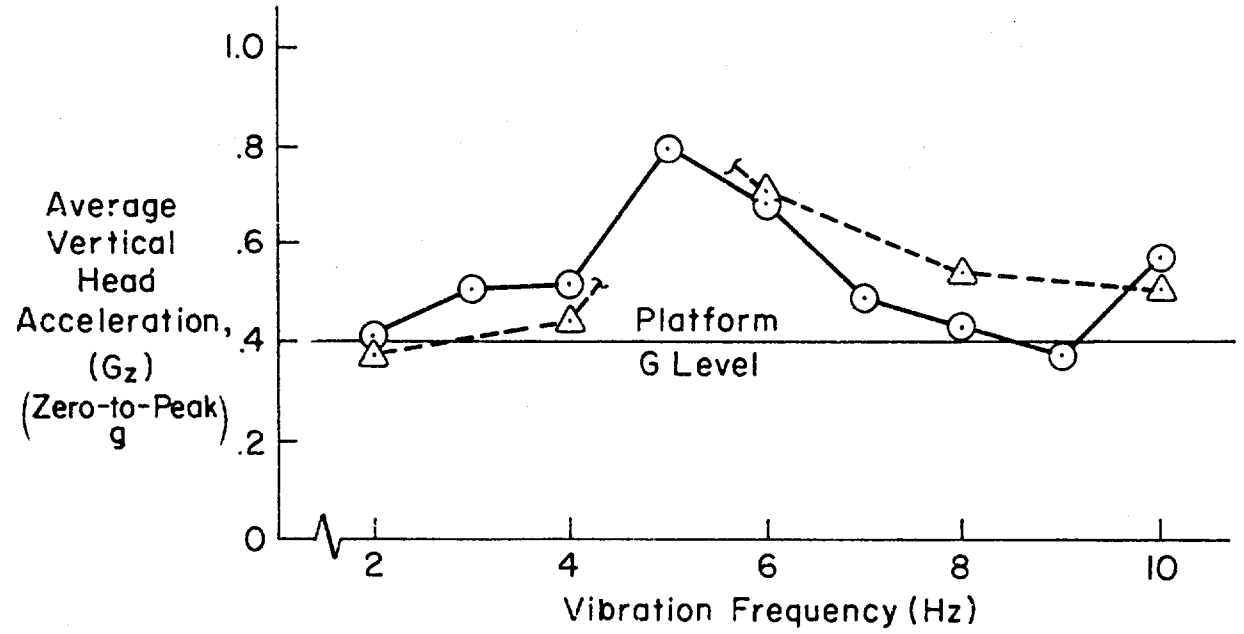

Figure 14. Vertical Head Vibration Averaged Over Subjects

Subjects commented that there was visual blurring out to the region of 10 Hz, which is consistent with the measured head resonance. However, they also commented that this did not seem to interfere with their tracking ability, because both the reference and the horizon lines on the display were blurred to the same degree and could still easily be perceived and aligned. Consideration of the luminous density distribution of a line vibrating sinusoidally with respect to the eye shows that the highest luminous density is near the extremes of travel, thereby providing sharp edges for alignment.

The zero-to-peak-amplitude control stick output incurred while the subjects stabilized the short-period dynamics is plotted in Fig. 15.* Note that, although the character of the feedthrough is slightly different for each subject, the general effects are quite similar. The average feedthrough over subjects for both the spring and stiff sticks is compared in Fig. 16 which illustrates the following effects:

1. Maximum feedthrough for both sticks occurs in the region of whole body resonance.

2. The spring stick gives greater high-frequency attenuation of feedthrough.

3. The stiff stick yields a greater amount of feedthrough (although it should be recalled that the stick gains were set according to subjective acceptability, which makes the comparative feedthrough magnitudes somewhat arbitrary).

*It was desired to make a common comparison between the outputs of the two control sticks which have basically different physical dimensions (i.e., force for the stiff stick and displacement for the spring stick). To accomplish this, stick amplitudes were multiplied by the appropriate controlled element gain, K_c, given in Table 1. The scaled stick signal, $K_c c$, then represents the electrical output of the two sticks which are equivalent in the simulation. The stick feedthrough results here and in Section V are plotted on this equivalent basis, with physical units given on the right hand ordinates of the graphs.

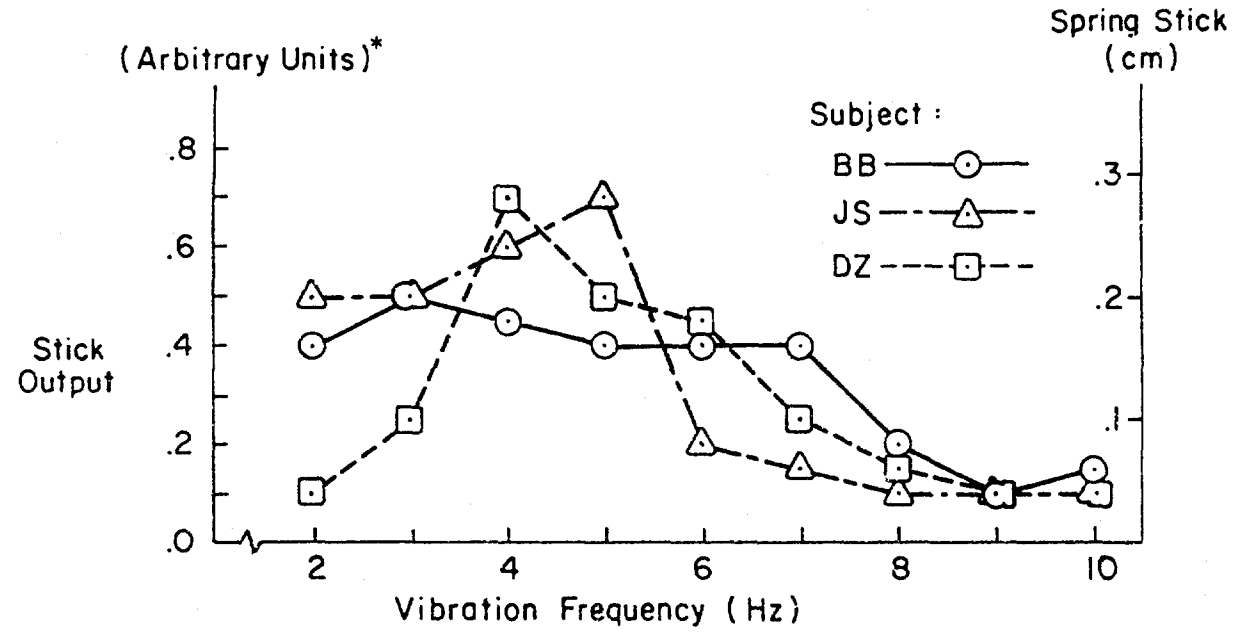

a) Spring Stick

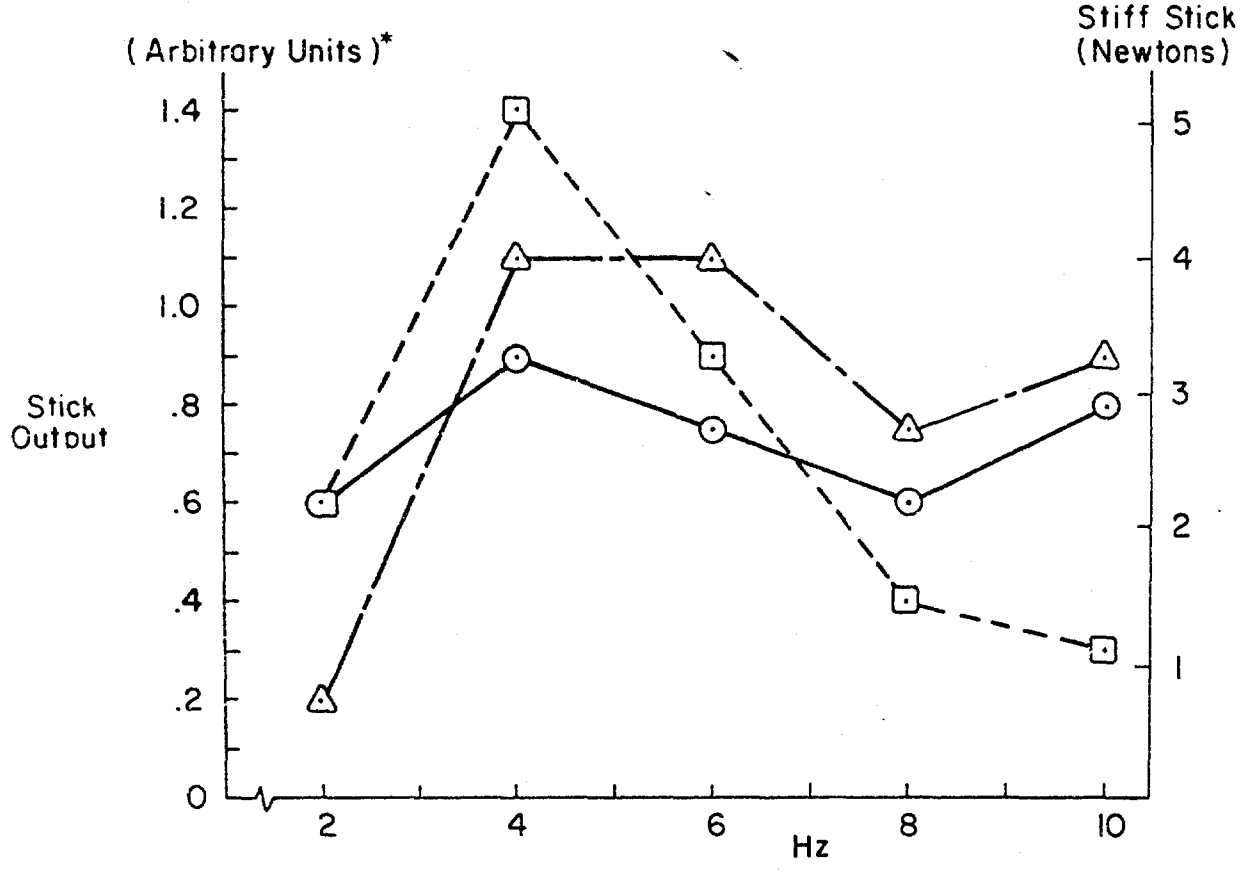

b) Stiff Stick

* See footnote on page 43 for explanation of stick output scaling

Figure ... Control Stick Output Due to Vibration Feedthrough

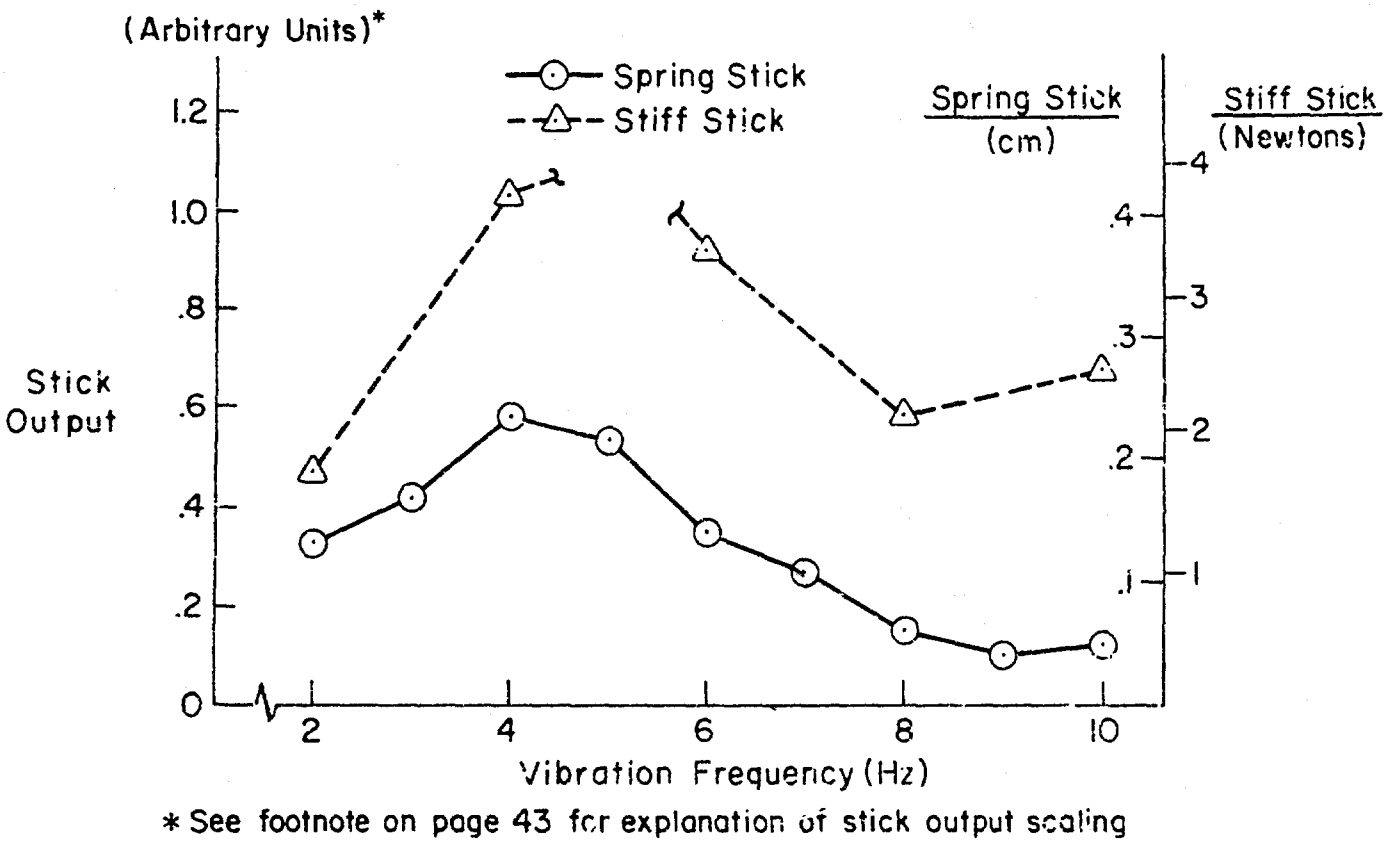

Figure 16. Stick Vibration Feedthrough Averaged Over Subjects

An interesting observation in Section VII is that, while significant stick output power results from vibration feedthrough, this power is small at the error point (because of attenuation in going through the controlled element). A quick calculation of display displacement corresponding to the stick output given in Fig. 16 shows that display deflections due to the direct feedthrough effects are below 0.1 mm. This is not to suggest that feedthrough effects are unimportant, however, since high stick power at high frequencies could have adverse effects on the flight control system of an aircraft, and could also excite the flexible body modes of large slender vehicles.

C. PERFORMANCE AND DYNAMIC RESPONSE EFFECTS

The effect of vertical vibration on error performance and dynamic response bandwidth ($\sim \omega_c$) and stability ($\sim \varphi_M$) is illustrated in Fig. 17, where the data have been averaged over two runs per subject and three subjects. It is apparent error variance consistently increased under higher vibration frequencies (6 and 10 Hz) for each task. For the first-order task and short-period task with stiff stick, the trends in input-correlated and total error follow each other, and in all cases uncorrelated error (remnant) shows a definite increase at 10 Hz vibration. As noted previously, subjects reported visual blurring at 10 Hz, which may account for some of the increase in remnant.

The effect of vibration on the dynamic response measures is somewhat different for each of the control tasks, as might be expected. For the first-order task (requiring no operator "lead"), there was little effect on gain crossover frequency (ω_c) or phase margin (φ_M); however, there was a large decrease in the phase crossover frequency (ω_u) at 10 Hz vibration. The first-order task allows phase crossover frequencies in the region of neuromuscular dynamics, and we have subjective reports that the 10 Hz vibration had a vaguely adverse effect on the dynamic properties of the neuromuscular system (i.e., tending to make motions more sluggish).

For the short-period task with spring stick the crossover frequencies remained quite stable while phase margin shows a slight increase under vibration. The relatively constant level of dynamic response behavior is consistent with the small changes observed in input-correlated errors.

As expected on the basis of prior research (Refs. 52, 53), use of the stiff stick control with the short-period dynamics has allowed higher crossover frequencies than with the spring stick, as shown in Fig. 17. However, the 6 and 10 Hz vibration conditions induced a decrease in ω_u which required the subjects to lower their gain (ω_c) as well, since some gain margin must be preserved. A rather dramatic increase in phase margin is noted also under 6 and 10 Hz vibration which is consistent with the large decrease in ω_c under the same conditions.

An analysis of variance was performed on the performance and dynamic response parameters in order to give quantitative estimates of the basic

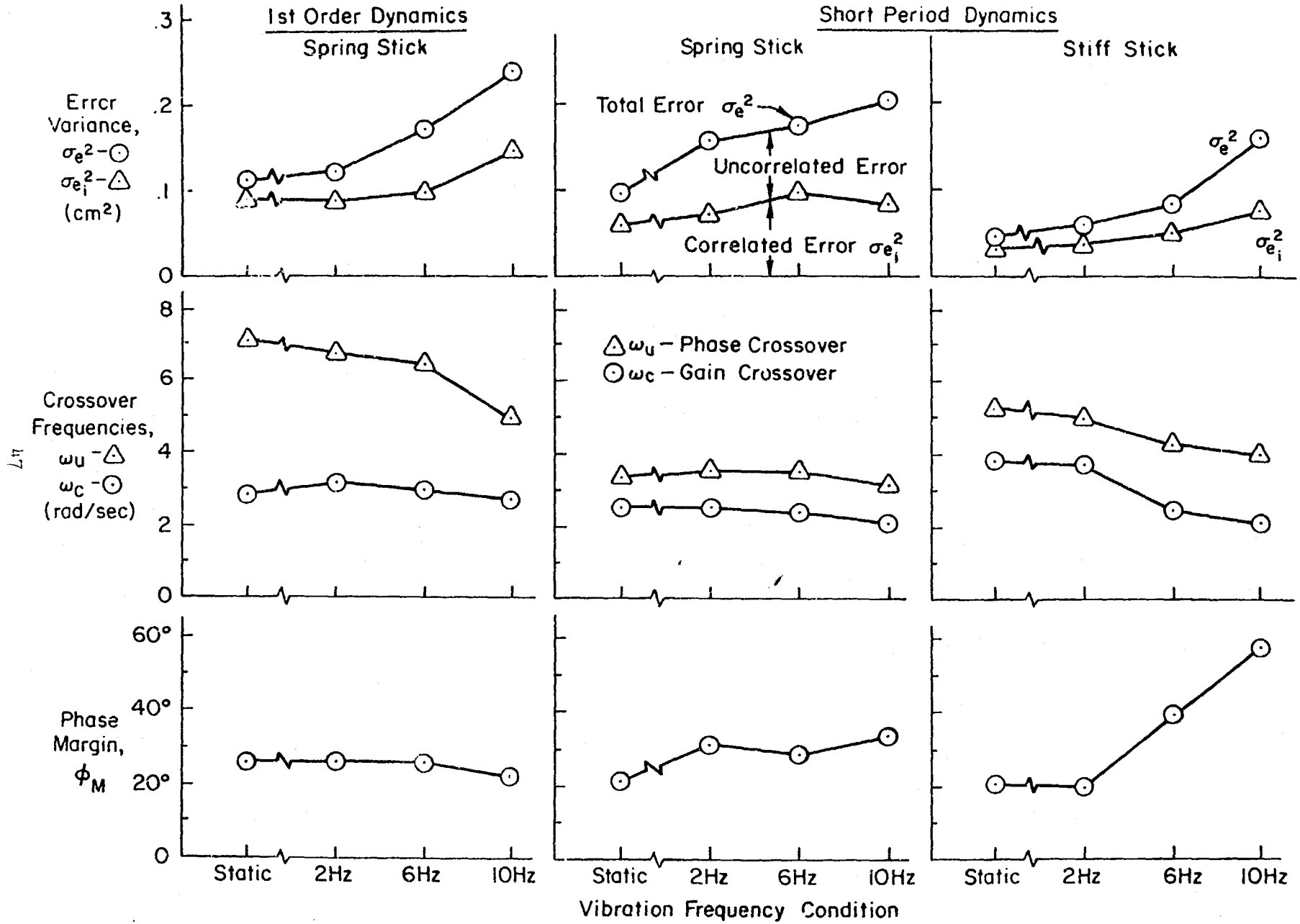

Figure 17. Performance and Dynamic Response Parameters Averaged Over Three Subjects in G_z Experiment

variability of the data and the importance of the various experimental treatments. The results are summarized in Table 5. A three-way model was used, with Subjects a random variable while Task and Vibration were considered fixed effects (Ref. 49). Representative response measures (ω_c, ω_u, and ϕ_M) and performance measures (σ_e^2, $\sigma_{e_i}^2$) were analyzed. Phase crossover frequency (ω_u) was the only significant task effect. Subject differences are significant for all parameters, and vibration frequency has a significant effect on all parameters except phase margin.

Some interesting relationships exist between the interaction effects given in Table 5. Task-by-Vibration interactions were significant for the dynamic response parameters and not for performance. This result is somewhat evident in Fig. 17. Further, the interactions involving subjects were quite significant in the case of performance parameters, while in only two of nine interactions was there a significant effect on dynamic response parameters (i.e., T × S for ω_c and S × V for ω_u). Based on these results it would appear that the subjects were more consistent in their dynamic response behavior than in overall performance, which also includes remnant as well as input correlated behavior.

D. DETAILED DESCRIBING FUNCTION RESULTS

In Fig. 18 detailed subject describing functions, $Y_p(\omega)$, are compared for the static and vibration conditions for each subject. On an overall basis the 10 Hz condition seems to have caused a more serious degradation in subject dynamic behavior than the more stressful resonant condition at 6 Hz. The subjective comment of Subject BB to the effect that there seemed to be "increased neuromuscular sluggishness" under 10 Hz vibration may be related to the generally poor performance at that condition. It is apparent that the 10 Hz vibration condition consistently incurs a phase penalty at the highest DFA measurement frequency (10.2 rad/sec) with the 6 Hz vibration condition causing a similar, albeit smaller, effect. There does not seem to be any consistent change with vibration in the operator's lead break frequency. Based on the $|Y_p|$ plots for the short-period dynamics, the lead break occurs at approximately 2 rad/sec (T_L = 0.5 sec) as expected.

TABLE 5

ANALYSIS OF VARIANCE SUMMARY FOR THE VERTICAL VIBRATION EXPERIMENT†

SOURCE OF VARIATION	DEGREES OF FREEDOM	PERFORMANCE PARAMETERS				DYNAMIC RESPONSE PARAMETERS					
		TOTAL ERROR VARIANCE, σ_e^2		CORRELATED ERROR VARIANCE, $\sigma_{e_i}^2$		GAIN CROSSOVER FREQUENCY, ω_c		PHASE CROSSOVER FREQUENCY, ω_u		PHASE MARGIN φ_M	
		MEAN SQUARES	F RATIO	MEAN SQUARES	F RATIO	MEAN SQUARES	F RATIO	MEAN SQUARES	F RATIO	MEAN SQUARES	F RATIO
Task (T)	2	0.04215	2.76 NS	0.01829	4.33 NS	2.079	5.96 NS	50.936	252.***	589.01	4.65 NS
Subjects (S)	2	0.10593	160.***	0.02081	69.4***	8.128	109.0***	10.972	116.***	497.08	4.97*
Vibration (V)	3	0.04370	7.9*	0.00632	7.44*	2.494	16.6**	5.342	11.9**	760.91	4.39 NS
T × S	4	0.01525	23.1***	0.00422	14.1***	0.349	4.7**	0.202	2.14 NS	126.58	1.27 NS
T × V	6	0.00177	0.39 NS	0.00110	1.08 NS	1.055	9.43***	1.161	6.11**	684.61	7.38
S × V	6	0.00549	8.33**	0.00085	2.8*	0.150	2.0 NS	0.448	4.73***	173.34	1.73 NS
T × S × V	12	0.00453	6.86***	0.00102	3.4**	0.112	1.5 NS	0.190	2.01 NS	92.94	0.92 NS
Residual	36	0.00066		0.00030		0.075		0.094		100.93	
RESIDUAL STANDARD DEVIATION		0.00256 cm^2		0.00173 cm^2		0.273 rad/sec		0.307 rad/sec		10.0 degrees	

Significance levels: * = 0.05, ** = 0.01, *** = 0.001.

†A three-way mixed effects model is employed where Subjects is a random variable, and Task and Vibration are fixed treatments.

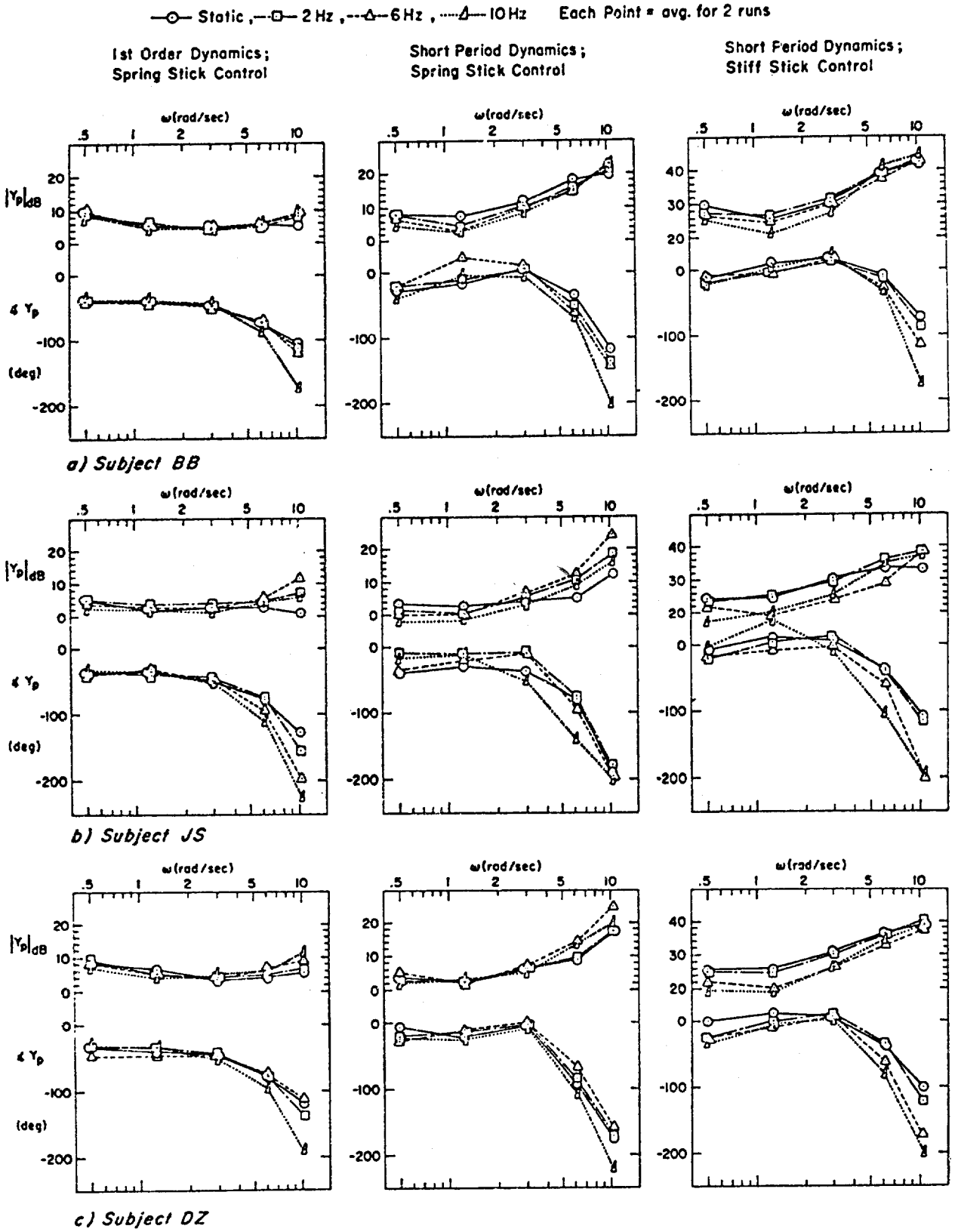

Figure 18. Human Operator Describing Functions (2 run averages) Compared Across Vibration Conditions in G_Z Experiment

Based on the describing function phase data of Fig. 18 and the related phase crossover frequency (ω_u) data in Fig. 17, we feel there is evidence that 10 Hz vibration has a significant effect on the neuromuscular system which is responsible for high-frequency phase lag properties. Guignard (Ref. 4) has speculated on direct effects of vibration on the neuromuscular system in the region of 10 Hz,* and the results obtained here would seem to support his suggestion.

E. DISCUSSION AND SUMMARY OF VERTICAL VIBRATION RESULTS

The subject population, although small, was reasonably well trained and exhibited biomechanical transmissibility properties under G_Z similar to previous measurements (Ref. 29). Appreciable vibration feedthrough to the control was measured, although it did not affect the displayed errors because of the filtering effect of the controlled element. Vibration control feedthrough was found to be significantly affected by control stick spring gradient, with a low spring gradient stick giving less feedthrough in general than a relatively stiff control stick. A model which accounts for vertical feedthrough effects in terms of biomechanical considerations is developed in Appendix A and summarized in Section VII.

Error performance was found to degrade with increasing vibration frequency, which is somewhat at variance with the results of Shoenberger (Ref. 31), who found a uniform performance decrement under sinusoidal G_Z vibration with little frequency sensitivity. The spring stick results are closest to Shoenberger's findings, and the stick gradient is similar although he used a side arm control rather than a joy stick. The stiff stick gave rather definite differential effects with frequency, and the various measurements obtained here have suggested underlying causes for

*From Ref. 4, p. 864, "It is occasionally suggested that, because the deep vibratory sense is mediated in the same end-organs as are concerned in the appreciation and regulation of posture, severe vibration might derange the action of muscles, and so degrade performance, by pre-empting the neuromuscular pathways involved in postural control. This would be most likely to occur at forcing frequencies around 10 Hz which coincide with the physiological tremor."

higher performance decrements at the high vibration frequencies. Increased operator phase lags (interpreted here as increased neuromuscular lags) are induced by high-frequency vibration, and cause an increase in correlated errors. Uncorrelated (remnant) errors also increased under high-frequency vibration. This effect corresponds with the reports of visual blurring at 10 Hz vibration which could induce increased perceptual remnant.* There may have been additional motor remnant as well, considering the adverse effect vibration had on the operator's dynamic response out in the frequency region of neuromuscular properties.

In summary, the effects of sinusoidal vertical vibration on manual control performance seem to be of a mainly involuntary nature. Control feedthrough can be largely accounted for by simple biomechanical models (see Section VII). Increased tracking errors seem to result from increased neuromuscular lags and greater remnant. Behavioral parameters which are under more voluntary control, such as human operator gain and lead (anticipation), do not seem to have been seriously affected by the vibration environment. It should be noted, however, that because of the small subject population and preliminary nature of the measurements used for this pilot study, the results require further verification before acceptance as general findings.

*As noted previously, sinusoidal vibration produces a relatively sharp-edged blur pattern, thus alleviating some of the expected difficulties in perception of errors under vibration. On the other hand, random vibrations at comparable frequencies will produce a fuzzy edge, which may be harder to perceive and align. These important differences may explain the absence, in these sinusoidal experiments, of large vibration-induced differences on the perceptual aspects of tracking; and they suggest possible significant differences that might be expected for a wideband random vibration case.

SECTION V

LATERAL VIBRATION EXPERIMENT RESULTS AND DISCUSSION

The lateral vibration experiment was more comprehensive and yielded more dramatic effects than the vertical study. Transmissibility, vibration control feedthrough, and tracking data are presented in this section, while models and further implications of the results are given in Section VII and Appendix B.

A. TRAINING

Performance measures obtained on each subject during the training and formal static trials are plotted in Fig. 19. In this experiment both the error and stick output variances were measured, along with the corresponding coherences or input-correlated power fraction. There are no significant learning trends apparent in Fig. 19. The improved error performance noted during the final formal session can be attributed to the improved dynamic response allowed with the stiff stick control. Subject JS seems to have the most consistent performance while SR shows the greatest variability. Finally, there seems to be no systematic performance differences between pre-vibration and post-vibration data for most of the subjects and controls. One interesting observation from Fig. 19 is that coherence in the error and stick signals is about equal, which is indicative of similar remnant power in both signals. Under certain vibration conditions there is a dramatic change in this situation, however, as will be shown in Section V-C.

Dynamic response parameters for the static training and formal sessions are compared in Fig. 20 for each subject. There are no strong learning trends. The increase in crossover frequency between the two formal sessions is due to the improved dynamic response allowed by the isometric stiff stick. Subject BC and JS appear to be the most consistent subjects, with SR showing the greatest variability, as was true with the performance measures. Also, most of the pre- and post-vibration dynamic parameters are the same, aside from some anomalous phase margin points for Subjects SR and DZ. (The latter had low margins in one case in which he later admitted trying a high gain technique.) Summarizing, it appears that all subjects were well trained for the lateral control tasks.

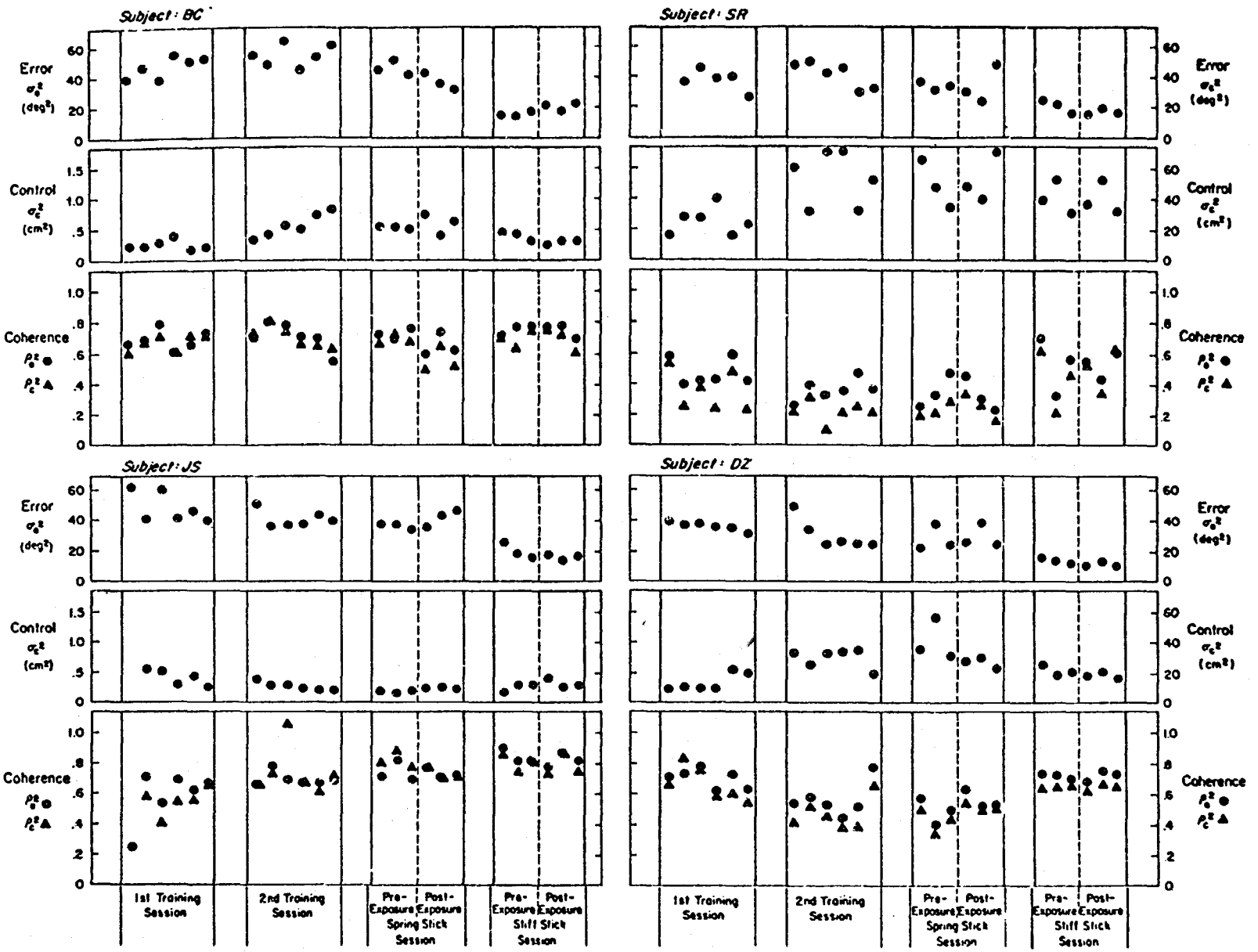

Figure 19. Comparison of Performance During Training and Formal Sessions of G_y Experiment [Note: Stiff stick variances set equivalent to spring stick variance for comparison. Physical scaling given by $\sigma_c^2(N^2) = (6.1\sigma_c)^2(cm^2)$]

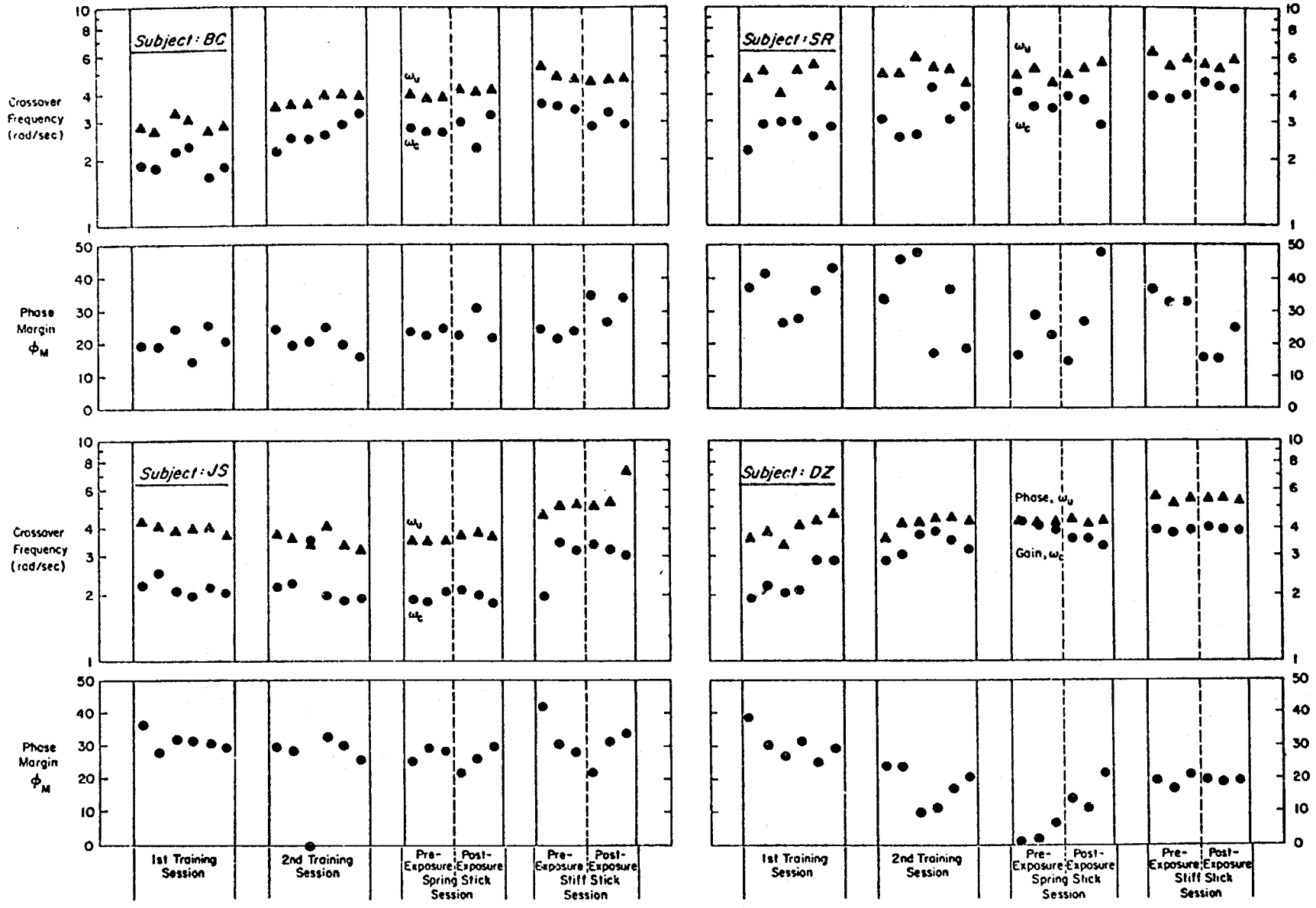

Figure 20. Comparison of Dynamic Response Measurements During Training and Formal Sessions of G_y Experiment

B. TRANSMISSIBILITY AND CONTROL FEEDTHROUGH

Lateral shoulder accelerations measured during the formal sessions are plotted in Fig. 21 for three of the test subjects. (Due to time limitations the fourth subject's data was not reduced.) Although the main trends are consistent, there is considerable variation in the detailed lateral transmissibility among the subjects during the two sessions. This coincides with experimenter observations as well as subjects' comments that various leg bracing and tensing techniques were attempted in order to "ride" the laterally-vibrating seat. These techniques may have varied between frequency conditions, even though the subjects were asked to maintain a consistent posture. Therefore, some variation in transmissibility and feedthrough measurements are expected which won't be accounted for in our average lateral dynamic response models developed in Appendix B.

Shoulder acceleration averaged over subjects is plotted in Fig. 22 for the two control sticks. In general, the maximum shoulder response occurs at low frequency (1-2 Hz) as opposed to the 5-6 Hz torso resonance typical for vertical vibration. This result is consistent with limited previous data (Refs. 6 and 40), as well as with our biomechanical response analysis of lateral torso motions described in Appendix B. At the higher frequencies shoulder response is slightly larger with the stiff stick because the shoulder is being driven by the rigid stick, as was hypothesized in the case of vertical vibration in Section IV-B.

Vibration feedthrough measured at the control stick output is plotted in Fig. 23. The stick output is multiplied by appropriate controlled element gains in order to make the stiff and spring stick results comparable.* There is considerable inter-subject variability with the stiff stick, while the spring stick gave more uniform behavior. The feedthrough for each stick averaged across subjects is compared in Fig. 24. The spring stick gives much greater attenuation of high-frequency feedthrough than the stiff stick. This effect is due to the difference in feedthrough dynamics between the two sticks and is discussed in Section VII. The spring stick also allowed much greater feedthrough at low vibration frequencies although the stick sensitivities were selected subjectively, which makes absolute comparison somewhat arbitrary.

*See footnote on page 43 regarding stick output scaling.

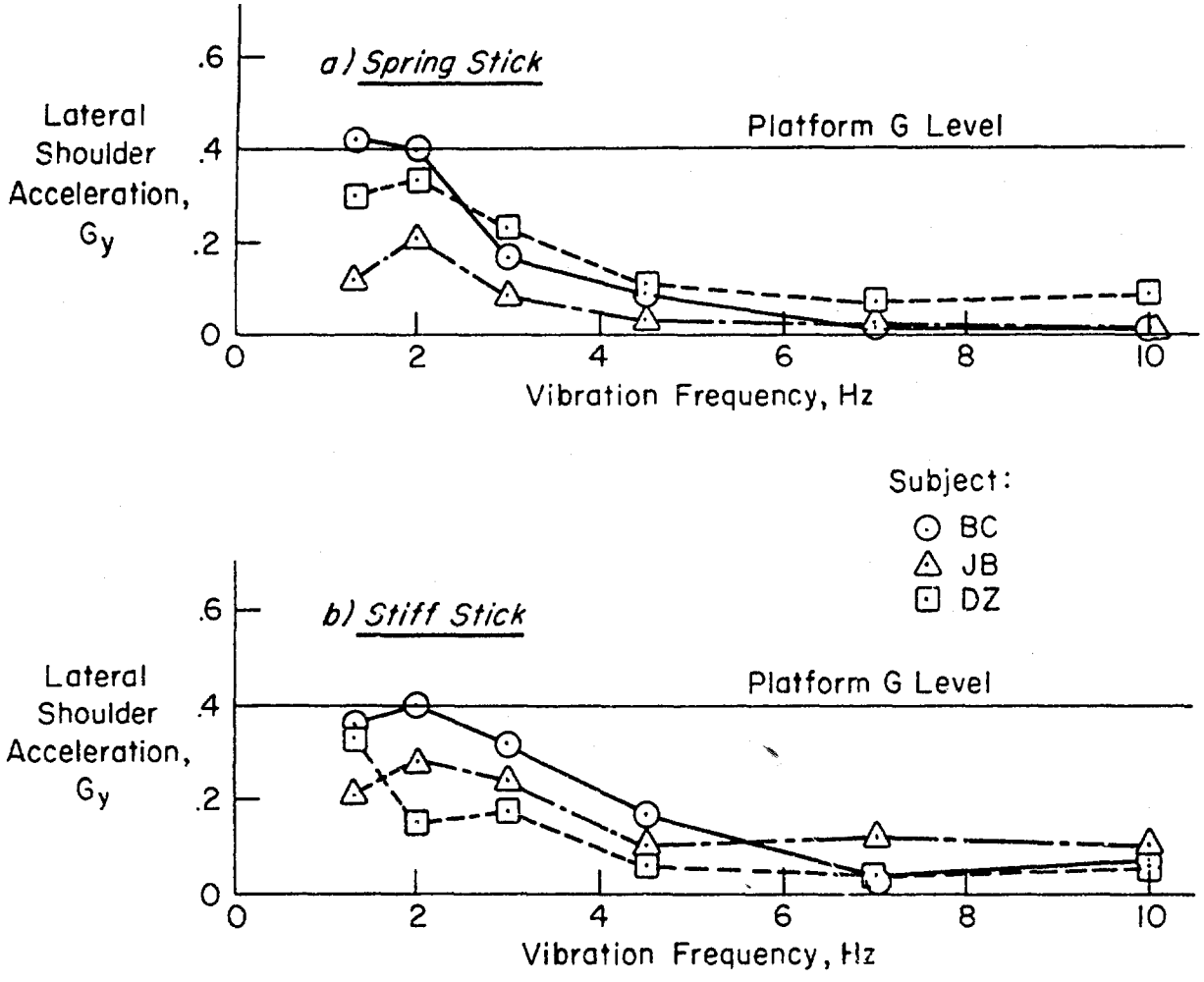

Figure 21. Lateral Shoulder Acceleration Measured During Formal Session Tracking Runs

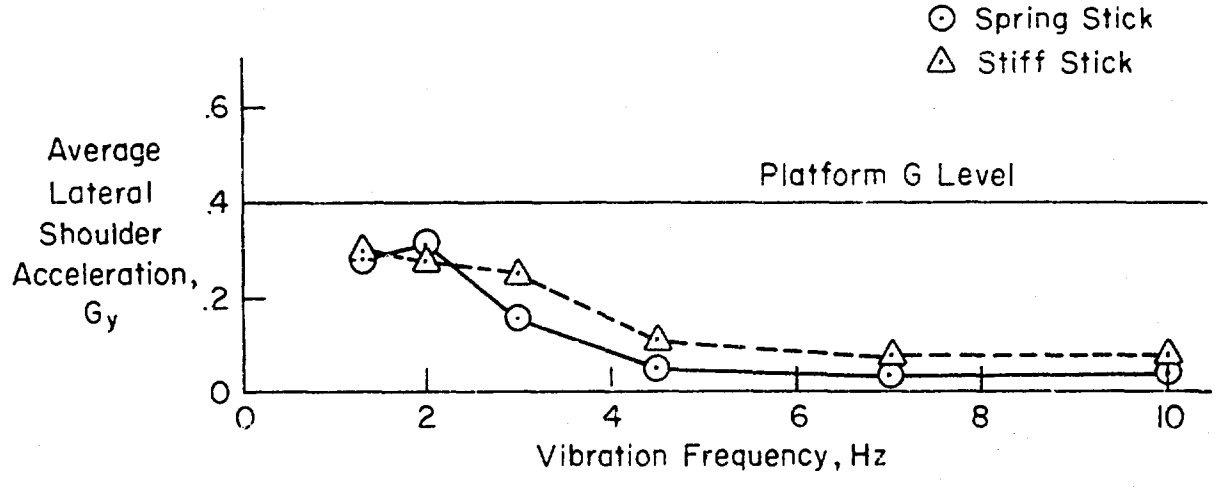

Figure 22. Shoulder Acceleration Averaged Over Subjects

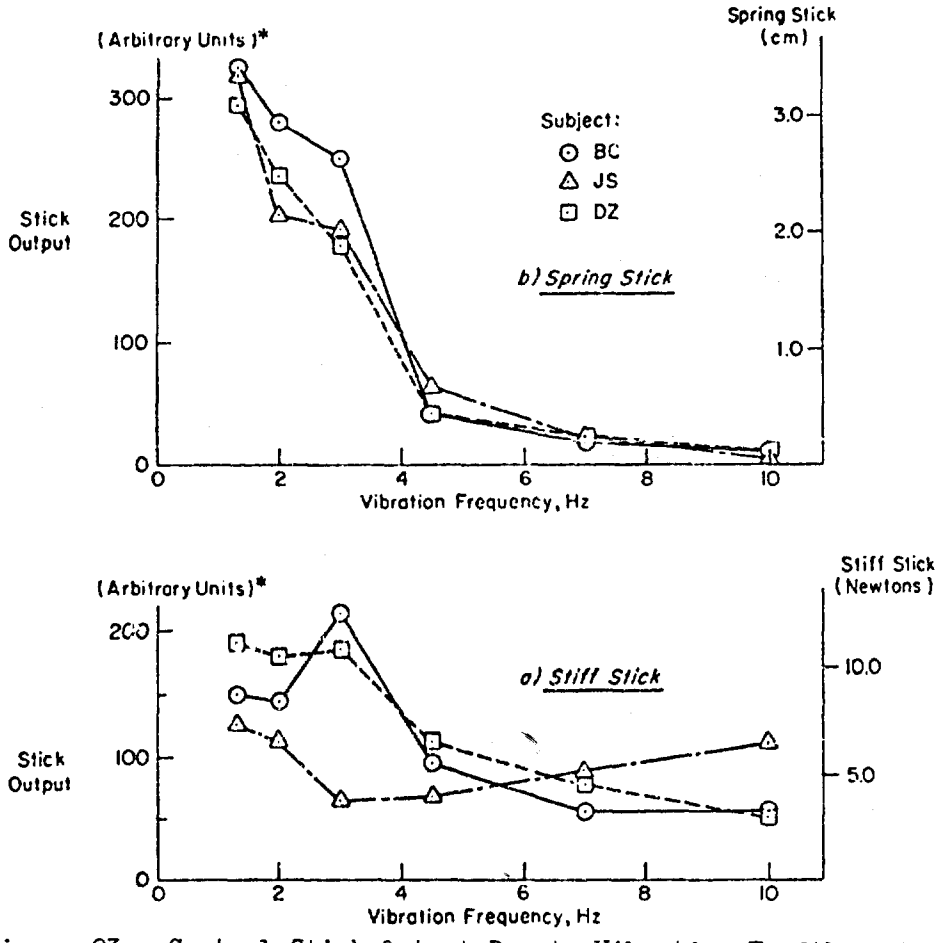

Figure 23. Control Stick Output Due to Vibration Feedthrough

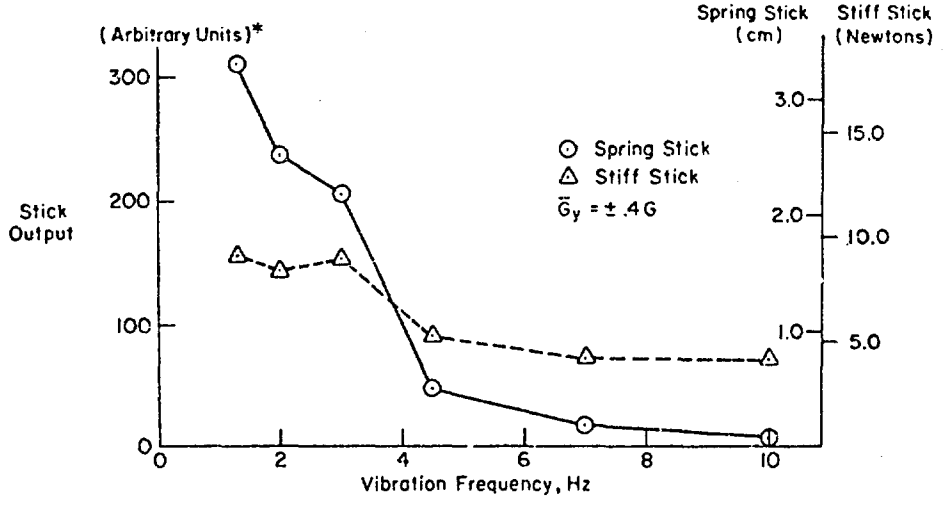

* See footnote on page 43 for explanation of stick output scaling

Figure 24. Stick Vibration Feedthrough Averaged Over Subjects

C. PERFORMANCE AND DYNAMIC RESPONSE EFFECTS

1. Performance Parameters

In the lateral study we were able to make the complete set of measurements necessary to partition performance into input-correlated, vibration-correlated, and total components, as described in Eq. 3 of Section II. The error performance data are presented in Figs. 25a (which shows each individual's data) and 25b (which shows the four-subject ensemble averages).* Although detailed differences among subjects do exist, comparison among the individual plots for each subject shows that the ensemble average plots presented in this section are indeed typical of any subject's dominant trends. Consequently, we will discuss only the features of the ensemble averages as representing the main effects of vibration and type of control stick.

Compared with the "static" points shown in Fig. 25b, it is apparent that low-frequency lateral vibration caused an order-of-magnitude increase in total error variance with the spring stick, which is consistent with the results obtained by Shoenberger (Ref. 31). The effects with the stiff stick were much smaller. The vibration-correlated feedthrough component is not a big contributor to the total roll control error, although its effect in the control feedthrough is quite large, as will be shown.

Tracking-input-correlated errors stay relatively constant with the stiff stick; and, while they increase at low frequencies for the spring stick, they do not account for the majority of tracking error. At low frequencies the lion's share of error is remnant and therefore arises from vibration-induced "noise" effects associated with the operator.

In Figs. 26a and 26b the various components of control stick output variance are shown. From the averaged data in Fig. 26b it is apparent that control variance is dominated by vibration feedthrough power at low vibration frequencies. Feedthrough attenuates much faster with increasing vibration

*Because of the large dynamic range of the components, the data in Figs. 25 and 26 are presented on log scales. This tends to suppress the relative dominance of the remnant component.

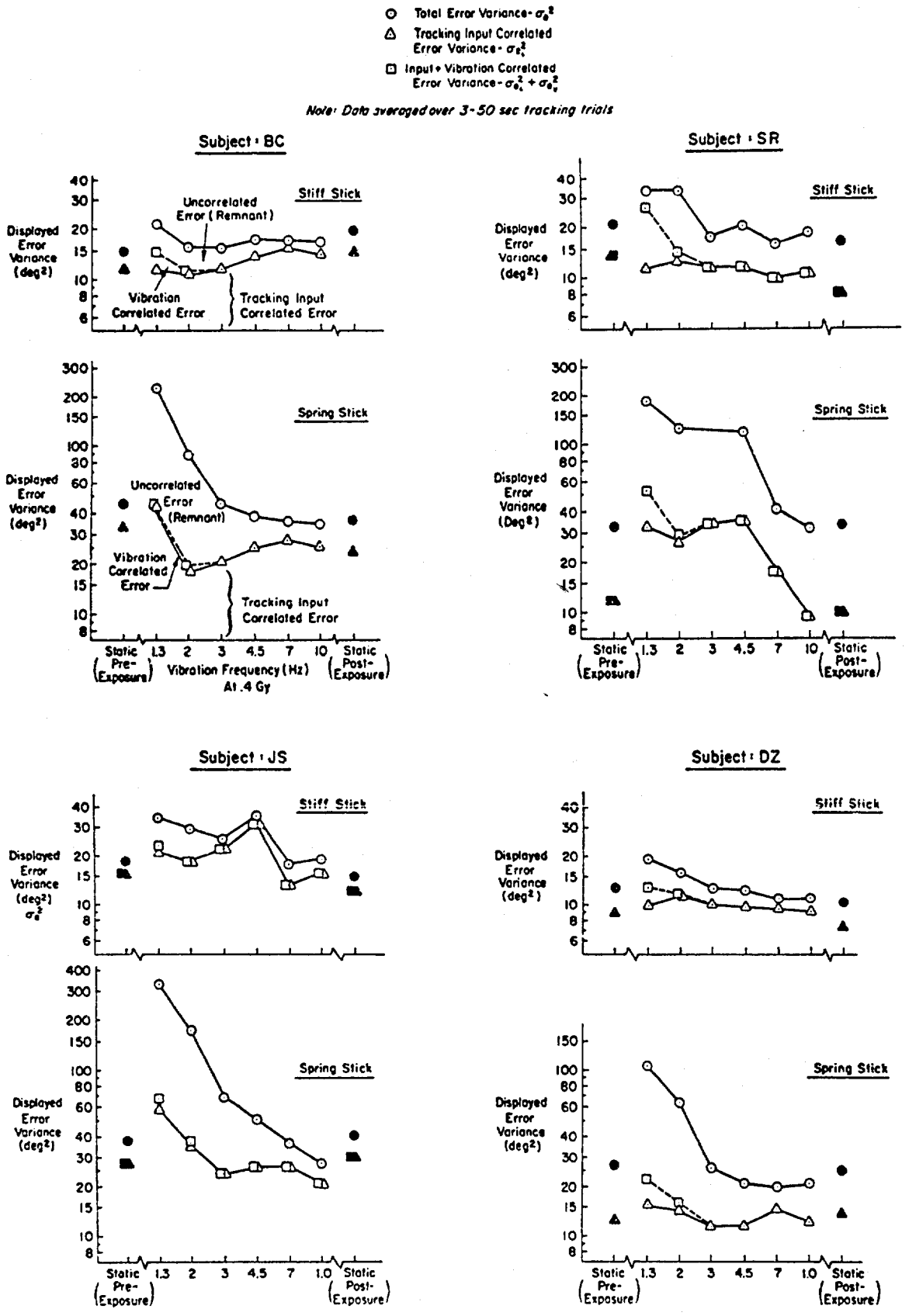

Figure 29a. Partitioned Error Variances for Each Subject

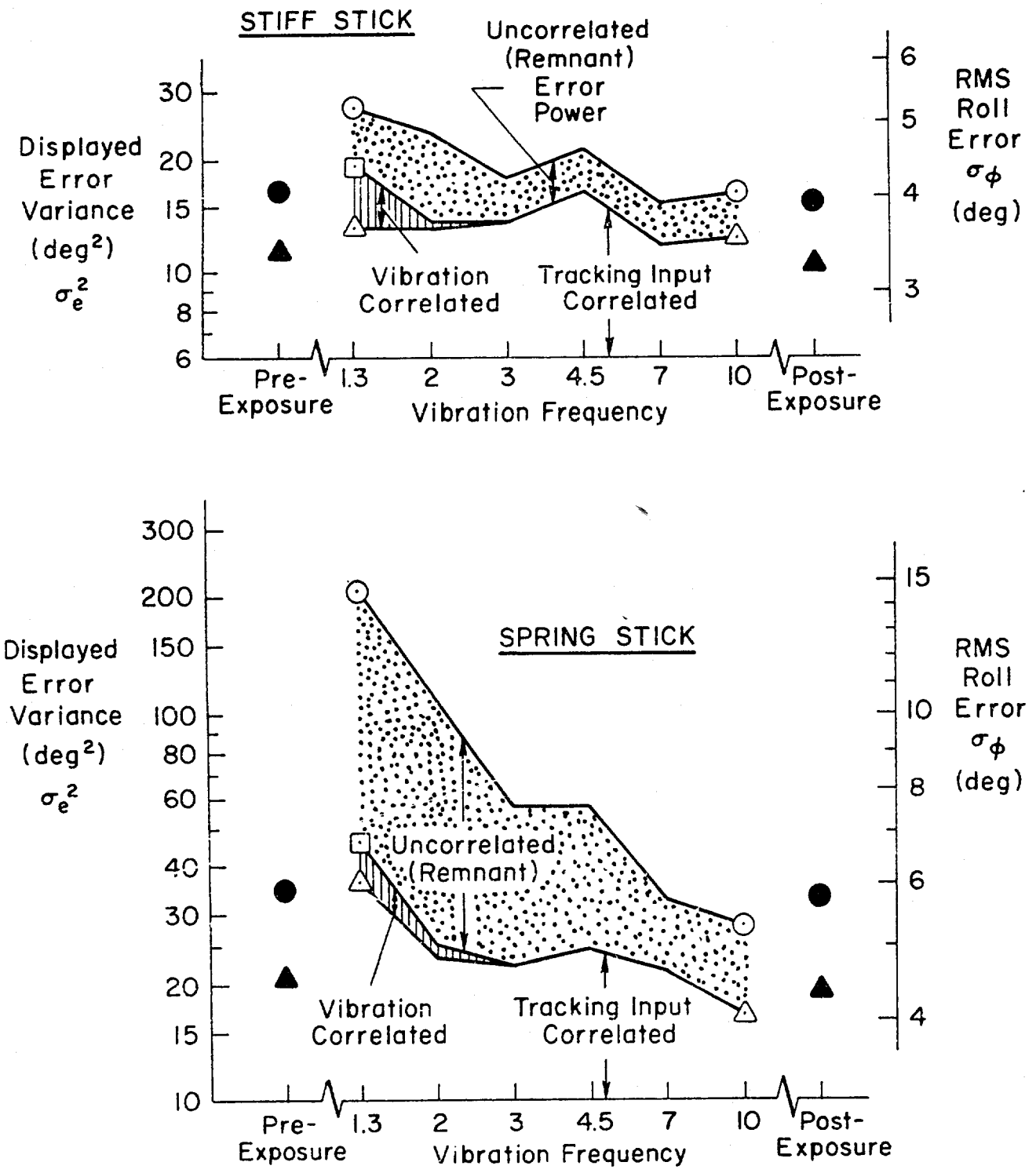

Figure 25b. Displayed Error Variance Components Averaged Over Subjects

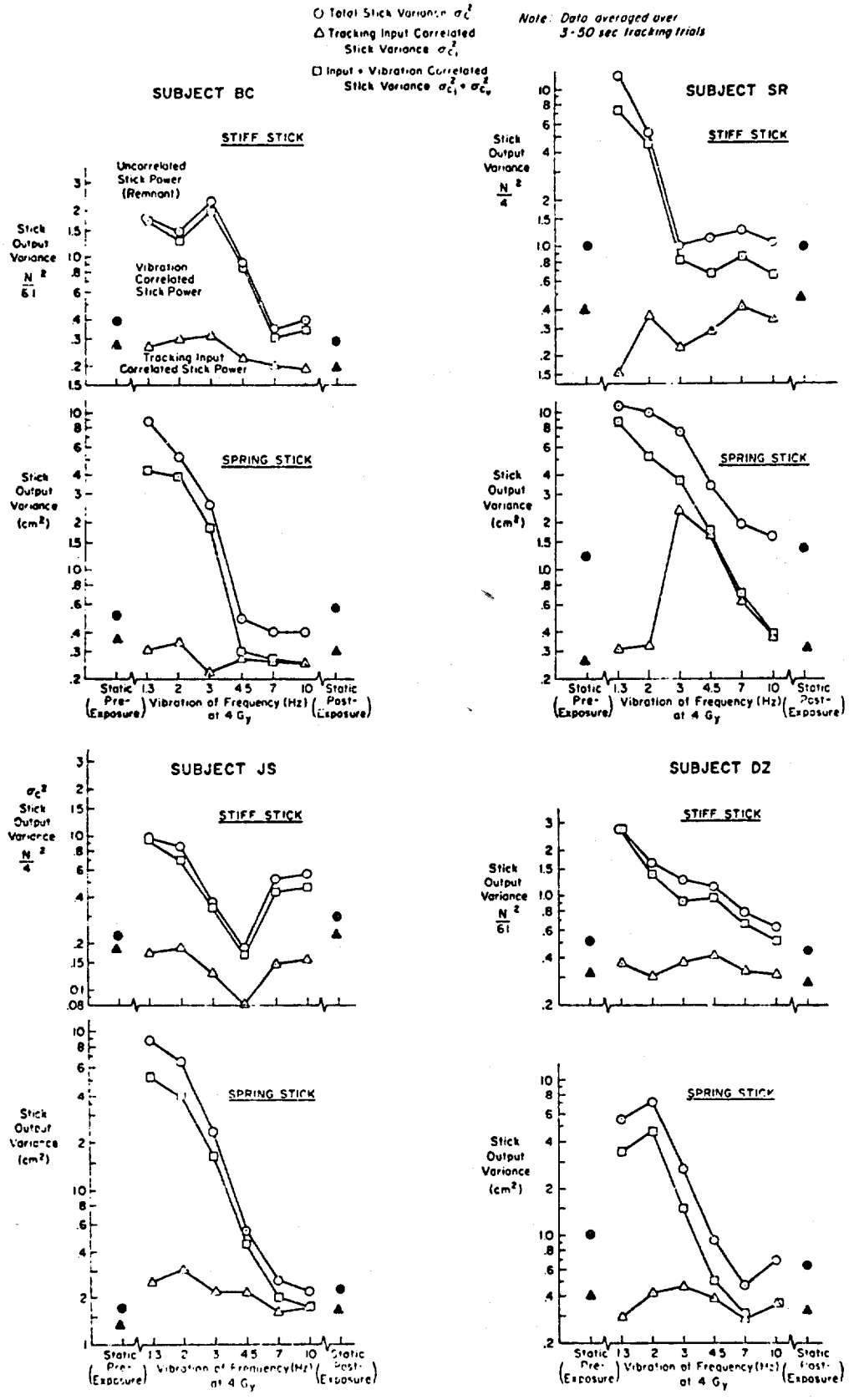

Figure 26a. Partitioned Control Variances for Each Subject

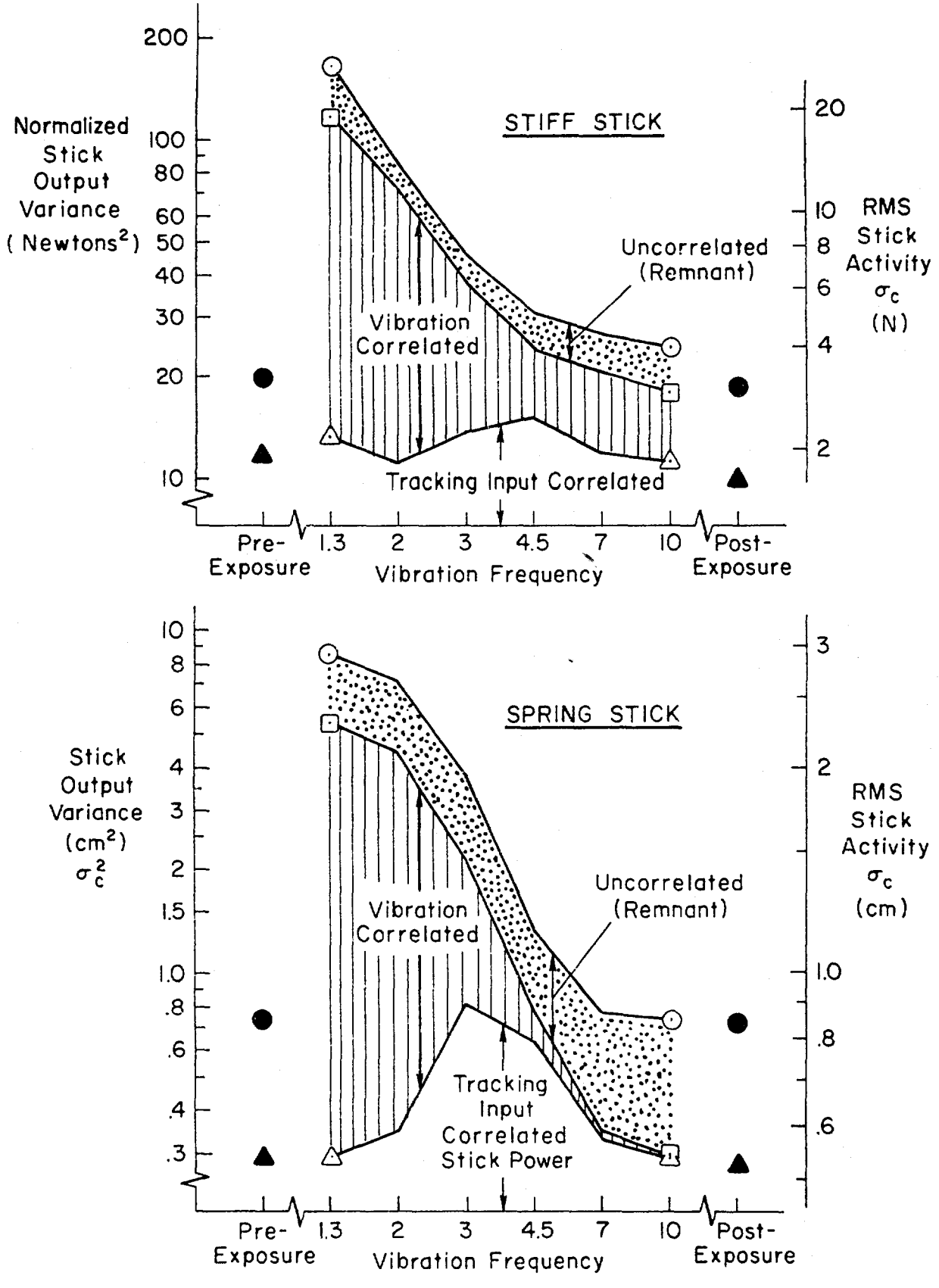

Figure 26b. Stick Output Variance Components Averaged Over Subjects

frequency in the case of the spring stick. This important result is consistent with the direct feedthrough measurements shown previously in Fig. 24, and it is properly accounted for by the lateral feedthrough model developed in Appendix B and summarized in Section VII. Remnant comprises only a small fraction of total control power at low vibration frequencies, in contrast to the error data.

The difference in relative importance of vibration feedthrough at the error versus control points is due to the attenuation effect of the controlled element, Y_c, in the range of the vibration frequencies. As discussed in Appendix B, the feedthrough appears directly at the control point due to biomechanical processes; in the error signal, however, the vibration-induced power is attenuated by the squared magnitude of the controlled element, which is considerable at the higher vibration frequencies (where $\omega >> 1$), as shown below:

Controlled Element: $$Y_c = \frac{K_c}{s(s+3)}$$

Variance Attenuation Factor: $$\left|\frac{Y_c}{K_c}\right|^2(\omega) = \frac{1}{\omega^2(\omega^2+9)}$$

Frequency:	Ref				
f_v =	(0.16)	1.3	3	10	(Hz)
ω_v =	1.0	8.1	18.8	62.8	(rad/sec)
Attenuation:					
$\lvert Y_c/K_c \rvert^2$ =	1×10^{-1}	2×10^{-4}	8×10^{-6}	6×10^{-8}	

In contrast to the vibration feedthrough effects, the operator's remnant dominates tracking error at low frequencies but is a small fraction of the control power. This effect has a possible explanation in terms of a low-frequency "motor noise" process appearing at the operator's output. In terms of the controlled element attenuation at very low frequencies, as $\omega \to 0$, $|Y_c| \to \infty$, so that low-frequency noise at the control stick point will be considerably amplified in the error signal. Subject impressions seem to

agree with the above assertion. One subject specifically commented that he was so unsure of the null position of the spring stick control under low-frequency vibration that he actually glanced at the control stick occasionally in order to make up for the lack of proprioceptive feedback on control position. The remaining subjects indicated increased uncertainty in spring stick control position due to large control motion induced by low-frequency vibration. Apparently, this vibration-induced uncertainty in control position manifests itself as low-frequency motor noise. On the other hand, because the stiff stick is firmly centered, position motor remnant is eliminated, which results in much better tracking performance. Further investigation of the source and variation of vibration-induced remnant is of great importance.

2. Dynamic Response Parameters

The dynamic response results are shown in Figs. 27a and 27b. There is remarkably little variation over the range of vibration conditions, considering the large performance effects noted earlier. There were significant individual differences in dynamic response behavior between the subjects, however, whose individual data are compared in Fig. 27a. In general, the variability is greatest with the rather loose spring stick at the lower frequencies of vibration.

Considering now the averaged trends shown in Fig. 27b, we find that during vibration with the stiff stick control a consistent increase in phase margin (Φ_M) is evident. For the spring stick, phase margin seems to be highest at the low vibration frequencies, which is consistent with trying to cope with the increased remnant observed at low vibration frequencies. These changes are small, however, in comparison to the changes in performance noted previously. This further substantiates the finding here that lateral vibration has little effect on the human operator's input-correlated behavior (i.e., the visual-motor describing function).

3. Analysis of Variance

An Analysis of Variance was performed on the performance and dynamic response parameters in order to quantitatively assess the reliability and relative magnitude of the various effects. A two-way mixed effects model,

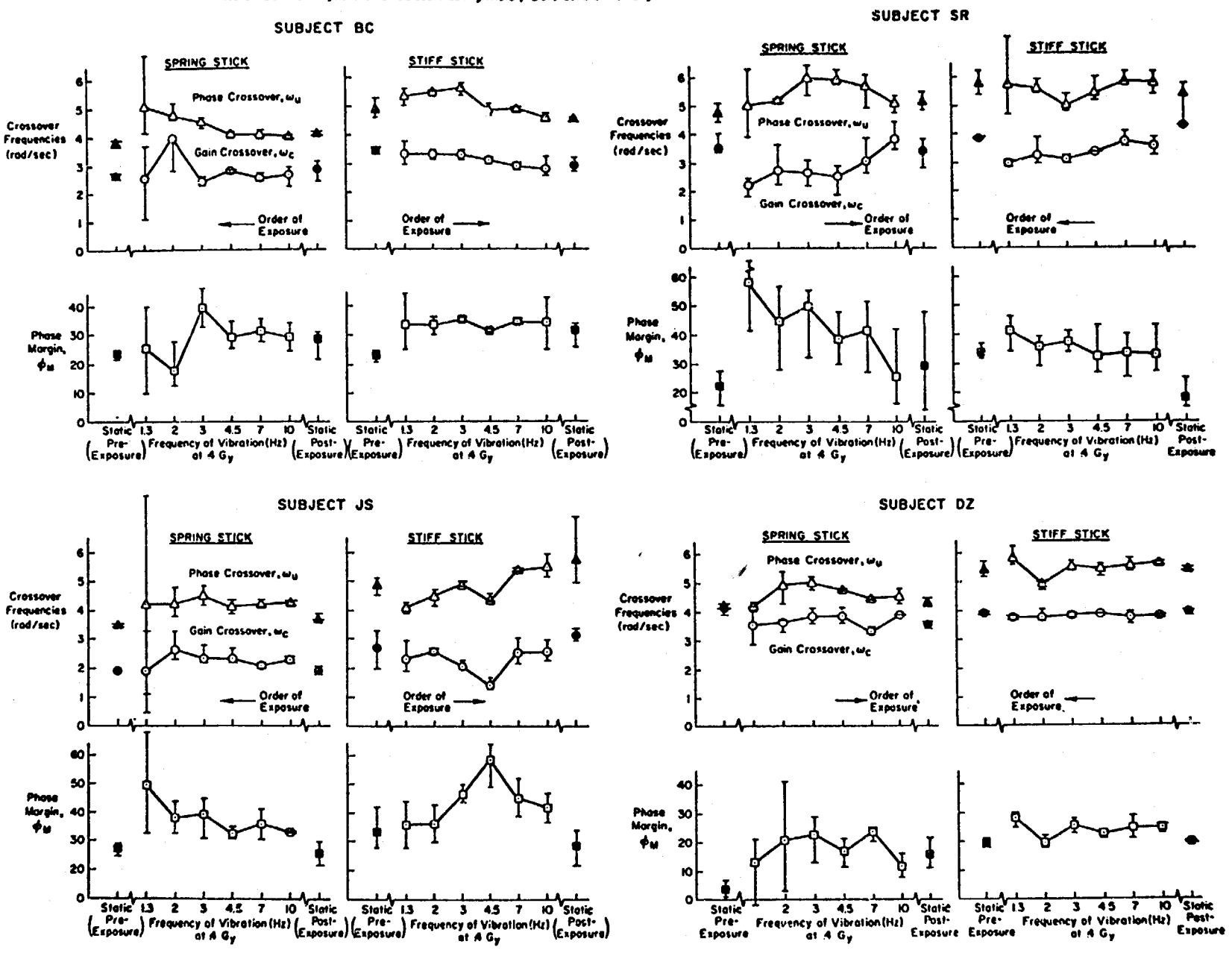

Figure 27a. Dynamic Response Measurements for Each Subject

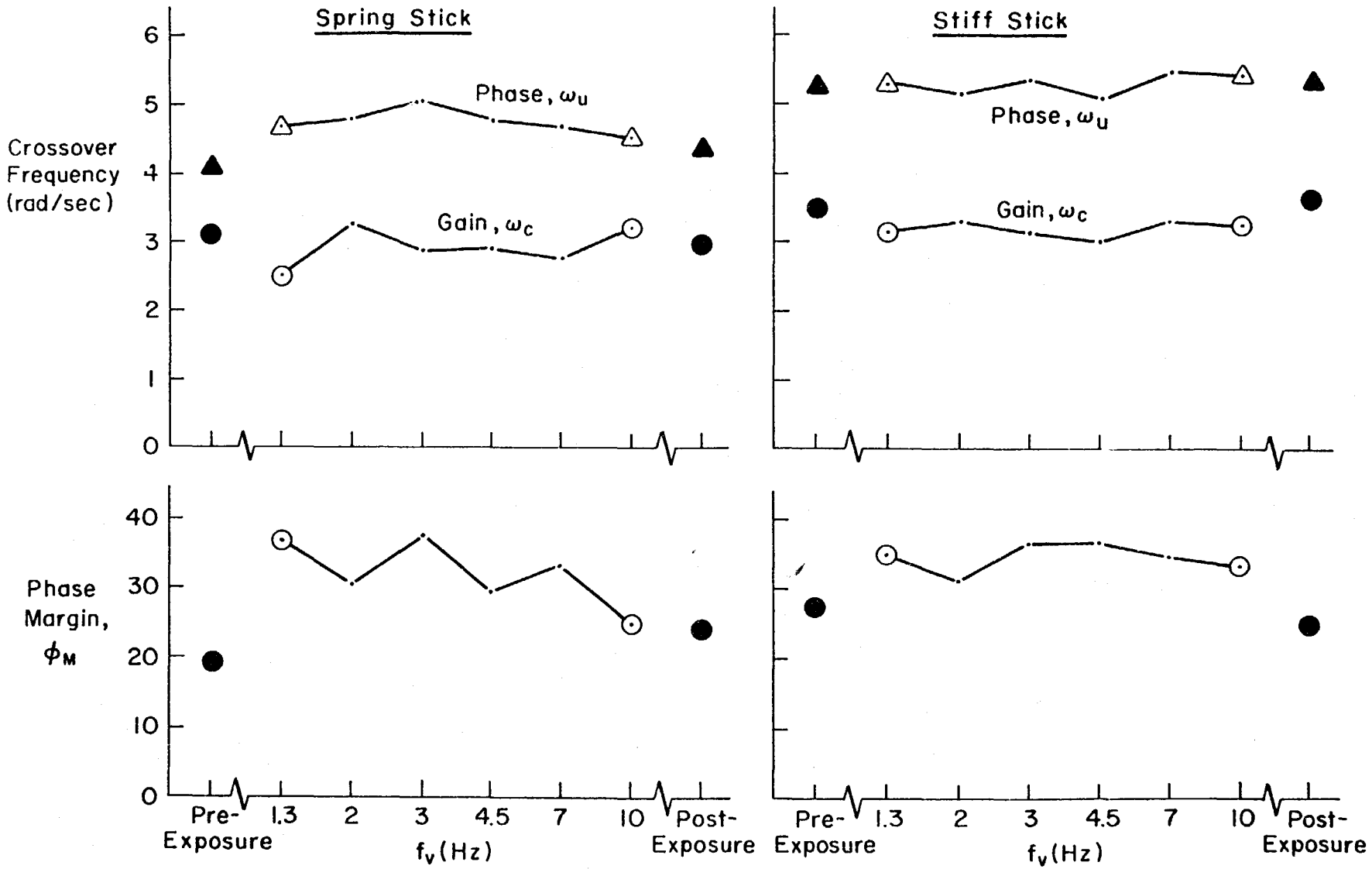

Figure 27b. Dynamic Response Parameters Averaged Over Subjects in G_y Experiment

with subjects considered a random variable, was used (Ref. 49). Separate analyses were performed for the two control sticks because of the obviously different trends and levels versus vibration frequency noted in the data plots previously discussed. The ANOV results (summarized in Table 6) show that vibration frequency (V) produced large and very significant mean-square contributions to the total variances in the total error and control measures (σ_e^2, σ_c^2) but resulted in non-significant effects in most of the other measures. This means that the dynamic response behavior and the resulting input-correlated measures, $\sigma_{e_i}^2$ and $\sigma_{c_i}^2$, were not as significantly affected by vibration as the totals. This is consistent with the main lateral vibration effects occurring in control feedthrough and remnant components as discussed previously.

Subject differences are significant in all cases except for total spring stick control power (σ_c^2). In most cases differences between subjects represent the largest source of variation; however, for the spring stick total error and control power (σ_e^2 and σ_c^2) vibration represents the largest source of variance.

Most of the highly significant interactions (S × V) between subject and vibration frequency, especially for the stiff stick case, are due to the very low repeat-trial residuals which accentuate any difference. Remembering that the data on which the residual variances are based were three consecutive trials, rather than three separate test replications, the question remains as to the true session-to-session repeatability of a given subject's dynamic response and performance measures.

Comparison between the two analyses for the two sticks shows some interesting results. The stiff stick data had considerably lower residual variability, almost an order of magnitude lower in the performance measures but only about a factor of one-half for the dynamic response parameters. This again reflects the dominance of the remnant (noise) effects on the total measures.

TABLE 6

ANALYSIS OF VARIANCE SUMMARY FOR THE LATERAL VIBRATION EXPERIMENT†

a. SPRING STICK DATA		PERFORMANCE PARAMETERS								DYNAMIC RESPONSE PARAMETERS					
		σ_e^2		$\sigma_{e_i}^2$		σ_c^2		$\sigma_{c_i}^2$		ω_c		ω_u		φ_M	
SOURCE OF VARIATION	DEGREES OF FREEDOM	MEAN SQUARES	F RATIO	MEAN SQUARES	F RATIO	MEAN SQUARES	F RATIO	MEAN SQUARES	F RATIO	MEAN SQUARES	F RATIO	MEAN SQUARES	F RATIO	MEAN SQUARES	F RATIO
Subjects (S)	3	14351.2	42.6***	1410.1	11.6***	38.08	1.68NS	1.537	4.68**	9.428	35.5***	7.428	11.3**	2481.5	24.8***
Vibration (V)	7	47552.3	11.9***	436.6	2.52*	117.83	4.38**	0.484	1.47NS	0.673	1.38NS	0.945	1.44NS	506.7	3.94**
SXV	21	3996.1	11.9***	173.0	1.43NS	26.86	1.18NS	0.464	1.42NS	0.489	1.84*	0.277	0.422NS	128.6	1.29NS
Residual (R)	64	337.6		121.3		22.73		0.328		0.266		0.656		100.7	
Residual Standard Deviation		18.3 (deg)^2		11.0 (deg)^2		4.76 (cm)^2		0.572 (cm)^2		0.515 rad/sec		0.81 rad/sec		10.0 deg	

b. STIFF STICK DATA		PERFORMANCE PARAMETERS								DYNAMIC RESPONSE PARAMETERS					
		σ_e^2		$\sigma_{e_i}^2$		σ_c^2		$\sigma_{c_i}^2$		ω_c		ω_u		φ_M	
SOURCE OF VARIATION	DEGREES OF FREEDOM	MEAN SQUARES	F RATIO	MEAN SQUARES	F RATIO	MEAN SQUARES	F RATIO	MEAN SQUARES	F RATIO	MEAN SQUARES	F RATIO	MEAN SQUARES	F RATIO	MEAN SQUARES	F RATIO
Subjects (S)	3	638.8	58.6 ***	416.1	66.2 ***	29.98	95.2***	0.167	52.8 ***	8.597	124.8 ***	2.223	12.4 ***	1328.4	46.1***
Vibration (V)	7	228.0	4.16***	39.4	1.22NS	23.13	2.19*	0.006	0.36NS	0.501	1.55NS	0.221	0.373NS	222.5	2.6*
SXV	21	54.7	5.02***	32.2	5.12***	10.57	33.6***	0.015	4.82***	0.324	4.70***	0.594	3.32***	85.6	2.97**
Residual (R)	64	10.9		6.3		0.32		0.003		0.069		0.179		28.8	
Residual Standard Deviation		3.29 (deg)^2		2.50 (deg)^2		0.561 $(\frac{\text{Newtons}}{6.1})^2$		0.0561 $(\frac{\text{Newtons}}{6.1})^2$		0.26 rad/sec		0.423 rad/sec		5.26 deg	

†The ANOV is a two-way mixed effects model (with subjects as random samples, vibration frequencies as fixed treatments, and three replications per cell). The F ratio for "Subjects" effects is MS_S/MS_R, while the F ratio for "Vibration" effects is MS_V/MS_{SV}.

Significance Level: * = 0.05; ** = 0.01; *** = 0.001.

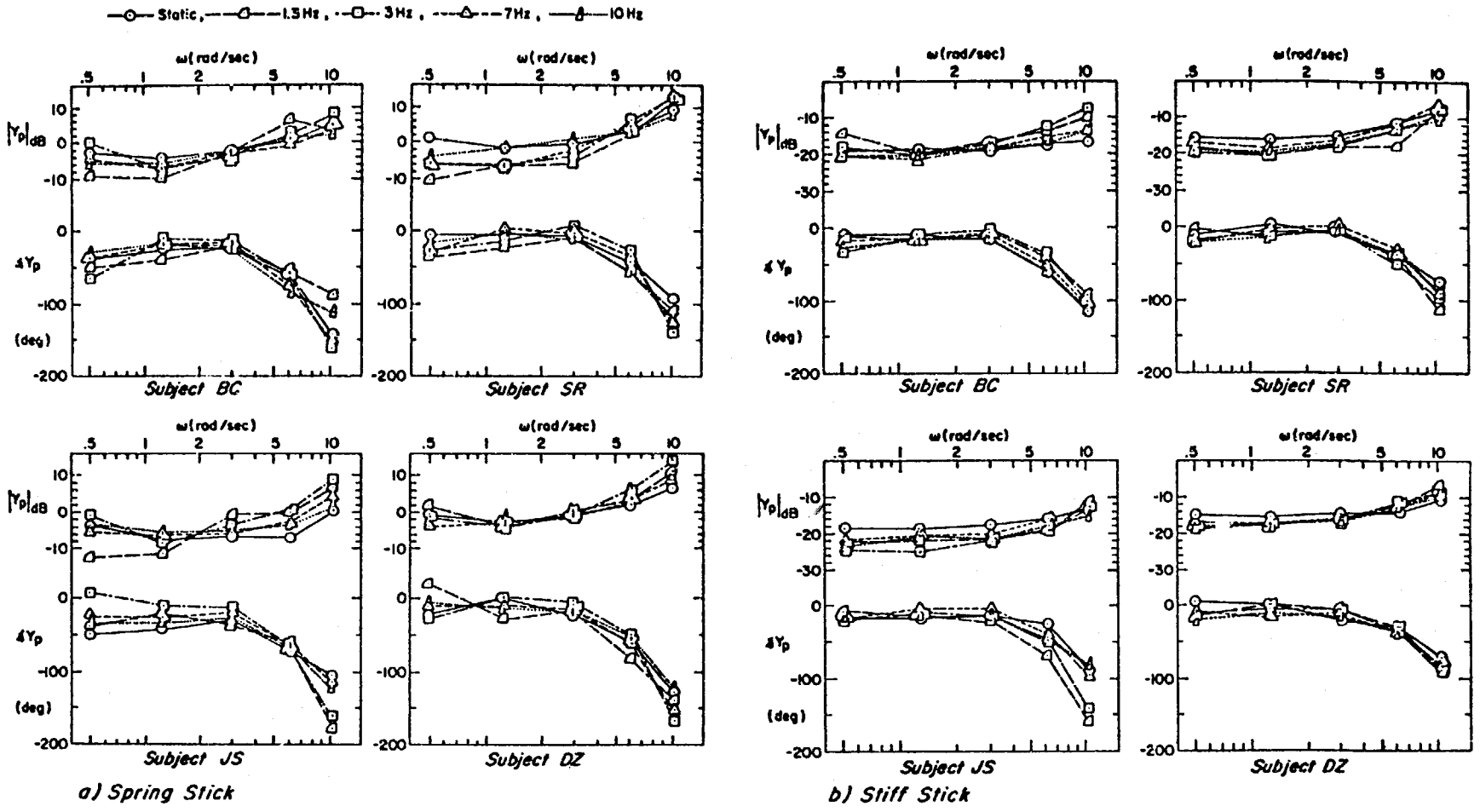

Figure 28. Human Operator Describing Functions Compared Across Vibration Conditions in G_y Experiment

4. Detailed Describing Functions

In Fig. 28 describing functions for each subject, averaged over 3 consecutive runs, are shown for static and four vibration frequency conditions. The stiff stick data seem to be most consistent, which ties in with the dynamic response parameters previously discussed. Despite large effects on the total performance and control measures, lateral vibration seems to have remarkably little effect on the detailed control loop behavior, as measured by the describing functions. Few consistent effects can be discerned, except for a tendency for 3 of the subjects to use less gain under vibration with the stiff stick. The transmissibility results (given previously) showed that high-frequency lateral vibration is not transmitted to the shoulder so that the increased neuromuscular lags found for vertical vibration would not be expected here, and the describing functions bear this out.

D. DISCUSSION AND SUMMARY OF LATERAL VIBRATION RESULTS

The major findings of the lateral experiment were the dramatic increase in tracking error and control activity under low-frequency lateral vibration, compared with the pre- and post-vibration "static" cases.

- The increase in tracking error was most pronounced for the light spring gradient control stick and was primarily due to vibration induced pilot remnant.
- The increased control activity occurred with both the spring and stiff sticks and resulted primarily from biomechanical vibration feedthrough effects.
- Changes in dynamic response behavior were minor with a small, but significant, increase in the control loop stability margin under vibration.

The error performance results obtained here for the rather loose spring stick are similar to Shoenberger's (Ref. 31), while the stiff stick data show much smaller effects. This emphasizes the task-specific nature of vibration effects and the need for using multi-factor measurements and models to provide a basic understanding of the various man-machine processes involved. Such an approach permits comparisons among research studies and extrapolation to new situations.

SECTION VI

FORE-AFT VIBRATION EXPERIMENT RESULTS AND DISCUSSION

The fore-aft (G_X) vibration experiment was conducted with experimental conditions, procedures, and measurements similar to those used in the lateral study, as explained in Section III. This allowed efficiencies in planning and preparation for the experiment, and gave results that can be compared with those obtained under G_y vibration.

A. TRAINING

Performance and dynamic response results obtained during training and formal session static conditions are compared in Figs. 29 and 30, respectively. As with the previous studies there are no strong learning trends apparent. The stiff stick has allowed better performance, which is attributed to the better dynamic response properties allowed by this control stick rather than any learning effect, per se.

Two of the subjects (JS, BB) had participated in the prior vertical vibration experiment and their averaged formal session data at that time is included via tagged symbols in Figs. 29 and 30. Comparison among the prior and current tests shows good agreement in general, and implies the achievement of stable performance levels and good test-retest reliability.

B. TRANSMISSIBILITY

Body motions induced by the fore-aft vibration were quite complex, including flexing of the spine and head nodding, which resulted in significant vertical motions at the shoulder and head. Fore-aft and vertical acceleration measurements are given in Fig. 31. Significant body accelerations (both horizontal and vertical) were measured throughout the vibration frequency range (1.3-10 Hz). Some evidence exists of the vertical resonance peak near 4-6 Hz, seen in the prior G_Z experiment. The vertical torso and head accelerations are of the same level as fore-aft levels. The vertical head motion measured with the mouth appliance (see Section III)

includes a component due to head nodding, and this is close to the motion experienced by the eyes. The vertical eye motion relative to the display led to visual blurring at higher motion frequencies, as indicated by subject comments.

It is apparent from Fig. 31 that there was considerably greater variability in biomechanical response among subjects in this G_x case than in the G_z and G_y experiments, which probably led to the significant inter-subject performance variability noted in the next section. Nevertheless, a given subject tends to rank high or low at each location measured, especially in the range beyond 3 Hz. It is difficult to deduce a "typical" or average transmissibility for fore-aft vibration from the results in Fig. 31. Observations during the experiment indicated a variety of subtle and complex postural differences between subjects (even though they wore shoulder and lap belts tightened according to identical instructions), and this led to the large differences in biodynamic responses. Postural effects appear to be inherently difficult to control in fore-aft vibration situations. Because there is reason to expect the same idiosyncratic adjustments and postural variations in operational situations, generalizing G_x effects may be intrinsically risky.

Another factor to be considered is anthropometric variability between subjects that may lead to biodynamic vibrational nodes (nulls) and antinodes (peaks) at different locations on different people under the same experimental setup. This might explain some of the wide differences in chest and shoulder motions at 4.5 Hz. (Note that a given subject tends to be high or low in most cases.)

C. PERFORMANCE AND DYNAMIC RESPONSE

1. Performance

The performance data in Fig. 32a show considerable variation among the four subjects, reflecting the biodynamic effects noted in the transmissibility data. The stiff stick error data appear to exhibit the least idiosyncratic differences, followed by the spring stick error data. The control stick variances show the greatest variability between subjects.

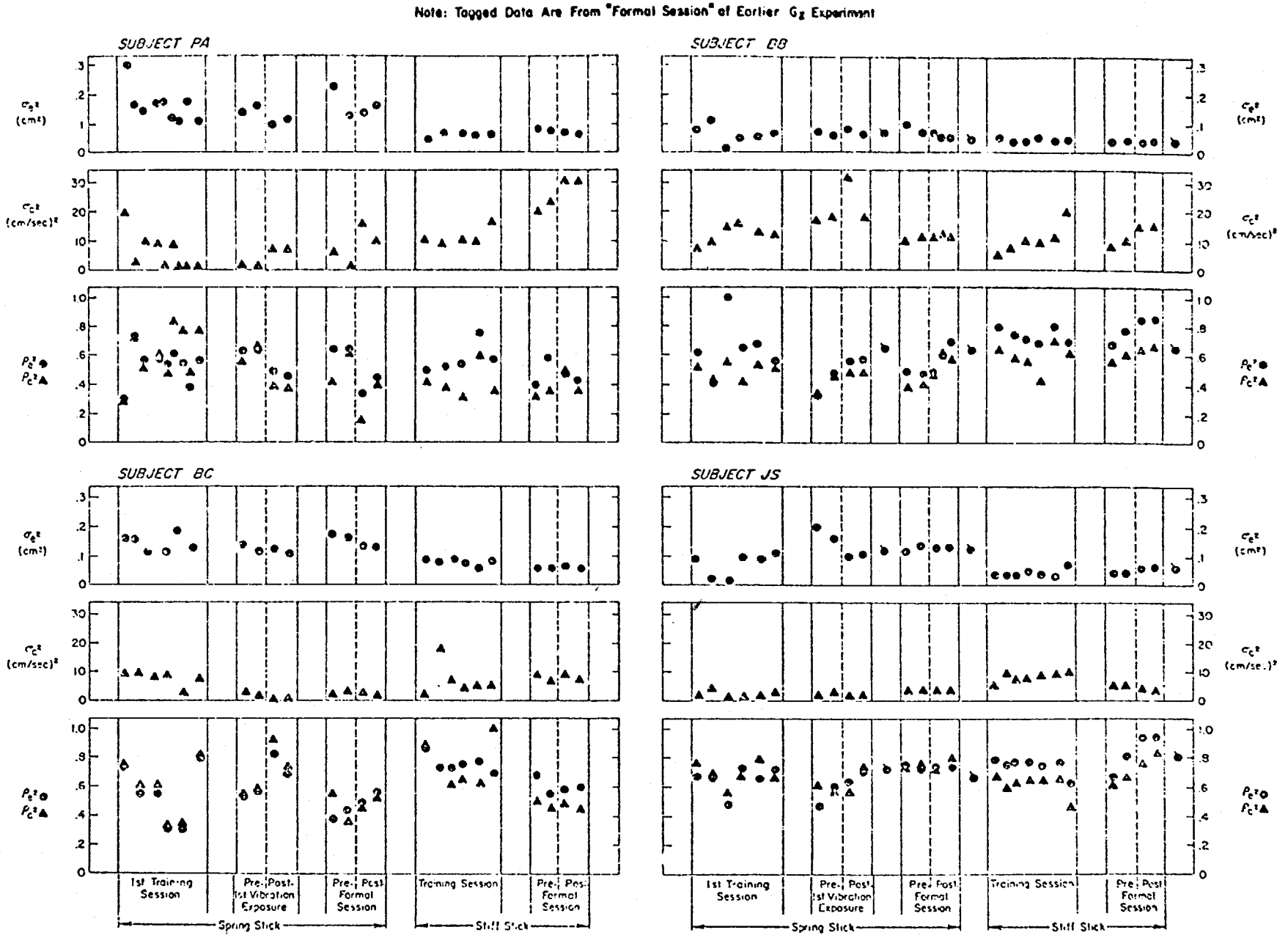

Figure 29. Comparison of Performance During Training and Formal Sessions of G_X Experiment

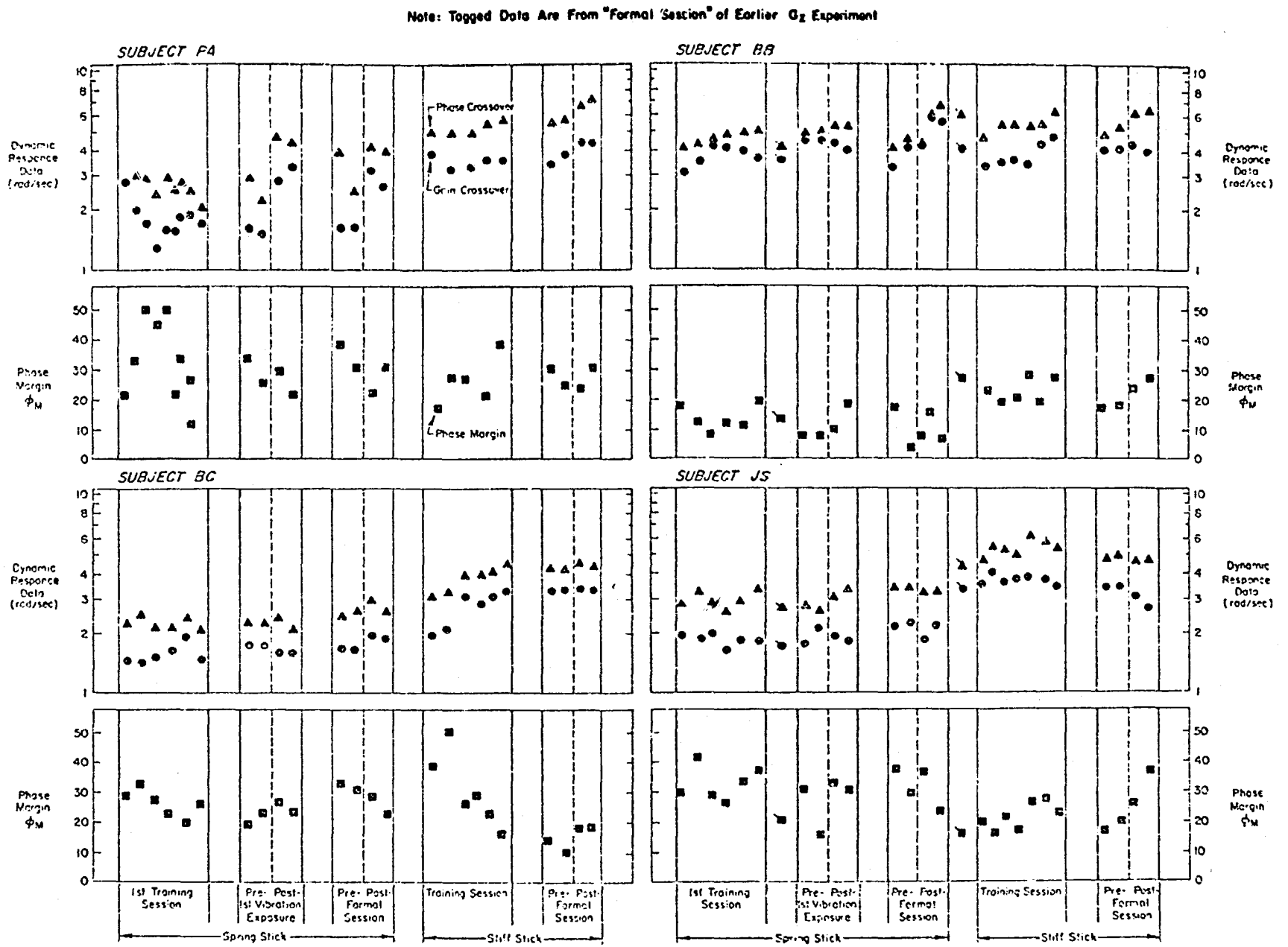

Figure 30. Comparison of Dynamics Response Measurements During Training and Formal Sessions of G_X Experiment

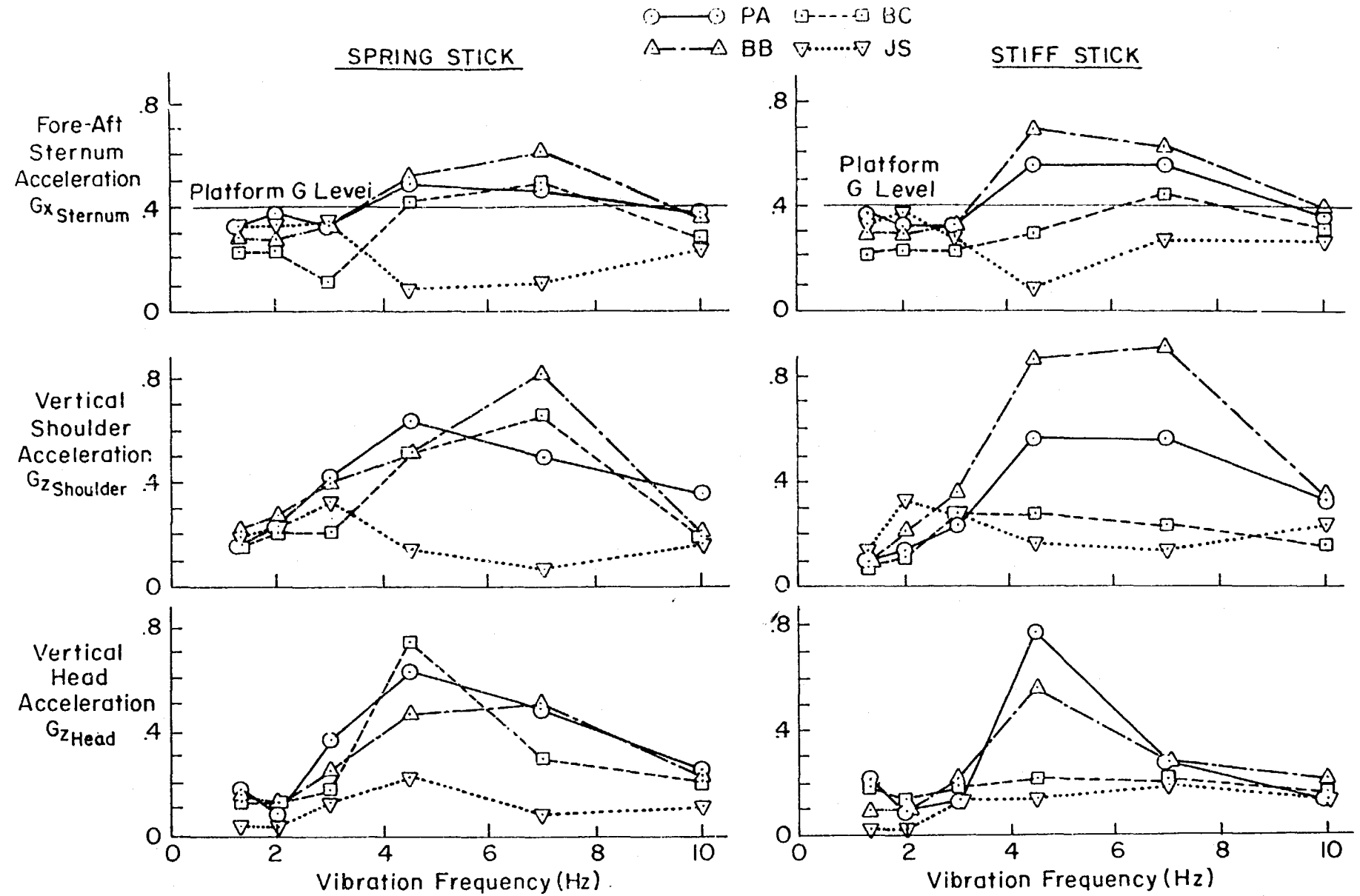

Figure 31. Sternum, Shoulder, and Head Motions During 0.4 g Fore-Aft Sinusoidal Vibration

The performance data averaged across subjects are plotted in Fig. 32b. Vibration generally caused an increase in total error, although the spring stick data are not statistically reliable, due to individual differences, as the following Analysis of Variance results will show. Almost all of the appreciable control-feedthrough from vibration is filtered out by the controlled element before it reaches the display, thus resulting in minimal vibration correlated errors. The spring stick gave a greater proportion of remnant while the stiff stick allowed a greater fraction of feedthrough.

The nature of fore-aft vibration feedthrough is illustrated by the averaged control stick variance data in Fig. 32b. A peaking or resonance of fore-aft feedthrough is apparent, and it occurs at higher frequency with the stiff stick (4.5 Hz) than for the spring stick. Also the spring stick gives much greater attenuation of high frequency feedthrough than the stiff stick, this being consistent with the previously given G_z and G_y results (Sections IV-B and V-B).

2. Dynamic Response

The dynamic response parameters for each subject, given in Fig. 33a, show considerable variability in trends across frequency of vibration. In contrast to other measures, the loose spring stick yields more consistent crossover frequencies (ω_u, ω_c). The averaged dynamic response parameters in Fig. 33b show that the main effects of sinusoidal G_x vibration occur in the region near 7 Hz G_x. Crossover frequencies declined and phase margin increased showing a tendency towards conservative closed loop tracking behavior. Subject BB reported arm sluggishness at the 7 Hz condition, which corresponds to his same comment in response to 10 Hz vertical vibration (Section IV-D).

3. Analysis of Variance

An Analysis of Variance was performed on these data to determine the sources and significance of variability in the experimental measurements. As in the prior ANOV, data for each control stick were analyzed separately. The ANOV results are given in Table 7. In general, stiff stick errors showed the highest consistency with vibration, while the high S × V interaction

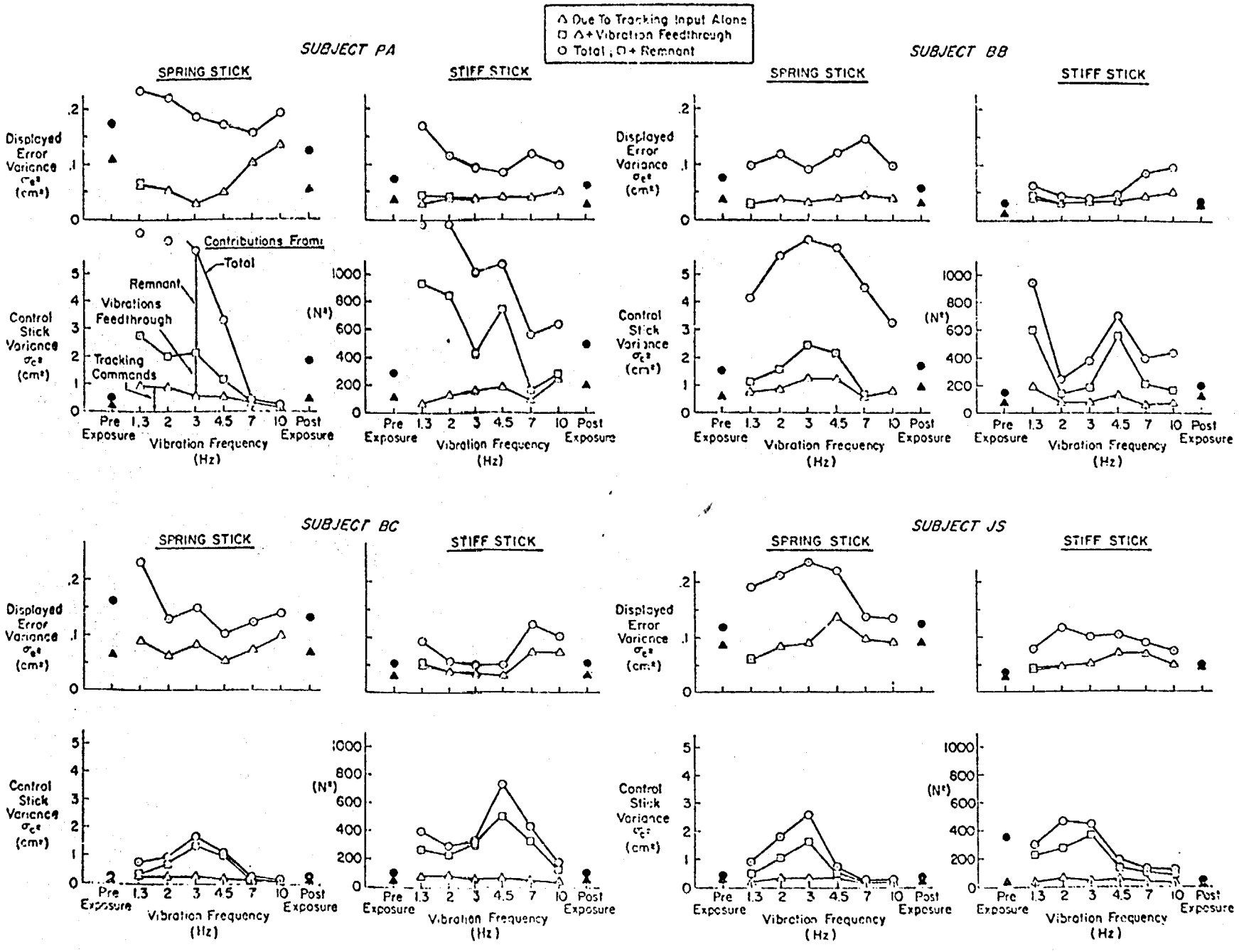
Δ Due To Tracking Input Alone
□ Δ + Vibration Feedthrough
○ Total ; □ + Remnant
SUBJECT PA
SUBJECT BB
SUBJECT BC
SUBJECT JS
SPRING STICK
STIFF STICK
Displayed Error Variance $\sigma_{e^*}^2$ (cm²)
Control Stick Variance $\sigma_{c^*}^2$ (cm²)
(N²)
Contributions From:
Total
Remnant
Vibrations Feedthrough
Tracking Commands
Pre Exposure
1.3
2
3
4.5
7
10
Post Exposure
Vibration Frequency (Hz)

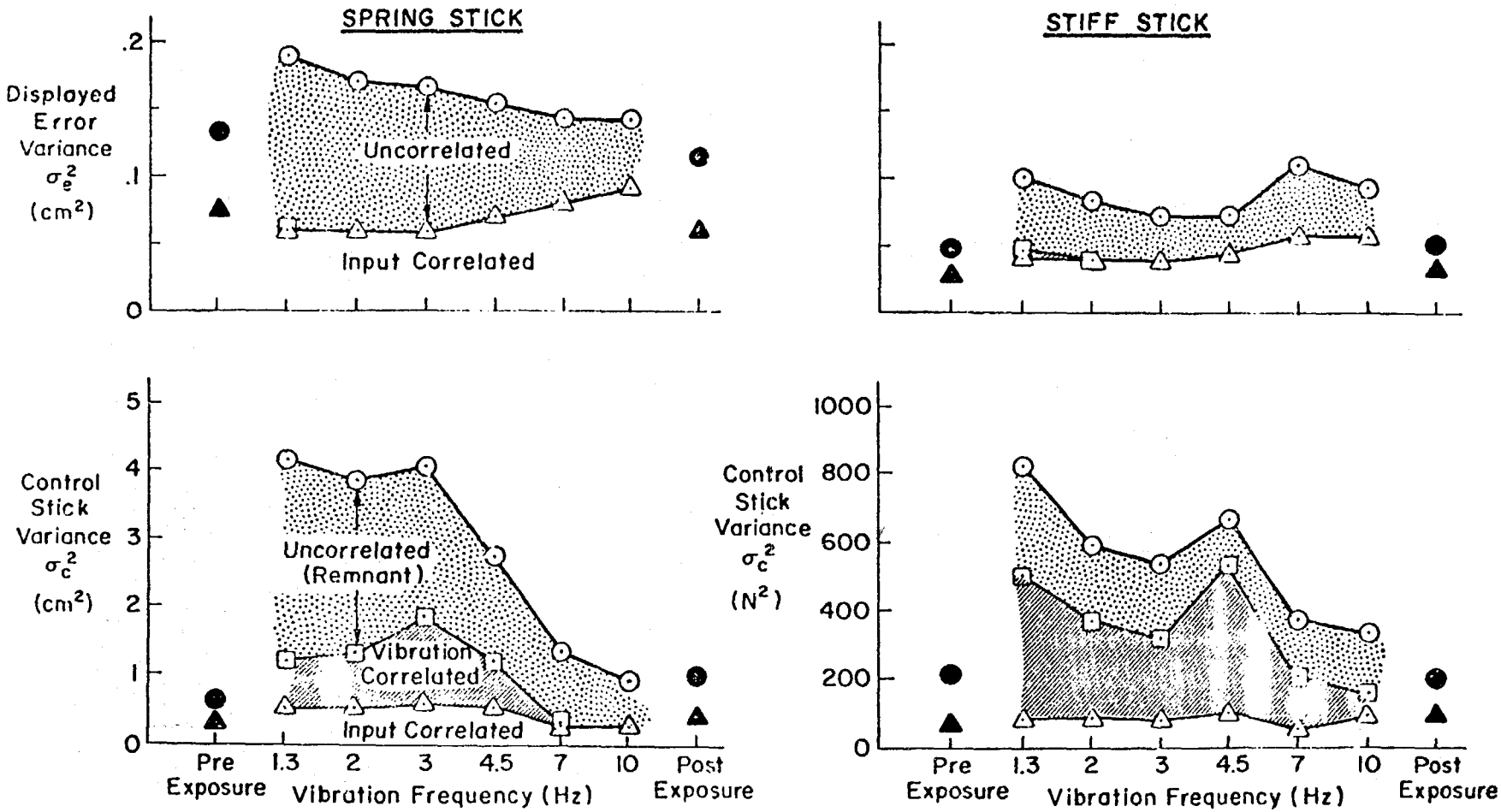

Figure 32b. Performance Effects Averaged Over Subjects in G_X Experiment (Averaged Over 2 Runs Per Subject and 4 Subjects)

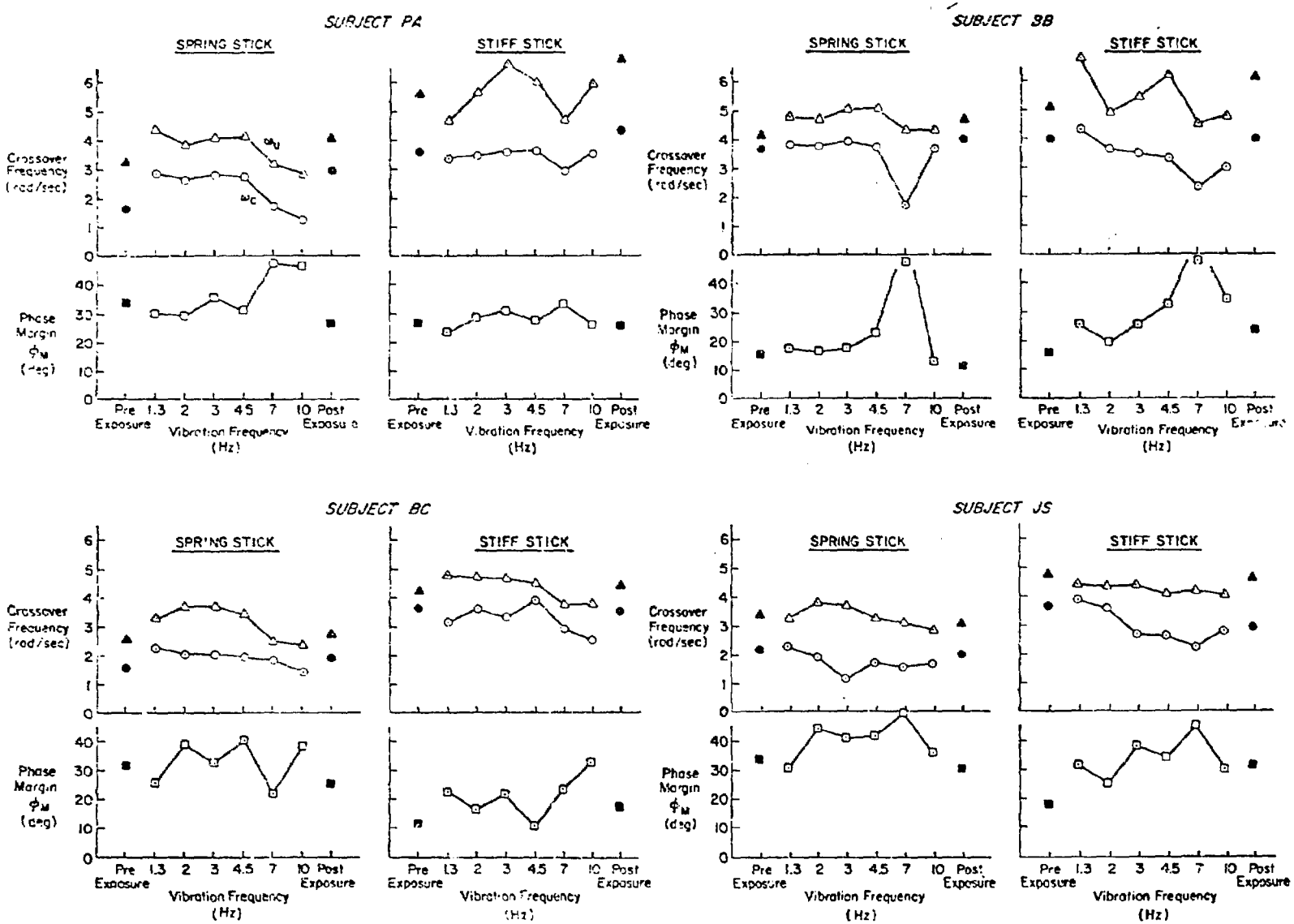

Figure 33a. Dynamics Response Measurements for Each Subject in G_X Experiment (2 Run Averages)

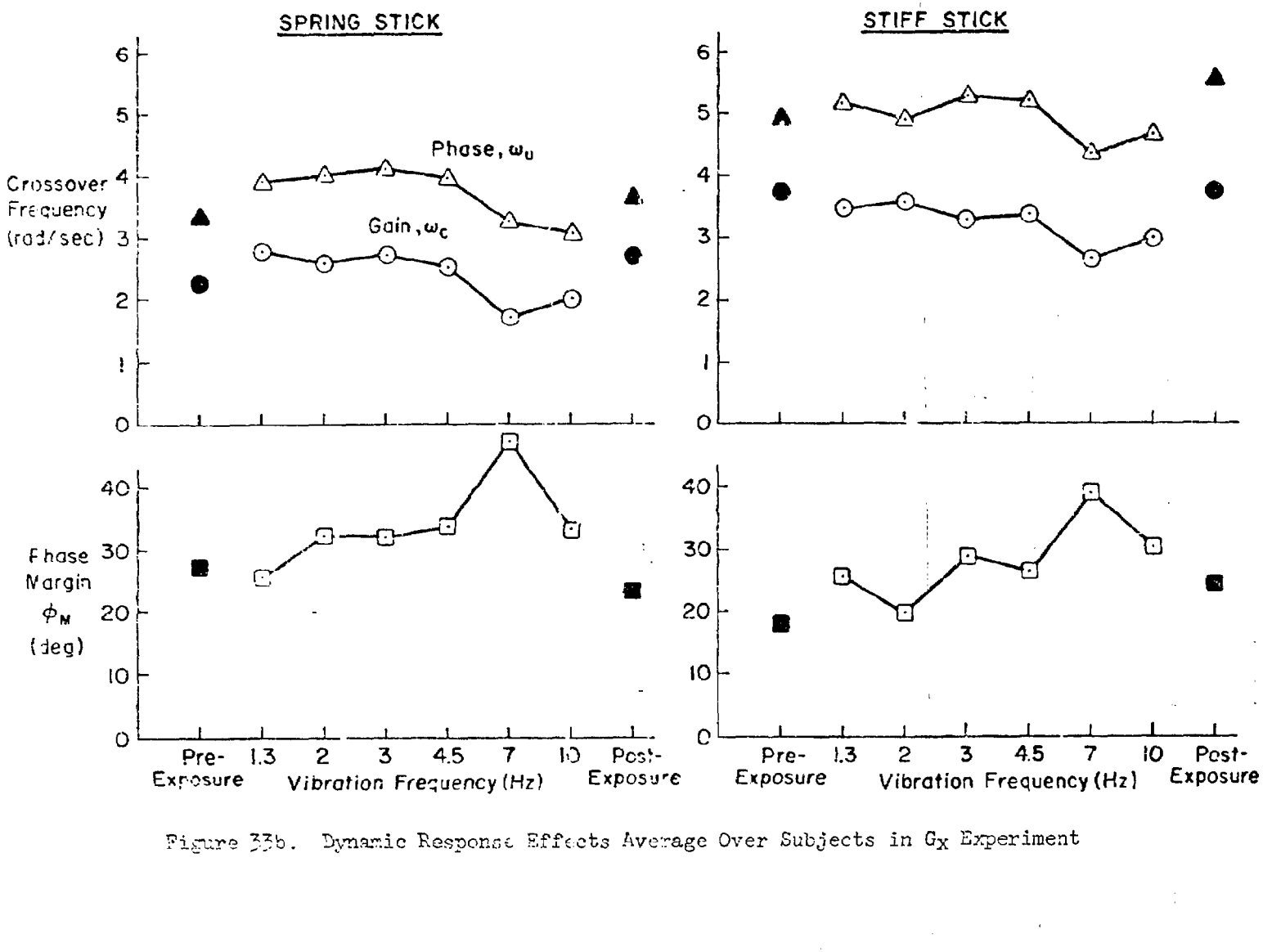

Figure 33b. Dynamic Response Effects Average Over Subjects in G_X Experiment

TABLE 7

ANALYSIS OF VARIANCE SUMMARY FOR THE FORE-AFT VIBRATION EXPERIMENT*

a. SPRING STICK DATA

		PERFORMANCE PARAMETERS								DYNAMIC RESPONSE PARAMETERS					
		σ_e^2		$\sigma_{e_i}^2$		σ_S^2		$\sigma_{\xi_i}^2$		ω_c		ω_u		ω_M	
SOURCE OF VARIATION	DEGREES OF FREEDOM	MEAN SQUARES	F RATIO	MEAN SQUARES	F RATIO	MEAN SQUARES	F RATIO	MEAN SQUARES	F RATIO	MEAN SQUARES	F RATIO	MEAN SQUARES	F RATIO	MEAN SQUARES	F RATIO
Subjects (S)	3	illegible	illegible***	0.00009	18.0***	54.24891	96.0***	1.51709	59.4***	illegible	109***	7.94986	105***	734.84021	10.1***
Vibration (V)	7	0.00163	2.04 NS	0.00102	1.03NS	18.70186	2.74*	0.14631	3.56*	1.19406	7.38*	1.04693	8.40***	223.71369	1.93NS
S x V	21	0.00080	2.89	0.00101	2.11*	6.97803	10.6***	0.04109	2.24*	0.35873	4.03***	0.14884	1.99*	223.71369	3.01**
Residual (R)	30	0.00027		0.00048		0.63159		0.02546		0.08909		0.07479		72.19001	
Residual Standard Deviation		0.031 $(cm)^2$		0.0219 $(cm)^2$		0.795 $(cm)^2$		0.16 $(cm)^2$		0.298 rad/sec		0.238 rad/sec		8.48 deg	

b. STIFF STICK DATA

		PERFORMANCE PARAMETERS								DYNAMIC RESPONSE PARAMETERS					
		σ_e^2		$\sigma_{e_i}^2$		σ_c^2		$\sigma_{c_i}^2$		ω_c		ω_u		ω_M	
SOURCE OF VARIATION	DEGREES OF FREEDOM	MEAN SQUARES	F RATIO	MEAN SQUARES	F RATIO	MEAN SQUARES	F RATIO	MEAN SQUARES	F RATIO	MEAN SQUARES	F RATIO	MEAN SQUARES	F RATIO	MEAN SQUARES	F RATIO
Subjects (S)	3	0.00670	illegible***	0.00066	5.5**	1315128.28521	35.8***	39394.87651	21.0**	1.51128	10.1***	8.04807	91.8***	367.62291	7.38***
Vibration (V)	7	0.00409	4.10**	0.00194	4.2**	398509.90977	5.45*	2138.79917	0.691 NS	1.14222	4.15**	1.17856	1.95NS	245.26639	4.07**
S x V	21	0.00096	4.26***	0.00080	1.67 NS	1155411.59937	3.14**	3087.41747	1.65 NS	0.27488	1.88NS	0.60644	6.25***	84.72277	1.71 NS
Residual (R)	30	0.00023		0.00012		36794.86818		1877.61030						49.71577	
Residual Standard Deviation		0.0151 $(cm)^2$		0.0109 $(cm)^2$		606 N^2		432 N^2		0.386 rad/sec		0.312 rad/sec		7.05 deg	

Significance Level: * = 0.05; ** = 0.01; *** = 0.001.

*The SICV is a two-way mixed effects model (with subjects as random samples, vibration frequencies as fixed treatments, and three replications per cell). The F ratio for "Subjects" effects is MS_S/MS_R, while the F ratio for "Vibration" effects is MS_V/MS_{SV}.

reduced the reliability of the spring stick error effects. The ANOV verifies the significant effects of vibration on the crossover frequencies noted earlier for the spring stick case.

The residual variances in Table 7 compare with the relevant ones found in the G_z and G_y studies, proving that the run-to-run data variability has not increased in this experiment. We have already noted that the test-retest "static" data for Subjects BB and JS show good repeatability. However, the S × V interaction for the spring stick are typically higher than those observed in the G_y study. Thus it appears that one of the major differences between control sticks under G_x vibration is the larger variability among subjects associated with the spring stick, whereas in the G_y experiment the spring stick led to larger performance decrements in general.

4. Describing Functions

The dynamic response results are supported by detailed describing function data shown in Fig. 34, where it is apparent that the high-frequency phase lags of the human operator increase with increasing G_x frequency. This result is similar to that found in the G_z study, where it was attributed to a direct vibration effect on neuromuscular response properties (Section IV-D). Comparison of G_z and G_x shoulder transmissibility results (Figs. 12 and 31) show that similar levels of high-frequency vibration occur at the shoulder, and persist to higher frequencies in the fore-aft case. Thus, the G_x describing function results are taken as further evidence of a direct vibration effect on neuromuscular dynamics.

D. DISCUSSION AND SUMMARY

Fore-aft G_x vibration led to considerable vertical motions of the torso and head, which induced visual blurring and neuromuscular impairments at higher frequencies. Considerable variability in biomechanical response was measured between subjects, however, which probably led to the large idiosyncratic performance differences encountered as a function of vibration frequency. Vibration-induced body motions are quite complex under fore-aft motion and seem to lead to greater inherent idiosyncratic behavior among subjects than under G_z and G_y vibration.

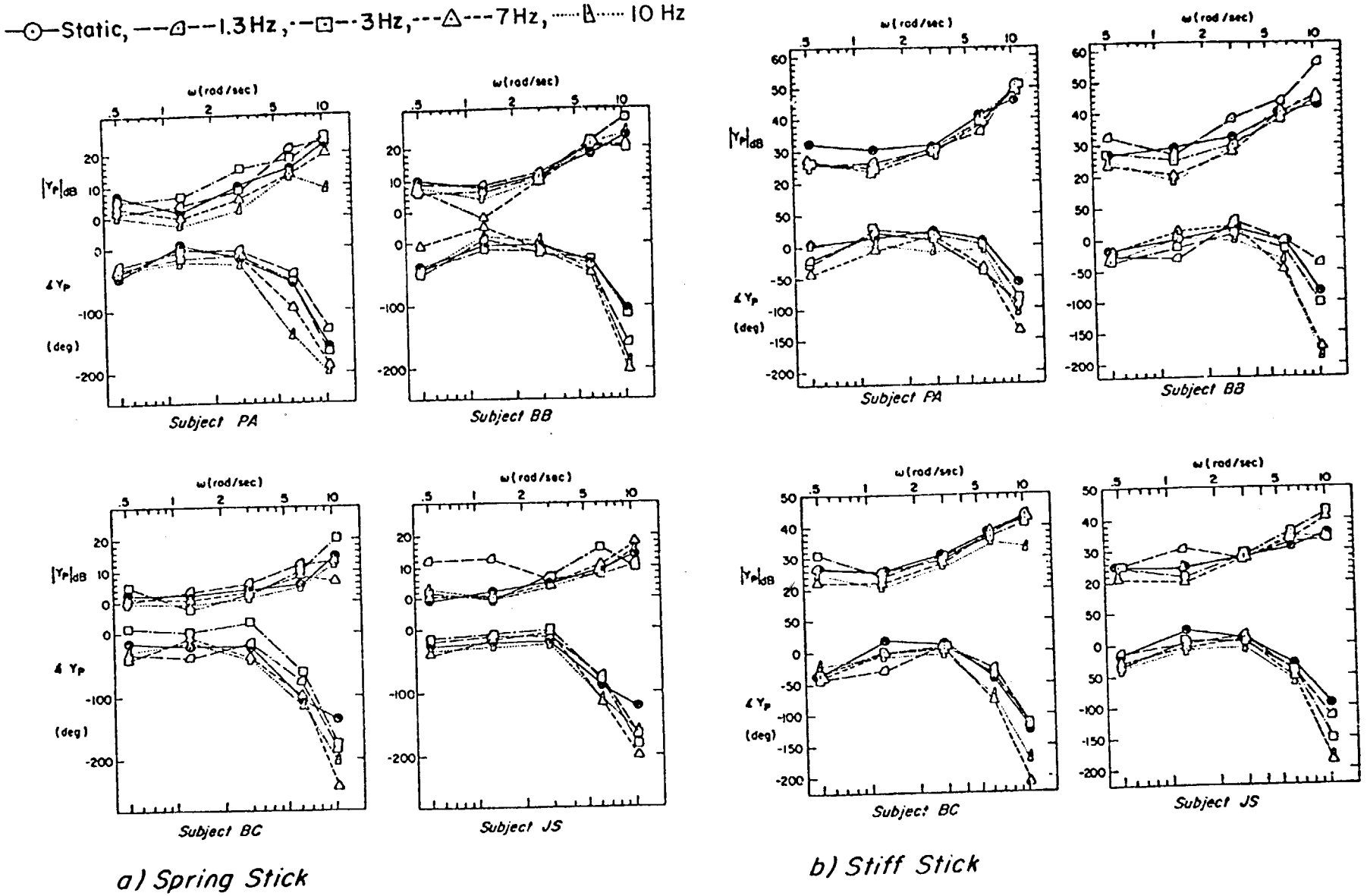

Figure 34. Human Operator Describing Functions (2 Run Averages) Compared Across Vibration Conditions in G_x Experiment

The stiff stick (nearly isometric) control led to less idiosyncratic effects and stick remnant than the spring (low spring gradient) stick. However, it also promoted higher vibration feedthrough because the rigid stick acts as an additional body support under vibration. Vibration generally degraded tracking errors with either control stick, which is consistent with the findings of Shoenberger (Ref. 31) and Hornick (Ref. 40). The shape of the tracking errors vs. frequency trend with the spring stick were not statistically reliable, however.

Finally, high-frequency fore-aft vibration had a consistent effect on the operator's dynamic response, which is similar to the results obtained in the G_Z study. In both situations, high-frequency phase lags increase under high-frequency vibration and seem to be related to an adverse effect of vibration on the neuromuscular system as suggested by Guignard (see Section IV-D). The neuromuscular impairment and visual blurring found here deserve more detailed investigation as to their cause and possible alleviation.

SECTION VII

VIRRATION FEEDTHROUGH MODELS

Development of models for the various biodynamic processes under investigation aids in their understanding, and validated models are essential to predict complex vibration effects in new situations. Models for the visual-motor dynamics of the human operator involved in continuous compensatory tracking tasks without vibration present are well developed (e.g., Refs. 18-21). The main objective of the present modeling work was to identify the biomechanical processes which alter the existing models and/or parameters, and to provide first-approximation models for those additional processes which allow motion inputs to feed through to the control response. Results presented in Sections IV, V, and VI show control feedthrough to be the major biodynamic effect, so we have concentrated on its modeling. The data also show that remnant induced by vibration is important, but modeling of this effect was beyond the scope of the present investigation.

Following the conceptual models presented earlier in Section II, the derivation, analysis and simplified approximations of the feedthrough models are given in Appendices A and B. This section provides a summary of the simplified models, correlation with our experimental data, and implications for other situations.

A. VERTICAL VIBRATION FEEDTHROUGH MODEL

One objective of the G_z experiment was to determine the feasibility of modeling the vibration feedthrough process. In this regard, only the spring stick (low spring gradient) data were analyzed for simplicity, and the following results are based on this initial effort.

1. Model Summary

In the vertical vibration experiment, the operator's task was pitch attitude control via fore-aft movements of a centerstick using an outstretched arm (see Fig. 4). Vibration inputs not only affect the

operator's loop closure parameters and remnant, but also feed directly through to cause control motions via induced motions of the seat, torso, limb and grip. (Refer to Figs. 1 and 3 for overall conceptual models of these elements.) Examination of the G_z data led to an exceptionally simple biomechanical model for the whole chain of elements, as developed in Appendix A. A version of this model is shown in Fig. 35, for which the following assumptions are justified in Appendix A:

- At vibration frequencies (1-10 Hz) the extended arm can be treated as a quasi-rigid link whose length is changed at low frequencies for tracking purposes, but is constant at vibration frequencies. It forms a bar having an average angle, θ, from the vertical.
- The shoulder and wrist act as pin-joints having negligible impedance.
- The upper body (limb root) acts as a vertically moving effective mass having, in general, a transmissibility defined as $Y_{T_z}(j\omega)$. This can be approximated for lower vibration frequencies (1-6 Hz) by a single mass, spring, damper system, as shown.

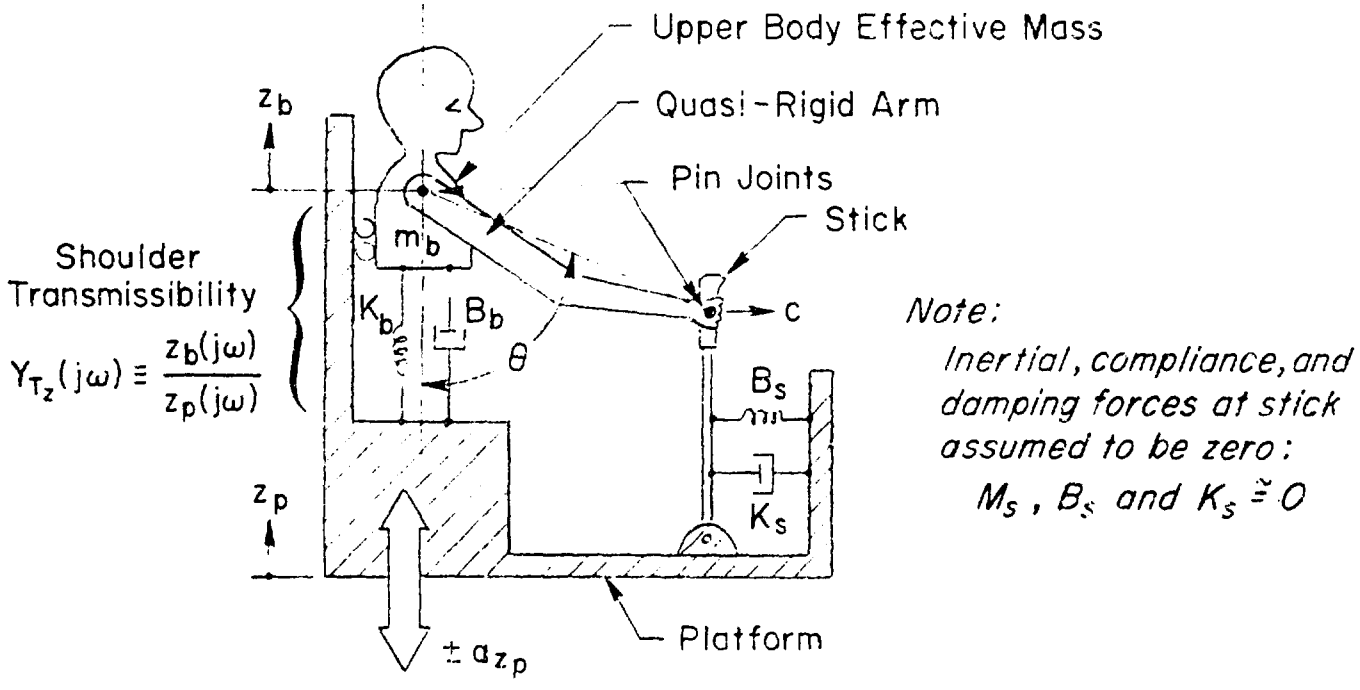

Figure 35. Simplified Biodynamic Model for Vertical Vibration Feedthrough to Pitch Control

- For the weakly restrained spring stick, the stick compliances are negligible compared with the torso-limb driving forces, making M_s, B_s and $k_s \cong 0$.

Under these assumptions, the stick merely acts as a linked transducer, and its motions reflect predominantly the upper body transmissibility, $Y_{T_z}(j\omega)$. Variations in the stick grip location and operator's arm length can affect the angle, θ, and thus lead to more or less attenuation of the shoulder motions. Converting the dimensionless transmissibility, $Y_{T_z}(j\omega)$, to a feedthrough component, $Y_{v_z}(j\omega) = c_v/a_{z_p}$ (in control units per acceleration unit), gives the following equation, derived in Appendix A:

$$Y_{v_z}(j\omega) \equiv \frac{c_v}{a_{z_p}}(j\omega) = \left(\frac{1 - Y_{T_z}(j\omega)}{(j\omega)^2}\right) \cot\theta \qquad (11)$$

where $$Y_{T_z}(j\omega) \equiv \frac{z_b}{z_p}(j\omega)$$

At this point we have retained the $(j\omega)$ argument to remind the reader that $Y_{T_z}(j\omega)$ and $Y_{v_z}(j\omega)$ represent measured describing functions which include the combined effects of the many small biodynamic nonlinearities, and are, in general, frequency and input-dependent (Ref. 6). In presenting simple mechanistic analytical models for these describing functions, we will drop the awkward $(j\omega)$ for the simpler (s), remembering that describing functions are still involved.

The limb-root transmissibility, Y_T, can be complicated, but our data seem to fit a single-degree-of-freedom model (such as that due to Coermann, Ref. 29) for an effective upper body mass-spring-damper system, as shown in Fig. 35 and developed in Appendix A. Thus the vertical shoulder-transmissibility can be written as:

$$Y_{T_z}(s) = \frac{z_b}{z_p}(s) \doteq \frac{(B_b s + K_b)}{M_b s^2 + B_b s + K_b} \qquad (12)$$

Combining the manipulating Eqs. 11 and 12 yields a remarkably simple second-order equation for the feedthrough dynamics:

$$Y_{v_z}(s) = \frac{c_v}{a_{z_p}}(s) = \frac{\cot\theta}{s^2 + (B_b/M_b)s + (K_b/M_b)} \qquad (13)$$

With this model for the injected vertical vibration feedthrough component, c_v, we can analyze the consequences of feedthrough on the complete closed-loop control signal, c. From the control system block diagram given in Fig. 2 (Section II) the transfer function between stick output and vertical vibration inputs is as follows:

$$\frac{c}{a_z}(s)\Big|_{\text{system}} = \frac{Y_{v_z}(s)}{1 + Y_p(s) \cdot Y_c(s)} \qquad (14)$$

Using the short-period dynamics employed in the experiment for Y_c, and assuming pilot dynamics (Y_p) comprising a gain, Padé time delay approximation, and appropriate lead equalization, yields the theoretical closed-loop vibration feedthrough response shown in Fig. 36. (Details are in Appendix A.) The low frequency amplitude peak (near 0.3-0.4 Hz) in Fig. 36 is the resonant peak of the closed-loop pilot vehicle system. This frequency region is below the range usually attributed to mechanical vibrations. The high frequency (f = 4-6 Hz) peak is due to the biomechanical transmissibility, Y_{v_z}. This peak is a decade above the closed-loop pilot-vehicle response peak and is realtively independent of the closed-loop response, as can be shown from Eq. 14, noting that $Y_pY_c << 1$ for frequencies beyond 10 rad/sec (1.5 Hz). Thus Eq. 14 can be approximated by the relationship:

$$\frac{c}{a_{z_p}}(s) \doteq Y_{v_z}(s) \quad ; \quad |s| > 10 \text{ rad/sec} \qquad (15)$$

This equation effectively describes the vibration feedthrough component that would be transmitted to the flight control system of an aircraft.

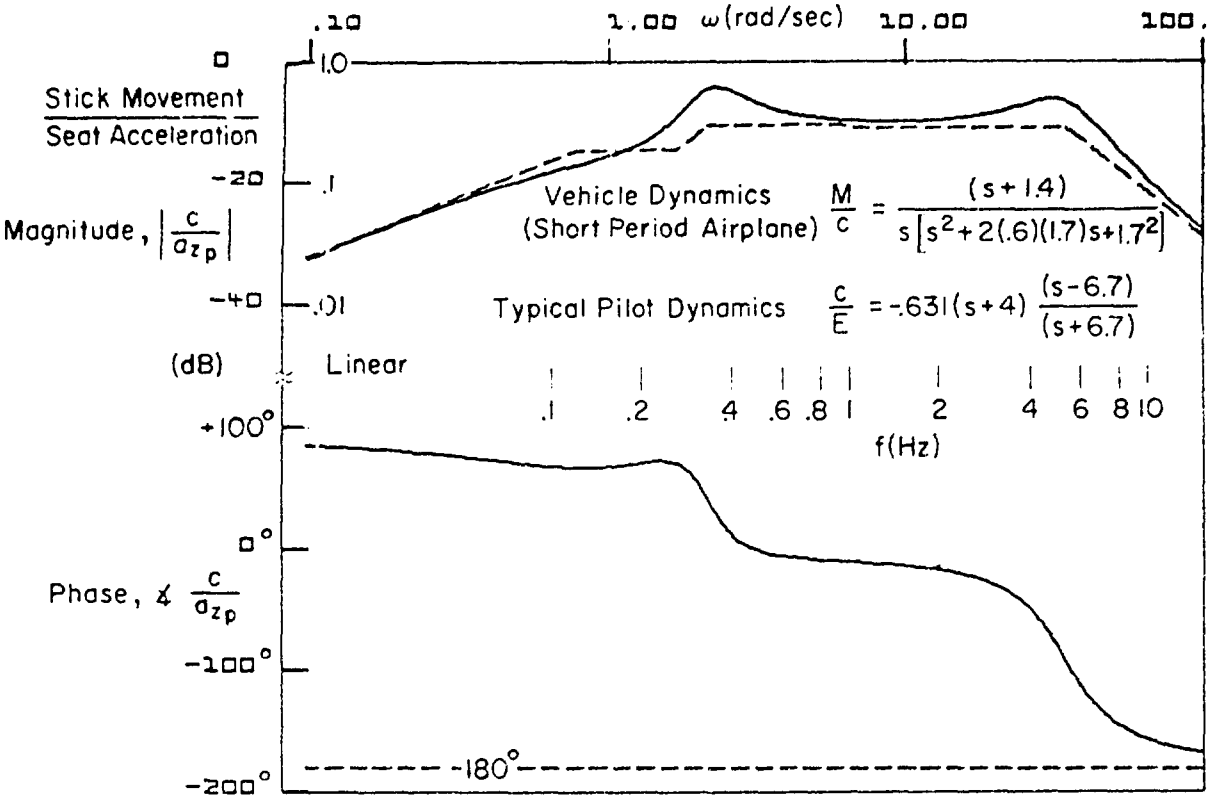

a) Stick Response to Platform Vibration

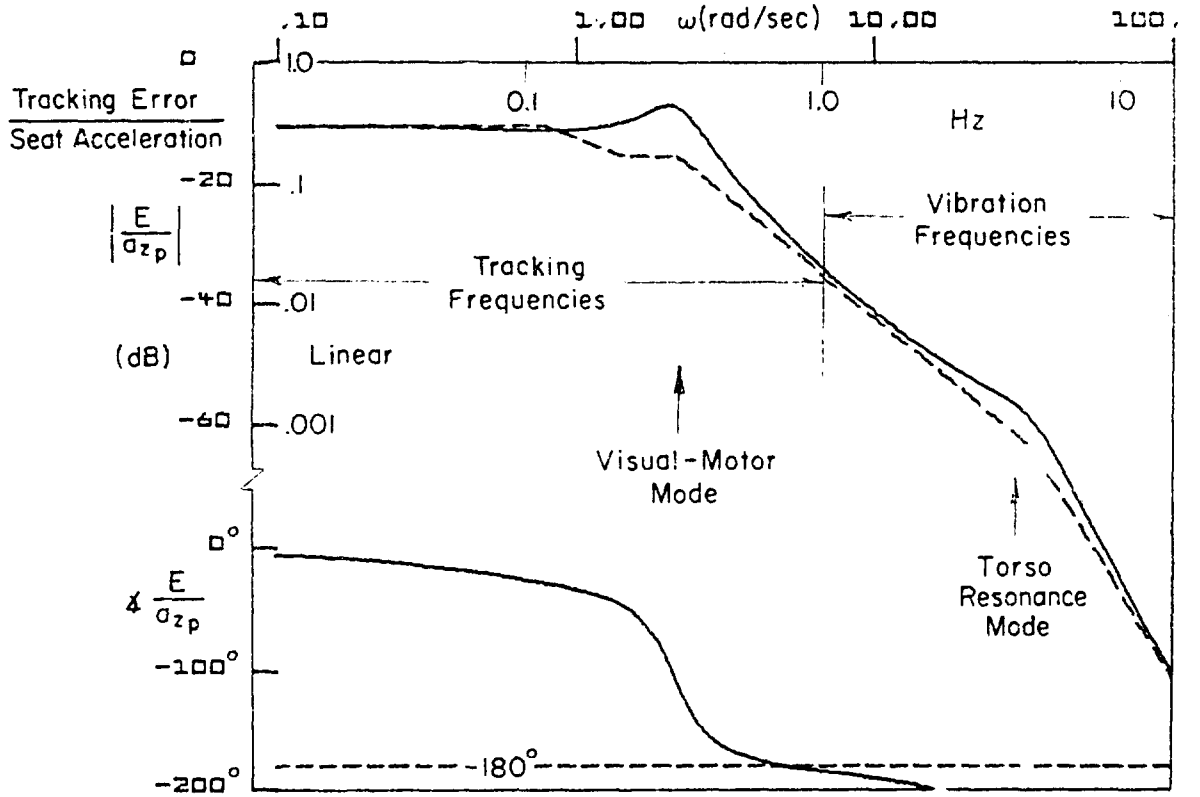

b) Displayed Error Response to Platform Vibration

Figure 36. Vertical Vibration Feedthrough Transfer Functions With the Pilot-Vehicle Loop Closed

The direct effect of vibration feedthrough on tracking error is of much less importance than its effect on the control system because feedthrough is fairly heavily filtered by the time it reaches the pilot's display. This can be seen by deriving the transfer function between vibration inputs and the pilot's display:

$$\frac{E}{a_{z_p}}(s) = \frac{Y_c(s) \cdot Y_{v_z}(s)}{1 + Y_p(s) \cdot Y_c(s)} \tag{16}$$

Since Y_pY_c is generally much less than unity in the vibration frequency range, Eq. 16 can be simplified to

$$\frac{E}{a_{z_p}}(s) \doteq Y_c(s) \cdot Y_{v_z}(s) \tag{17}$$

Thus the feedthrough term is filtered by the controlled element or vehicle dynamics, Y_c. A plot of Eq. 16 is shown in Fig. 36b. It is clear that above 3 rad/sec (0.5 Hz) the displayed feedthrough component is highly attenuated and probably not even apparent to the operator.

An exception to this can occur with a very elastic aircraft or booster rocket where the pilot sits at front, often near an antinode of the main fuselage-bending modes. In this case control motions at fuselage-bending frequencies can excite significant angles and large accelerations at the pilot's station, and this is manifested by resonant peaks in the normally attenuated $Y_c(j\omega)$ (e.g., Ref. 50). In such cases the simplification to Eq. 17 may not be justified, because significant tracking errors can result from control feedthrough, and the pilot-vehicle analysis demands visual-motor models valid at bending frequencies

2. Model and Data Comparison

The vibration training runs reported in Section IV used vibrations of 0.4g (zero-to-peak) at frequencies from 2 to 10 Hz. Stick position as well as head, shoulder and elbow accelerations were recorded. Figure 37a shows representative traces of c and a_{z_s} (at the shoulder) at 4 Hz for

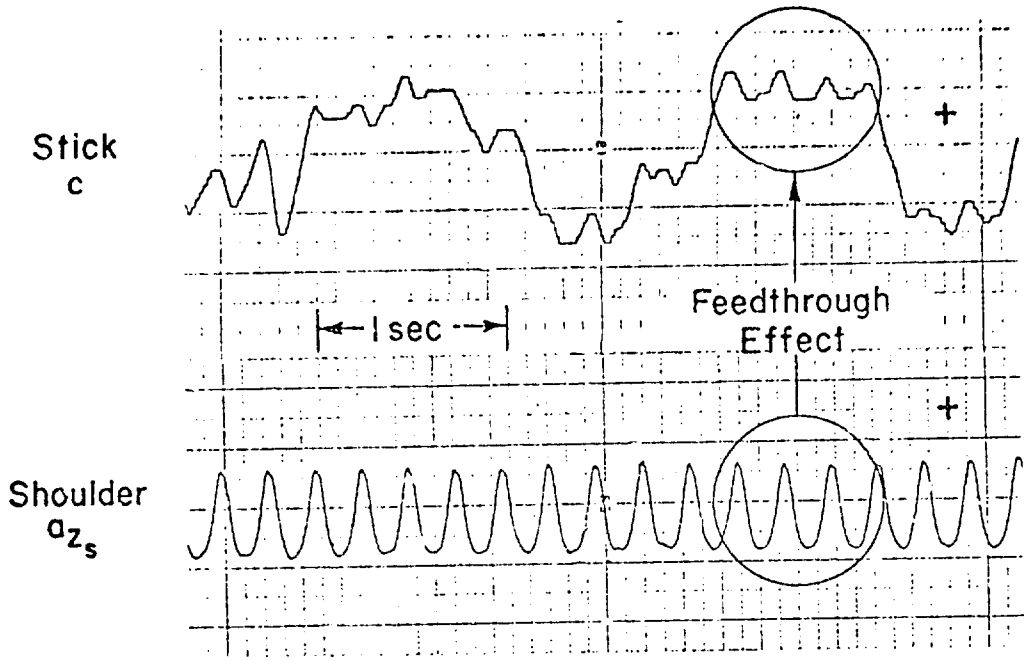

a) Typical Time Trace

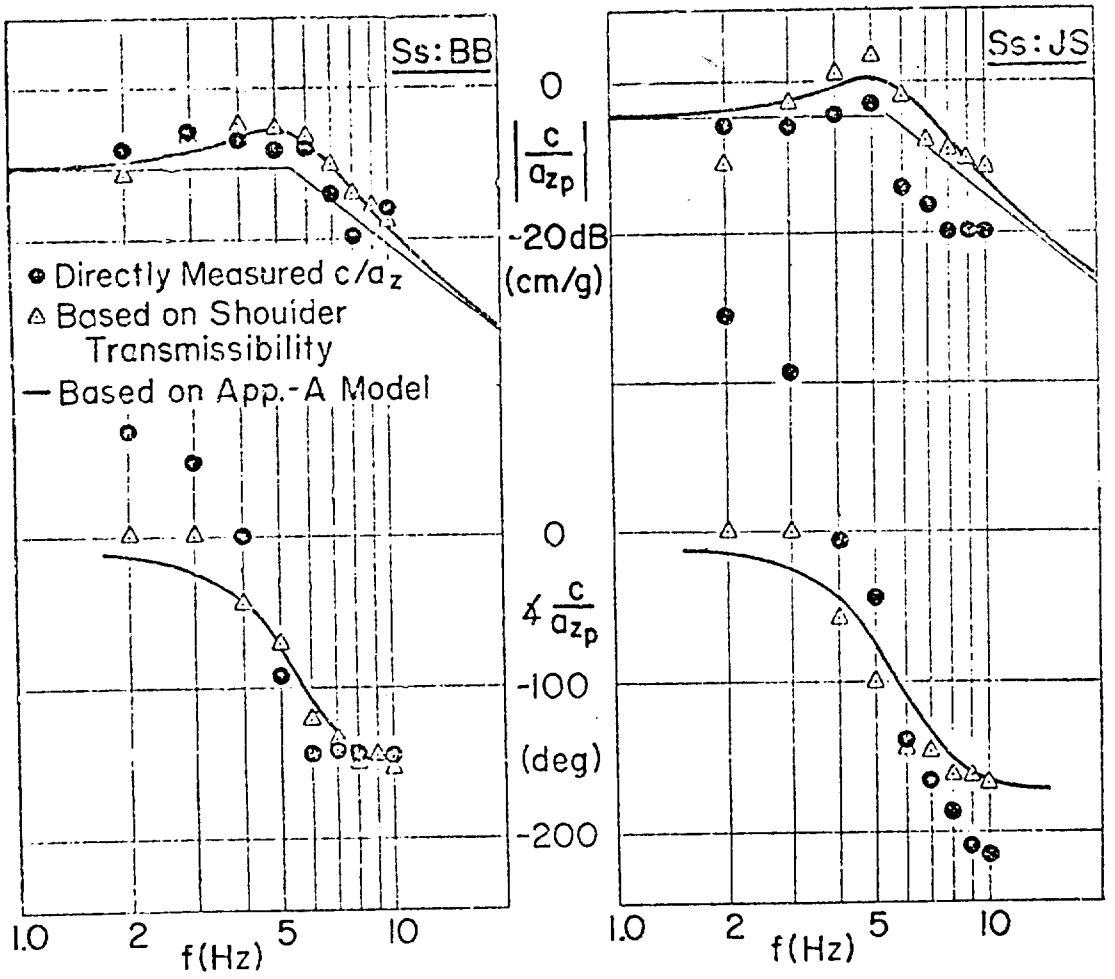

b) Frequency Responses of Control / Acceleration

Figure 27. Comparison of Measured and Modeled Vertical Vibration Feedthrough Response

the spring-stick case. Others are shown and discussed in Appendix A, and the following points are noted therefrom.

- Shoulder and elbow vertical motions are closely in phase, justifying the quasi-rigid link assumption. This occurs at most frequencies up to 7-8 Hz (e.g., refer to Fig. 12).

- Stick feedthrough motion actually leads the shoulder acceleration somewhat because the stick motion depends on the difference between platform and shoulder motions.

- Although it tends to be masked somewhat by additional tracking control components, the feedthrough frequency <u>is</u> apparent in the control stick trace of Fig. 37a. Consequntly, measurements via the Φ_{cv} scheme of Fig. 7 should be reliable.

Figure 37b compares the measured feedthrough dynamics c/a_{z_p} with that predicted by the quasi-rigid linkage model (Eq. 11) using the subject's measured transmissibility dynamics. Also shown is the predicted feedthrough dynamics using the single degree of freedom upper body model of Eq. 12. The measured and predicted feedthrough dynamics agree quite well for Subject BB, who tracked with an extended-arm configuration. (The phase shifts at 3 Hz and below were hard to measure from the strip chart records and are not very reliable.) The feedthrough predictions for Subject JS are not in as good agreement with the measurements as for Subject BB, however, and the rigid link model may be a poorer approximation for this case. There was not enough time for more thorough analyes for other subjects.

Given the preliminary nature of the measurements and models, the simple vertical-vibration-to-centerstick feedthrough model developed here is surprisingly good in the following respects:

- It is quite simple, and is based on transmissibility dynamics which have been measured extensively by several investigators and are well understood.

- It exhibits the resonant second-order nature of the feedthrough dynamics in the 4-6 Hz region.

- The control feedthrough resonant peak and sharp phase shift is closely matched, and the attenuation of the feedthrough at the error point is clearly explained.

- The magnitude of the feedthrough effect is roughly correct, with one subject's data matching within 2dB or 30 percent.

As noted above, there was not time for more detailed investigation of other subjects' data, nor of the stiff-stick case. In the latter case as was noted earlier in the transmissibility data of Section IV, the rigid stick actually forces the arm (if the angle θ is acute enough) and thereby the upper body at the higher frequencies. A straightforward extension of the current model to include nonzero stick mass, damping and compliance effects would account for these observed effects. The good results obtained with the simple models indicates that further modeling efforts for the vertical case would be fruitful.

3. Implications of the Vertical Feedthrough Model

With a tentatively substantiated feedthrough model, some implications for situations not yet tested can be explored. For instance, using Eq. 11 one can assess the effect of changes in shoulder transmissibility due to passive or active seat dampers, seat belt restraints, etc. If one were able to achieve unity transmissibility (shoulder motions equal to floor motion) then the control feedthrough would be zero because the shoulder, arm, and stick would move in unison. Active vibration isolation seats have been considered by other investigators (Ref. 27), and control task performance has been found to be unaffected or even degraded under certain conditions although isolation leads to greater comfort (Refs. 56, 57). With a floor mounted center stick, our control feedthrough model reveals that unity transmissibility may be a more desirable design goal than the zero transmissibility goal of most isolation seats. Such a "vibration compensated" seat could be self-adjusted to any operator's resonant characteristics and would be much easier to design and install than a pure isolation seat. The present analysis shows that measures taken to isolate the pilot from cockpit vibrations will aggravate the control feedthrough effect (and in a similar vein aggravate

relative eye-display motion), giving undesirable inputs to the flight control system and/or unduly exciting the body-bending modes of a large aircraft. The simple models summarized here should be adequate as a first-cut improvement in the complex systems models needed to explore these potential problems and their solutions.

B. LATERAL VIBRATION FEEDTHROUGH MODEL

Measurements in the lateral experiment indicated a definite difference in the type of feedthrough characteristics between the spring and stiff stick. Because of the success of the limited G_Z model development, it was decided to pursue a much more intensive and comprehensive effort in modeling G_Y effects that would explain these differences.

1. Model Summary

It appeared necessary at first to include the complex effects of lateral motion transmissibility to the upper torso, closed-loop neuromuscular actuation dynamics, and coupled limb/manipulator characteristics. Nevertheless, because the torso is only weakly coupled to stick side motions via the outstretched arm, a remarkably simple mechanical representation of the lateral feedthrough model was developed in Appendix B, and is shown in Fig. 38. The stick, arm and torso have been unfolded, so to speak, so that they all lie in the same plane. Shoulder-to-platform transmissibility is described by the general function $Y_{T_Y}(j\omega)$. The arm and stick are characterized by both a mass and moment-of-inertia since they both translate and rotate, and are both restrained by spring/damper characteristics (effective closed-loop neuromuscular characteristics in the case of the arm). References 51 and 52 give background on the neuromuscular basis for the present model. Finally, the arm is coupled to the control stick through the interface dynamics, mainly due to compliance and damping in the wrist and fingers.

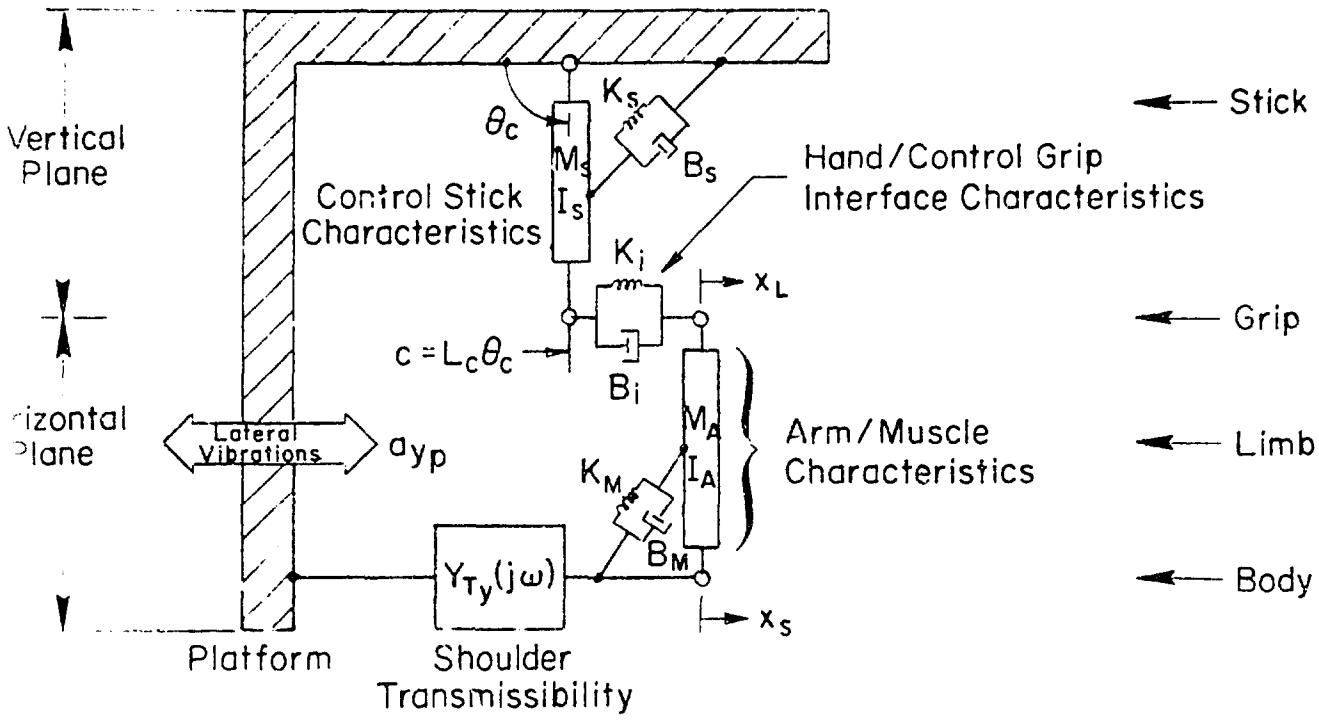

Figure 38. Lateral Vibration Control Feedthrough Model

2. Model and Data Comparison

The feedthrough dynamics $Y_{V_y}(j\omega)$ for the above model are too complex to review here, but are presented in detail in Appendix B. Here we will merely take the computed lateral feedthrough dynamics (Y_{V_y}) and consider the implications on the closed-loop manual control system:

$$\frac{c}{-a_{y_p}}(s) = \frac{Y_{V_y}(s)}{1 + Y_p(s) \cdot Y_c(s)} \qquad (18)$$

In Fig. 39 the computed closed-loop feedthrough dynamics between lateral stick output and vibration input is shown for both the spring and stiff sticks, using reasonable parameter estimates discussed in Appendix B. A crossover model approximation to the open-loop dynamics (Y_pY_c) was used with a Padé approximation for the time delay:

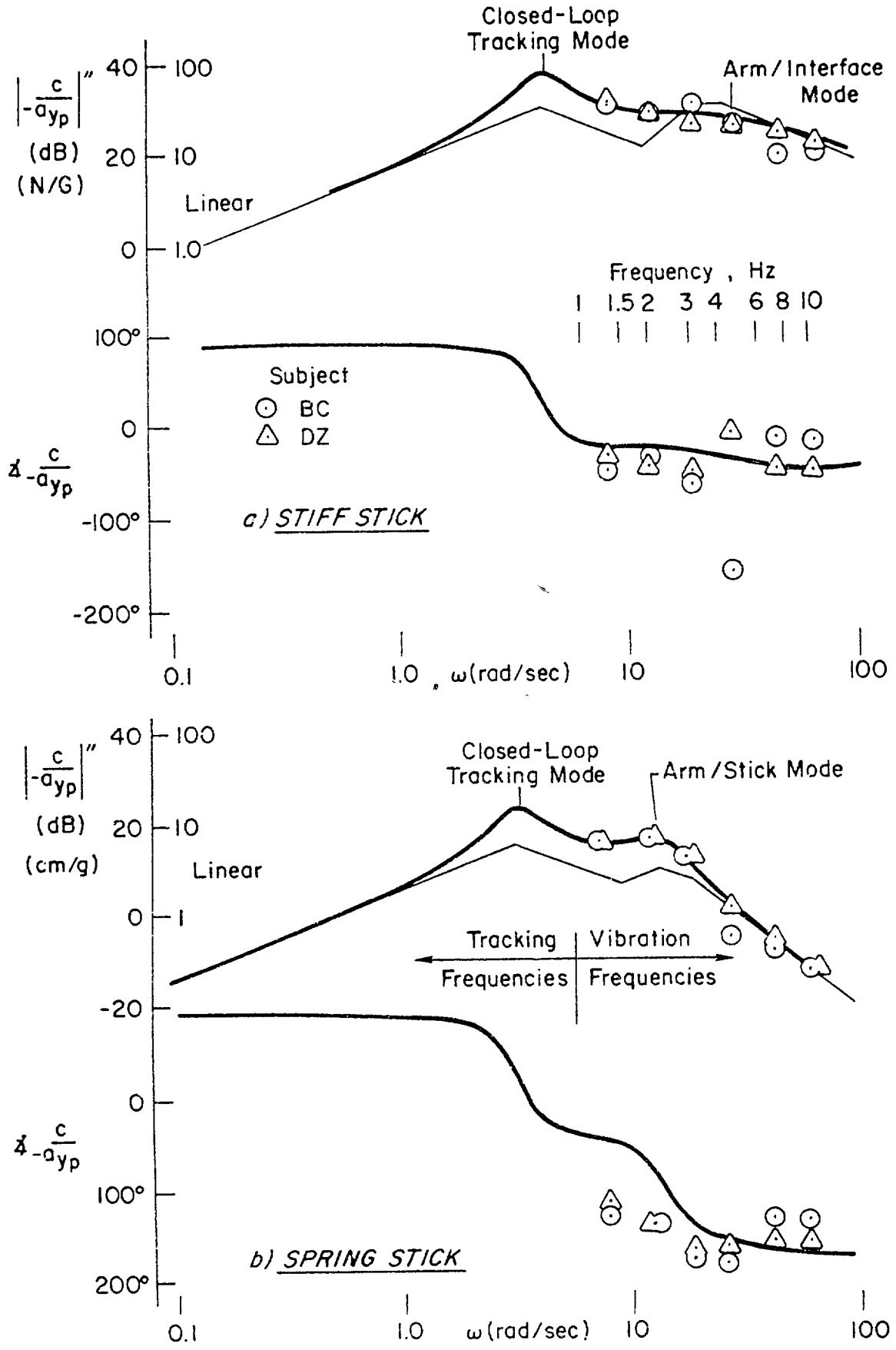

Figure 39. Comparison of Models and Data for Closed-Loop Responses Under Lateral Vibration

$$Y_p Y_c \doteq \frac{\omega_c}{s} \frac{\left(\frac{-\tau_e}{4}s + 1\right)^2}{\left(\frac{\tau_e}{4}s + 1\right)^2} \qquad (19)$$

where ω_c = 3.2 rad/sec (stiff stick)
2.5 rad/sec (spring stick)

τ = 0.33 sec (stiff stick)
0.42 sec (spring stick)

The above ω_c and τ values are close to the average values for Subject BC and are typical among all subjects.

Experimental measurements of the closed-loop feedthrough (obtained with the cross-correlation technique described in Section III) are compared with the theoretical curve in Fig. 39 for two subjects. The agreement is quite good considering the numerous factors involved.

3. Model Implications

Comparison of Fig. 39 with Fig. 36 shows that **lateral motion inputs produce significant control feedthrough at much lower frequencies than in the vertical case.** In fact, for motion frequencies somewhat lower than employed here, the effects would be magnified by the closed-loop resonance of the visual-motor tracking control loop. The difference in feedthrough characteristics between the spring and stiff sticks is apparent in Fig. 39. The stiff stick has a first-order roll-off characteristic at 5 Hz which is primarily due to the grip-interface characteristics, while the spring stick has a second-order roll-off at 2.5 Hz primarily due to the coupled arm/control stick dynamics. Thus the model reveals that the stiff stick will pass a greater amount of high frequency vibration feedthrough than the spring stick, in accord with the experimental finding.

The low frequency vibration feedthrough can be considerably aggravated at the error point as shown in Fig. 40. Here the closed-loop feedthrough transfer function shows that vibration inputs are rapidly attenuated at frequencies beyond the closed-loop resonance of the tracking loop.

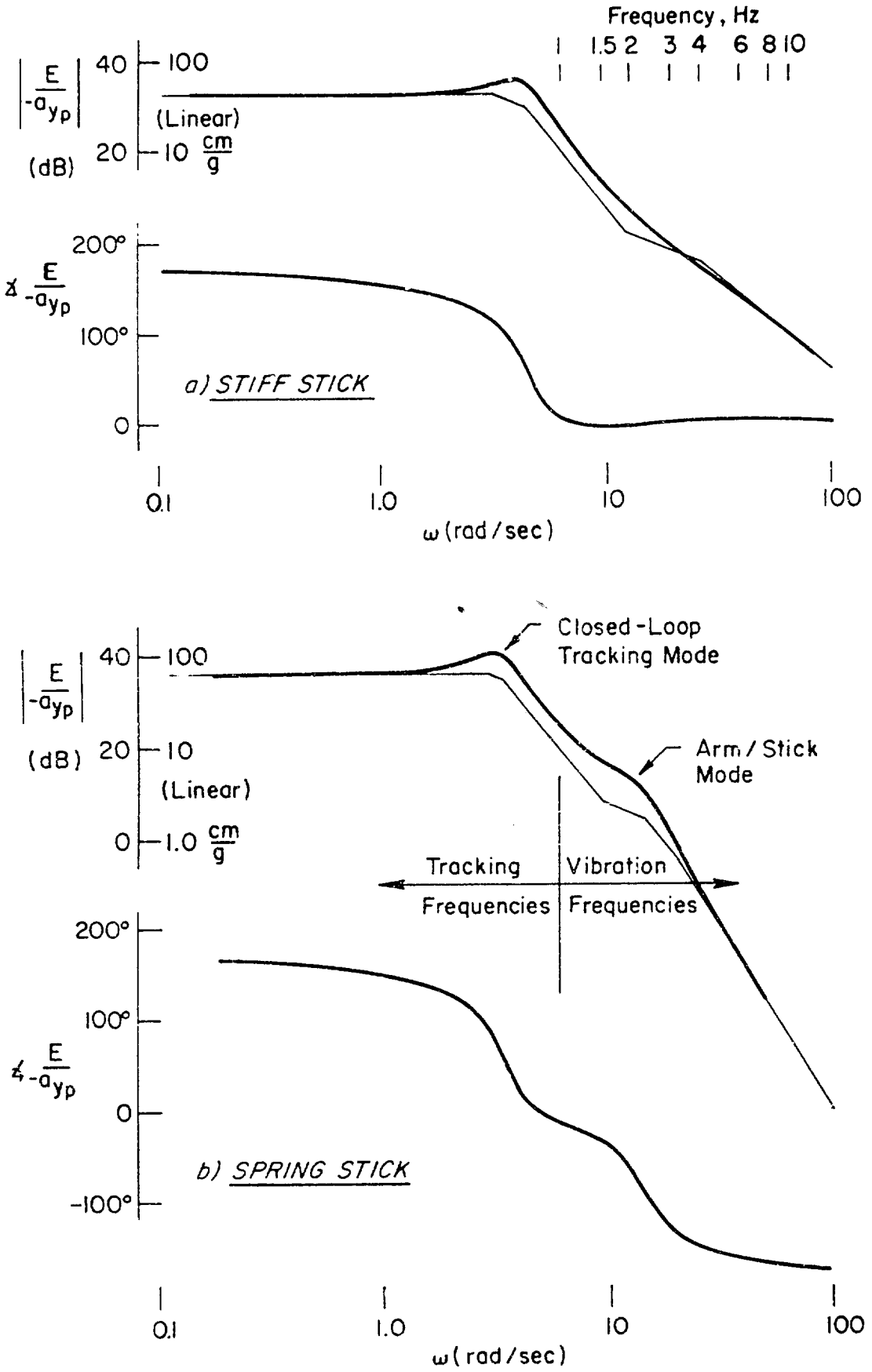

Figure 40. Closed loop Vibration-to-Error Transfer Functions

However, if the tracking loop resonant peak is approached at low vibration frequencies (around 0.5 Hz), the feedthrough may be greatly amplified. Judging from the feedthrough measurements obtained in this study in the error signal at 1.3 Hz, feedthrough at lower frequencies would be annoying enough to cause the operator to lower his gain in order to minimize feedthrough amplification. The high errors due to vibration at very low frequency are caused mainly by the direct quasi-static "bobweight" effect, whereby the combined arm-stick mass moves the stick against its spring gradient. An approximate formula for this is given in Appendix B (see Eq. B-26 et seq.).

The lateral model developed here is capable of handling a number of interesting effects such as: different stick/limb properties, gripping techniques, arm bracing, counterbalanced stick designs, torso restraints, and so on. Further investigation of these effects now seems warranted, both analytically and experimentally.

C. FORE-AFT VIBRATION FEEDTHROUGH MODEL

Development of a fore-aft vibration feedthrough model was beyond the scope of this investigation. Nevertheless, Y_{v_x} (feedthrough describing function) measurements were obtained, and due to similarities with the lateral vibration case, these measurements can be interpreted in a biomechanical model context.

1. Feedthrough Measurements

The feedthrough describing function measurements are given in Figure 41. Comparison with the lateral feedthrough measurements of Figure 39 reveals similar trends between the two sticks; the stiff stick feedthrough dynamics are relatively wideband while feedthrough with the spring stick shows a rapid attenuation out beyond 5 Hz.

In Appendix B expressions are developed for "hands off" stick-alone feedthrough response. The fore-aft stick characteristics were identical and the magnitude is plotted in Fig. 41. For the stiff stick it can be seen that the measured feedthrough amplitude ratio is a factor of 20 dB (or ten times) greater than the "stick-alone" value which implies

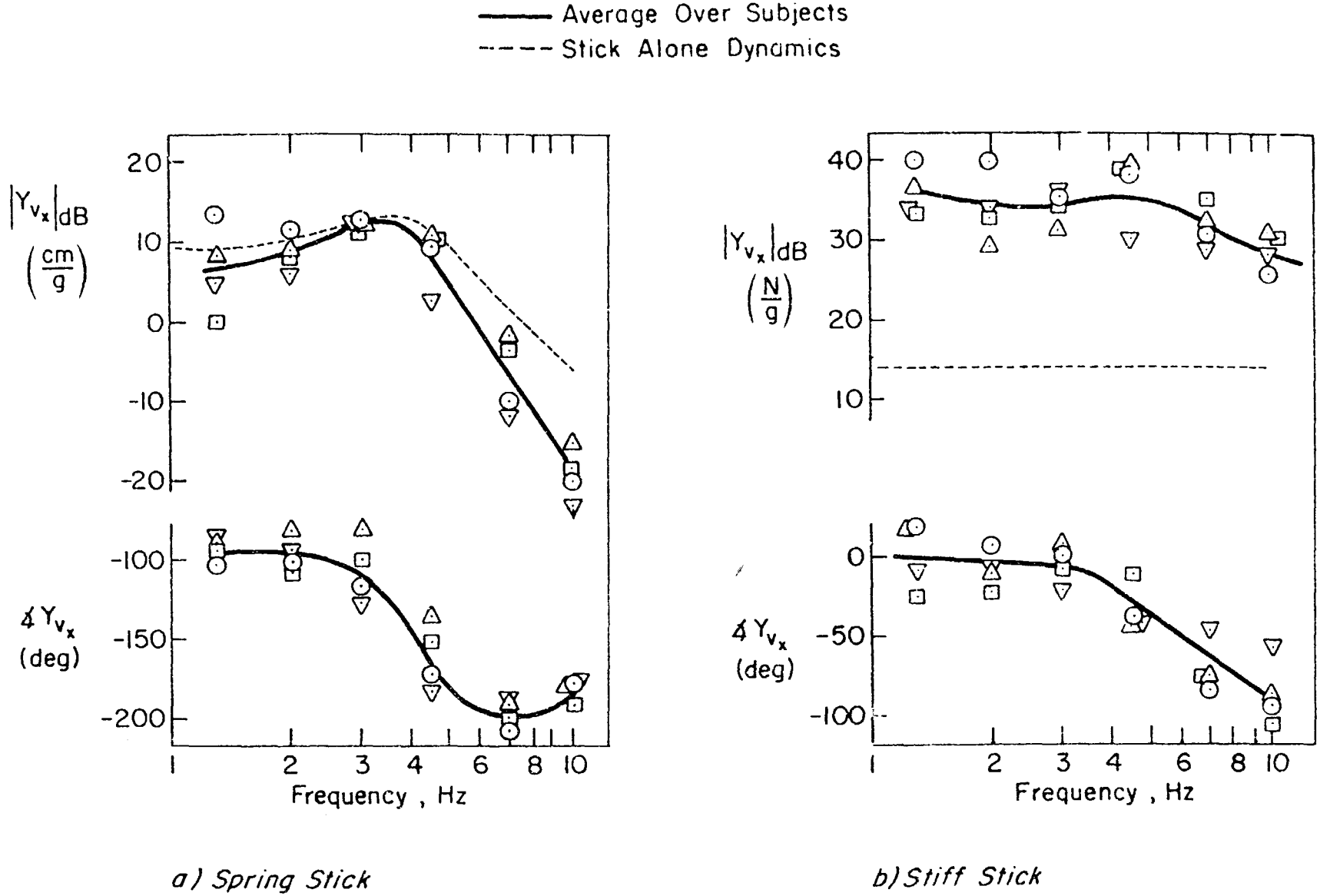

Figure 41. Fore-Aft Feedthrough Describing Function Measurements Averaged Over Two Runs Per Subject

that **the subjects use the stiff stick as an additional body restraint under vibration.** In Appendix B the increase in feedthrough under lateral vibration due to the subject holding the stick was found to be on the order of 11 dB or 3.5 times (Fig. B-10). This implies that about three times as much feedthrough is generated under fore-aft vibration as compared with lateral motion. This result is also consistent with the arm strength capabilities of the human operator. If the operator is restraining body motions by using the stick as a support, then the restraining forces must pass through the shoulder. Measurements of maximum force capability (Ref. 55) have shown that the push-pull strength of the arm is two to three times greater than strength in the sideward direction, which is consistent with the present results.

In contrast to the above, the feedthrough data for the spring stick shown in Fig. 41 are remarkably close to the stick-alone response. If we assume the torso-limb-stick system to be a roughly three-bar linkage, then these data suggest that torso (shoulder) response is similar to the stick-alone response. There are important differences, however, as the high frequency feedthrough attenuates at 40 dB per decade versus only 20 dB per decade for the stick alone. Also the feedthrough phase lag levels off at −90 deg at low frequencies, while the stick response would return to zero. Thus a fairly complex model will probably be required to account for G_x feedthrough effects.

One interesting final observation should be made regarding the G_x feedthrough data. While the G_x transmissibility data given in Fig. 31 are quite variable between subjects, the feedthrough data of Fig. 41 show a good deal of consistency in the major trends and should lead to a fairly general model for G_x feedthrough effects. It should be noted, however, that the transmissibility data are plotted in linear units while the feedthrough results are presented in log magnitude (dB) and phase angle with a log frequency axis. It appears that this latter format is most appropriate for biomechanical data, and in addition gives better insight into most dynamic properties than a linear format.

2. Conceptual Model

Based on the measured fore-aft transmissibility data and comparison with the lateral vibration model and data, a first-cut conceptual G_x feedthrough model is proposed, as illustrated in Fig. 42. The transmissibility portion of the model is similar to the G_y case (Appendix B); the hip translates with respect to the platform, with attendant shearing compliance (K_a) and damping (B_a). The torso rotates in pitch with respect to the hip with rotational compliance (K_T) and damping (B_T).

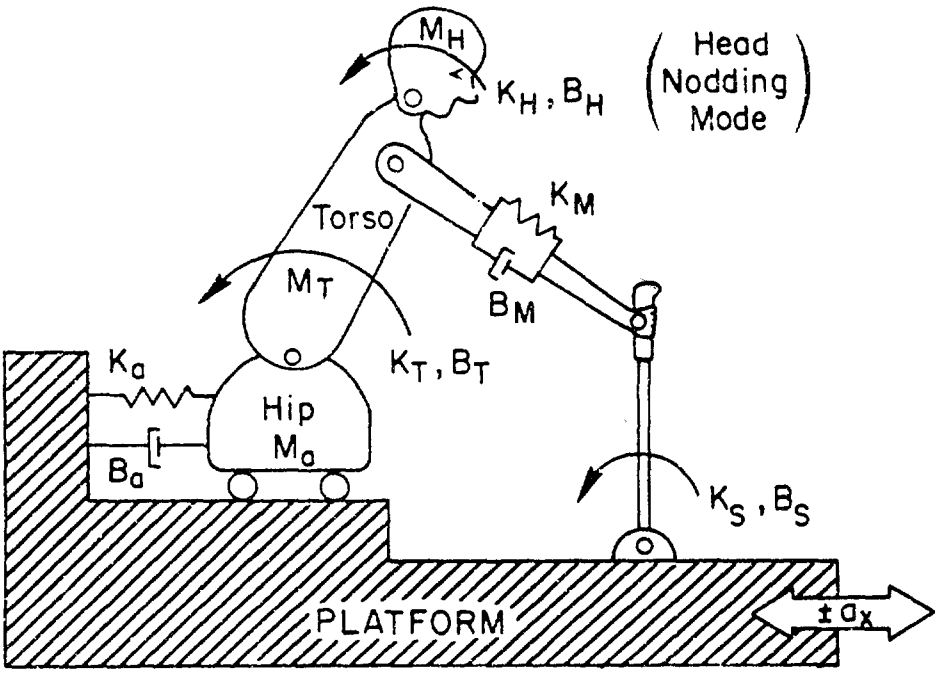

Figure 42. Conceptual Fore-Aft Vibration Feedthrough Model

A head nodding mode has been added to the model which will have some effect on shoulder transmissibility. The complete transmissibility model must produce significant vertical accelerations, as measured in the G_x study (Figure 31), and additional complexity may be required to include this effect.

The shoulder-stick coupling in Fig. 41 includes compliance and damping. This component accounts for movement of the shoulder and elbow joints which are restrained by equivalent muscle compliance and damping.

The control stick model is the same as that described in Appendix B. It should be noted that the torso and stick elements undergo both translation and rotation. The techniques for describing this motion are developed in Appendix B.

Because of the similarity of the G_x to elements of the G_y and G_z cases, and because of the excellent data obtained for the feedthrough describing function, we recommend further analytical development of the fore-aft feedthrough model with experiments to validate its use.

SECTION VIII

CONCLUSIONS AND RECOMMENDATIONS

A. GENERAL CONCLUSIONS

While some aspects of the exploratory research presented here (e.g., number of subjects and coverage of all frequencies and amplitudes) may not be as comprehensive as desired, the approach was quite successful in meeting the prime objectives, and the results should serve as an adequate foundation for further biodynamic research. Summaries have already been given for each of the experimental sections (IV-VI) and the modeling effort (Section VII), and will not be repeated in detail. Among the more general conclusions which can be drawn from these findings are the following, separated into effects on visual-motor behavior, feedthrough to controls, and performance (recall that G_z is vertical, G_y is lateral, and G_x is fore-aft vibration).

1. Visual-Motor Behavior

- The predominant effects of sinusoidal vibration on visual-motor behavior were found to be mainly involuntary in nature, including increases in neuromuscular lags and operator-induced remnant (noise). The neuromuscular effects occur when high-frequency vibration (near 10 Hz) reaches the shoulder as occurred under G_x and G_z vibration. Remnant increases occurred under both high-frequency G_x and G_z (>8 Hz) and low-frequency G_y (<5 Hz) vibrations.

- The increased remnant from high-frequency G_x and G_z vibration may be due to subject-reported visual blurring or to neuromuscular interference near tremor frequencies as discussed in the text.

- Based on the nature of the data and subjective reports, the remnant induced by low-frequency G_y vibration, in combination with the low spring gradient control stick, may arise from the masking of kinesthetic feedback of control position caused by the large torso and control motions which occur under this vibration condition.

- There is some indication of voluntary or "adaptive" changes in the human operator's visual-motor response under vibration, including slightly decreased tracking gain and increased phase margins. These effects are in the direction of more conservative closed-loop behavior, as might be expected in the face of the stressful nature of vibration.

2. **Vibration Transmissibility and Control Feedthrough**

- Vibration-induced control feedthrough was a significant component in control stick activity under most conditions. For G_z, whole-body resonance ($\cong$ 5 Hz) leads to the most significant feedthrough. At low frequencies (<4.5 Hz), G_y vibration causes inertial forces on the stick (i.e., the "bobweight" effect of the limb-stick ensemble) which leads to the majority of lateral feedthrough. For G_x vibration a combination of low- and mid-frequency (<7 Hz) vibration effects, including a complex coupling of fore-aft vibration into vertical torso motions, caused the majority of feedthrough.

- Biodynamic transmissibility results obtained here are consistent with the findings of previous investigators and tie in well with related feedthrough and performance effects measured in this study: e.g., G_z resonance in the region of 5 Hz which leads directly to vibration feedthrough at the control stick, and arm motions occuring under G_z and G_x high-frequency vibration which lead to increased neuromuscular phase lags.

- Stick spring gradient plays a dominant role in control feedthrough, with a lightly-sprung control resulting in considerable high-frequency attenuation, while a stiff stick gave relatively wide band feedthrough.

- The simple quasi-linear dynamic models developed here are consistent with transmissibility and feedthrough measurements, and give insight as to what factors (e.g., body motions, stick characteristics, etc.) contribute to the feedthrough phenomenon. The models include coupled sets of spring-mass-dampers representing the body, limb, and control stick subsystems, and are capable of representing most of the major effects measured in the present experiments. The models are formulated in terms of physical properties (mass, compliance, damping), so that changes in these factors can be accounted for in new situations (e.g., the effect of vibration isolation seats on control feedthrough).

3. Performance

- Considerable insight into the performance effects of vibration was gained by partitioning the error and control variances into factors correlated with the tracking input, vibration input, and a remaining uncorrelated portion (remnant). The performance measures themselves have shown the relative importance of various effects, while the related measurements of visual-motor behavior and vibration feedthrough processes have indicated the source of the effect in most cases.

- The most consistent overall vibration effect on tracking errors was an increase in human operator remnant. The most consistent effect on control activity was the addition of vibration-induced feedthrough. The feedthrough was generally filtered out by the controlled element dynamics, however, and did not have an appreciable effect on tracking errors, although in the G_y case extrapolation from the present results suggests that low-frequency motions (<1 Hz) represent a potential problem.

B. RECOMMENDATIONS

While the results presented here give new insight into vibration effects on manual control performance, the experimental setup was somewhat of an abstracted laboratory situation, and future research should be directed towards more operational conditions. Some suggestions follow for future research that could build on the present results:

1. Vibration Environment

The present results should be extended to the random vibration regime, including narrow and wide-band spectra (typical of fuselage bending and buffeting, respectively). The feedthrough models should be verified and extended with random describing function measurements. Two-axis vibration cases should also be considered, such as the cyclic x-y motions common to rotor craft. Finally, the problem of closed-loop-pilot/vehicle-induced bending vibrations in large flexible aircraft should be carefully simulated in order to determine how pilots behave under such conditions and to explore, both analytically and experimentally, various means for minimizing such problems.

2. Control Sticks

The results obtained here under lateral vibration demonstrate the profound effect control stick characteristics can have on manual control performance under vibration. Research should now be conducted with operational control configurations (such as centersticks, with appropriate detents and spring gradients and wheel columns). In view of the current interest in fly-by-wire systems, side-mounted controllers should be investigated, with attention devoted to the proper support of the forearm and elbow for vibration resistance.

3. Tasks

The single axis tracking tasks used in this research provided only a small workload to the subjects. This was adequate for the fundamental phenomena studied here, but they may be inadequate to reveal some of the subtler general stress effects of vibration (e.g., aversion, arousal, fatigue). Two axis tasks should be employed in the future, with some operational relevance, such as pitch/roll tracking. The task induced workload should be set at relatively high levels in order to make operator behavior more sensitive to vibration stress.

4. Modeling and Analysis

The modeling effort for the present research, while greatly simplified and somewhat preliminary, has yielded considerable insight into the basic vibration control feedthrough phenomenon. Further analysis and elaboration of the situations studied here should be pursued, and new situations should be analyzed (e.g., side sticks with various types of forearm supports).

Particularly important is a study of the detailed nature of the large error remnant observed under all vibration conditions. Because of the diffuse nature of possible remnant sources (such as: perceptual and motor thresholds, time delay variations, gain fluctuations, etc.), an ensemble of tasks, conditions, and analyses must be employed to isolate the various causes (e.g., see Ref. 24).

REFERENCES

1. Buckhout, Robert, A Working Bibliography on the Effects of Motion on Human Performance, MRL-TDR-62-77, July 1962.

2. Linder, Gerald S., "Mechanical Vibration Effects on Human Beings," Aerospace Medicine, Vol. 33, No. 8, Aug. 1962, pp. 939-950.

3. Chiles, W. Dean and Carolyn L. Custer, Summaries of Research on the Human Performance Effects of Vibration, AMRL TR 77-172, Nov. 1963.

4. Guignard, J. C., "Vibration," A Textbook of Aviation Physiology, J. A. Gillies, ed., Pergamon Press, New York, 1965, pp. 813-894.

5. von Gierke, H. E., "Response of the Body to Mechanical Forces, An Overview," Lectures in Aerospace Medicine, Sixth Series, School of Aerospace Medicine, Brooks AFB, Texas, 6-9 Feb. 1967, pp. 325-344.

6. Roth, Emanuel M., ed., Compendium of Human Responses to the Aerospace Environment, Vol. II, Sections 7-9, NASA CR-1205(II), Nov. 1968.

7. Beaupeurt, J. E., F. W. Snyder, S. H. Brumaghim, et al, Ten Years of Human Vibration Research, Boeing Co. Wichita Div. Rept. No. D3-7888, Aug. 1969.

8. Rustenburg, John W., Development of Tracking Error Frequency Response Functions and Aircraft Ride Quality Design Criteria for Vertical and Lateral Vibration, ASD-TR-70-18, Jan. 1971.

9. Grether, Walter F., "Vibration and Human Performance," Human Factors, Vol. 13, No. 3, June 1971. pp. 203-216.

10. Shoenberger, Richard W., "Human Response to Whole-Body Vibration," Perceptual and Motor Skills, Monograph Supp. 1-V34, 1972, pp. 127-160.

11. Weis, Edmund B., Neville P. Clarke, James W. Brinkley, et al, "Mechanical Impedance as a Tool on Human Response to Acceleration," Aerospace Medicine, Vol. 35, No. 10, Oct. 1964, pp. 945-950.

12. Lee, Richard A. and Fred Pradko, Analytical Analysis of Human Vibration, SAE Paper No. 680091, Jan. 1968.

13. Magid, Edward B., Rolf R. Coermann and Gerd H. Ziegenruecker, "Human Tolerance to Whole Body Sinusoidal Vibration Short-Time, One-Minute and Three-Minute Studies," Aerospace Medicine, Vol. 31, No. 11, Nov. 1960, pp. 915-924.

14. Mandel, Morris J. and Richard D. Lowry, One-Minute Tolerance in Man to Vertical Sinusoidal Vibration in the Sitting Position, AMRL-TDR-62-121, Oct. 1962.

15. Aspinall, D. T. and R. J. Oliver, Vehicle Riding Comfort—The Correlation Between Subjective Assessments of Vehicle Ride and Physical Measurements of Vehicle Motion, Motor Industry Research Assn. Rept. No. 1964/10, Feb. 1964.

16. Bryce, W. D., A Review and Assessment of Criteria for Human Comfort Derived from Subjective Responses to Vibration, National Gas Turbine Establishment Rept. No. R. 286, Dec. 1966.

17. Van Deusen, Bruce D., Human Response to Vehicle Vibration, SAE Paper No. 680090, Jan. 1968.

18. McRuer, Duane, Dunstan Graham, Ezra Krendel and William Reisener, Jr., Human Pilot Dynamics in Compensatory Systems — Theory, Models, and Experiments with Controlled Element and Forcing Function Variations, AFFDL-TR-65-15, July 1965.

19. McRuer, D. T., L. G. Hofmann, H. R. Jex, et al, New Approaches to Human-Pilot/Vehicle Dynamic Analysis, AFFDL-TR-67-150, Feb. 1968.

20. Jex, Henry R., "Modeling Man-Machine Control Behavior in Biodynamic Environments," 1971 IEEE Systems, Man and Cybernetics Group Annual Symposium Record, Anaheim, Calif., Oct. 25-27, 1971, pp. 91-96.

21. Jex, H. R. and R. W. Allen, "Research on a New Human Dynamic Response Test Battery," Proceedings of the Sixth Annual Conference on Manual Control, Wright-Patterson AFB, Ohio, April 1970, pp. 743-777.

22a. Allen, R. Wade and Henry R. Jex, "A Simple Fourier Analysis Technique for Measuring the Dynamic Response of Manual Control Systems," IEEE Trans., Vol. SMC-2, No. 5, Nov. 1972, pp. 638-643.

b. Magdaleno, R. E., "Serial Segments Method for Measuring Remnant," IEEE Trans., Vol. SMC-2, No. 5, Nov. 1972, pp. 674-678.

23a. Levison, W. H., S. Baron and D. L. Kleinman, "A Model for Human Controller Remnant," IEEE Trans., Vol. MMS-10, No. 4, Dec. 1969, pp. 101-107.

b. Jex, H. R. and R. E. Magdaleno, "Corroborative Data on Normalization of Human Operator Remnant," IEEE Trans., Vol. MMS-10, No. 4, Dec. 1969, pp. 137-139.

24. Jex, Henry R., R. Wade Allen and Raymond E. Magdaleno, Display Format Effects on Precision Tracking Performance, Describing Functions, and Remnant, AMRL-TR-71-63, Aug. 1971.

25. Allen, R. W. and Henry R. Jex, Visual-Motor Response of Crewmen During a Simulated 90-Day Space Mission as Measured by the Critical Task Battery, NASA CR- , forthcoming (published in part previously in NASA SP-261, pp. 421-435).

26. Braune, W., O. Fischer, J. Amar and W. T. Dempster, Human Mechanics: Four Monographs Abridged, AMRL-TDR-63-123, Dec. 1963.

27. Schubert, Dale W., Jerome S. Pepi and Frank E. Roman, Investigation of the Vibration Isolation of Commercial Jet Transport Pilots during Turbulent Air Penetration, NASA CR-1560, July 1970.

28. Ashkenas, Irving L., Henry R. Jex and Duane T. McRuer, Pilot Induced Oscillations: Their Cause and Analysis, Systems Technology, Inc., TR-239-2, 20 June 1964 (also Northrop-Norair Rept. NOR 64-143).

29. Coermann, Rolf R., The Mechanical Impedance of the Human Body in Sitting and Standing Position at Low Frequencies, ASD TR-61-492, Sept. 1961.

30. Primiano, F. P., Jr., R. D. Lowry and N. P. Clarke, Distortion Analysis of the Acceleration Produced by the Western Gear Corporation Model 4010 High Amplitude Vibration Machine, AMRL-TR-65-27, April 1965.

31. Shoenberger, Richard W., Human Performance as a Function of Direction and Frequency of Whole-Body Vibration, AMRL-TR-70-7, Oct. 1970.

32. Allen, R. W., The Effect of Measurement Duration on Describing Function Estimates, Systems Technology, Inc., WP-175-18, Oct. 1970.

33. Guignard, J. C. and A. Irving, "Measurements of Eye Movements During Low Frequency Vibration," Aerospace Medicine, Vol. 33, No. 10, Oct. 1962, pp. 1230-1238.

34. Drazin, D. H., Factors Affecting Vision During Vehicular Vibration, Royal Air Force, Farnsborough, Inst. of Aviation Medicine, May 1962.

35. Jones, G. Melvill and D. H. Drazin, Oscillatory Motion in Flight, Air Ministry, Flying Personnel Research Committee, FPRC/1168, July 1961.

36. Taub, Harvey A., Dial-Reading Performance as a Function of Frequency of Vibration and Head Restraint System, AMRL-TR-66-57, April 1966.

37. Rubenstein, L. and H. A. Taub, Visual Acuity During Vibration as a Function of Frequency, Amplitude and Subject Display Relationship, AMRL-TR-66-181, June 1967.

38. Shoenberger, Richard W., Investigation of the Effects of Vibration on Dial Reading Performance with a NASA Prototype Apollo Helmet, AMRL-TR-67-205, Feb. 1968.

39. Rubinstein, L. and R. Kaplan, Some Effects of Y-Axis Vibration on Visual Acuity, AMRL-TR-68-19, June 1968.

40. Hornick, Richard J., Charles A. Boettcher and Allison K. Simons, The Effect of Low Frequency, High Amplitude, Whole Body, Longitudinal and Transverse Vibration upon Human Performance, Bostrom Research Labs., July 1961.

41. Weisz, A. Z., R. W. Allen and C. J. Goddard, An Evaluation of Three Types of Hand Controllers under Random Vertical Vibration, Hughes Aircraft Company RM-837, Oct. 1965, reported in NASA SP-128.

42. Weisz, A. Z., Connie Goddard and R. W. Allen, Human Performance under Random and Sinusoidal Vibration, AMRL-TR-65-209, Dec. 1965.

43. Holland, C. L., Jr., Performance and Physiological Effects of Long Term Vibration, AMRL-TR-66-145, Oct. 1966.

44. Besco, Robert O., "The Effects of Cockpit Vertical Accelerations on a Simple Piloted Tracking Task," Human Factors, Vol. 3, No. 6, Dec. 1961, pp. 229-236.

45. Wempe, Thomas E., Effects of Gust-Induced and Maneuvering Acceleration Stress on Pilot-Vehicle Performance, NASA TM X-54,063 (paper presented at the 35th Aerospace Medical Assn. Meeting, Miami, Fla., 11-13 May 1964).

46. Soliday, S. M. and B. Schohan, A Simulator Investigation of Pilot Performance during Extended Periods of Low-Altitude, High-Speed Flight, NASA CR-63, June 1964.

47. Rosenberg, Bruce and Robert Segal, The Effects of Vibration on Manual Fire Control in Helicopters, Franklin Institute Research Labs. Tech. Rept. 1-168, Mar. 1966.

48. Gordon-Smith, M., An Investigation into Certain Aspects of the Describing Function of a Human Operator Controlling a System of One Degree of Freedom, Univ. of Toronto, UTIAS Rept. No. 149, Feb. 1970.

49. Hald, A., Statistical Theory with Engineering Applications, John Wiley and Sons, Inc., New York, 1952.

50. Jex, H. R., G. L. Teper, D. T. McRuer and W. A. Johnson, A Study of Fully-Manual and Augmented-Manual Control Systems for the Saturn V Booster Using Analytical Pilot Models, NASA CR-1079, July 1968.

51. Magdaleno, Raymond E., Duane T. McRuer, and George P. Moore, Small Perturbation Dynamics of the Neuromuscular System in Tracking Tasks, NASA CR-1212, Dec. 1968.

52. Magdaleno, R. E. and D. T. McRuer, Experimental Validation and Analytical Elaboration for Models of the Pilot's Neuromuscular Subsystem in Tracking Tasks, NASA CR-1757, April 1971.

53. Magdaleno, R. E. and D. T. McRuer, Effects of Manipulator Restraints on Human Operator Performance, AFFDL-TR-66-72, Dec. 1966.

54. Graham, Dunstan and Duane McRuer, Analysis of Nonlinear Control Systems, John Wiley and Sons, Inc., New York, 1961.

55. McCormick, Ernest J., Human Engineering, McGraw-Hill Book Company, Inc., New York, 1957.

56. DiMasi, Frank P., Rush E. Allen, and Peter C. Calcaterra, Effect of Vertical Active Vibration Isolation on Tracking Performance and on Ride Qualities, NASA CR-2146, Nov. 1972.

57. Schaffer, J. T., Vibration Isolation Effects on Pilot Performance, presented at the meeting of the Aerospace Medical Association, Houston, Texas, 26-29 April 1971.

APPENDIX A

DERIVATION OF A VERTICAL VIBRATION FEEDTHROUGH MODEL AND DATA COMPARISON

A. PHYSICAL SETUP

A preliminary model for the feedthrough dynamics for vertical sine wave acceleration was derived from an analysis of transmissibility and control feedthrough data. The data were taken over a frequency range or 2-10 Hz while the subject was nulling the CRT display (no forcing function) with approximate short-period dynamics as the controlled element*:

$$Y_c = \frac{K_c(s + 1/T_\theta)}{s(s^2 + 2\zeta_{sp}\omega_{sp}s + \omega_{sp}^2)} \qquad \text{(A-1)}$$

where $K_c = 2.56$ cm display/cm stick
$1/T_\theta = 1.42$ rad/sec
$\zeta_{sp} = 0.56$
$\omega_{sp} = 1.71$ rad/sec

A more complete description of the tracking task is given in Section III.

Figure A-1 shows the setup and anthropometric data for the three subjects used in the vertical vibration experiment. This first-cut modeling effort concentrated on the spring restrained stick for simplicity since the low spring rate resulted in low stick forces and thus would not load down or affect the basic body motion which takes place between seat and shoulder. Further, we assumed massless arm linkage elements connecting the shoulder to the stick; thus only arm linkage kinematics need be considered.

B. MODEL DERIVATION

Vertical body motion dynamics have been measured and modeled (Refs. A-1 — A-7), and in Ref. A-1 a multimode mass-spring damper model is used to explain

*The complex variable, s, has units of rad/sec. Transmissibility data have traditionally been plotted with a frequency axis in Hz (cycles/sec) where ω(rad/sec) = 2πf (Hz), and some figures here follow this precedent.

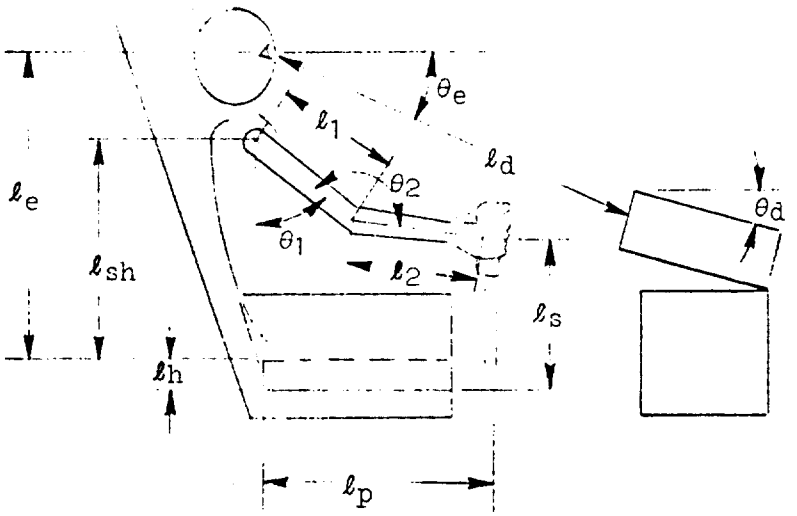

ℓ_h = 11 in. ℓ_s = 15 1/2 in.

ℓ_p = 18 in. θ_d = 20 deg

DIMENSION	SUBJECT		
	JS	BB	DZ
ℓ_1	13.5 in.	11.5 in.	14 in.
ℓ_2	13.75 in.	12 in.	14 in.
ℓ_d	22.5 in.	27 in.	30.5 in.
ℓ_e	27 in.	25.75 in.	29.5 in.
ℓ_{sh}	21 in.	17.75 in.	22 in.
ℓ_T	24.8 in.	23.4 in.	
℄ to Shoulder	8.5 in.	7.5 in.	8.5 in.
℄ to Elbow	7 in.	5 in.	6.5 in.
θ_1	30 deg	65 deg	45 deg
θ_2	130 deg	170 deg	160 deg
θ_3	25 deg	5 deg	10 deg
θ_e	30 deg	20 deg	32 deg

Figure A-1. Pilot Study Setup and Anthropometric Data

a variety of reasonance effects amongst whole body and internal organ motions. For our purposes we shall use the simple spring-mass-damper model shown in Fig. A-2 for the motion of the shoulder relative to the platform. The massless links then connect shoulder motion to the top of the stick.

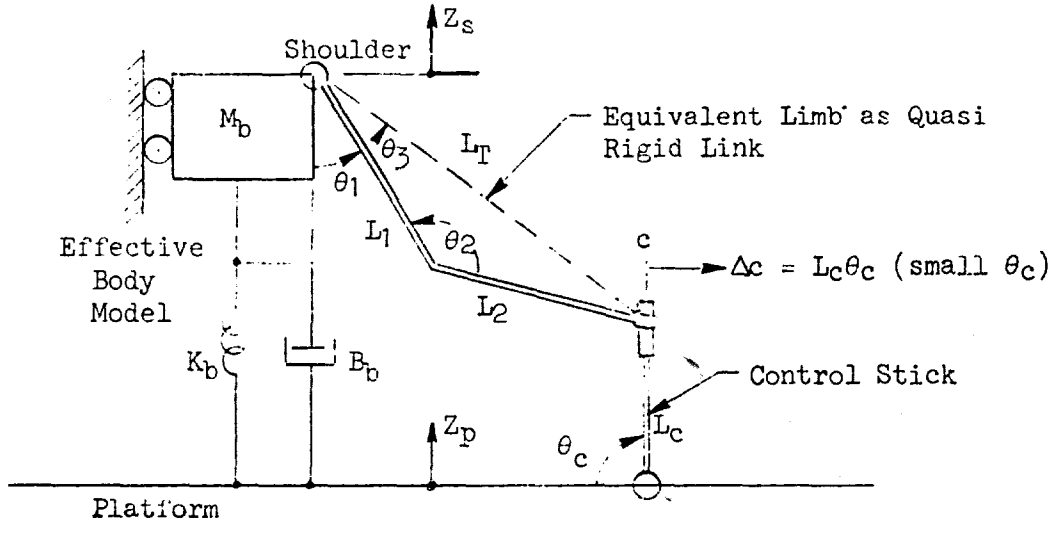

Assumption: No horizontal shoulder motion

Note: For convenience z axis assumed positive upwards.

Figure A-2. Simplified Body Motion Model and Arm Linkage to Center Stick

The transmissibility between the platform and shoulder is:

$$\frac{a_{z_s}}{a_{z_p}} = \frac{z_s}{z_p} = \frac{B_b s + K_b}{M_b s^2 + B_b s + K_b} \qquad \text{(A-2)}$$

where the spring and damper include some effects from the seat cushion. The same model form was considered in Ref. A-2 where data was obtained with no seat cushion. Complex impedance was measured which is the ratio of the transmitted force to the velocity at that point where the force is applied. Figure A-3 (from Ref. A-2) shows a comparison of the Fig. A-2 model form with data for the Sitting Erect situation. The fit is very good up to the resonant peak and gives a good approximation to the data out to 17 Hz.

For Sitting Erect Data

Spring = 131×10^6 dyne/cm

Damper = 1.9×10^6 dyne sec/cm

Mass = 84,000 dyne sec^2/cm

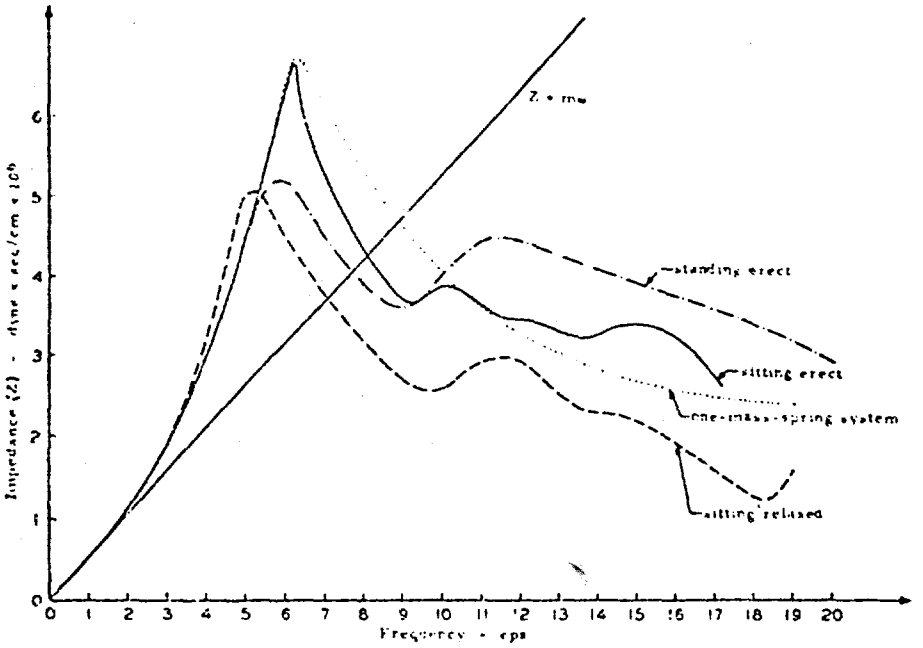

The Modulus of the Impedance of One Subject at Varied Body Postures Compared with the Impedance of a Pure Mass (mω) and of a One-Mass-Spring System with Damping

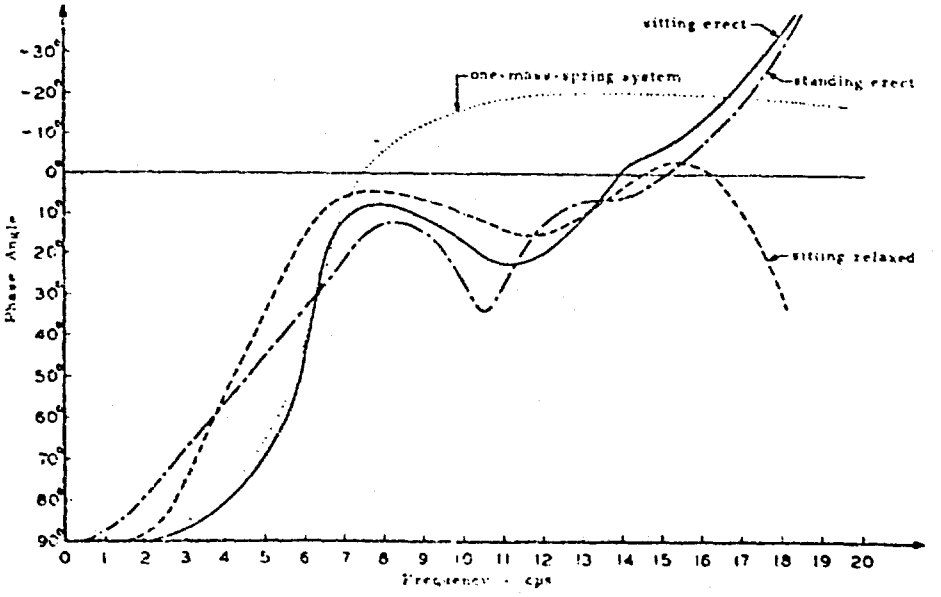

Phase Angle of the Impedance for One Subject at Varied Body Postures Compared with Phase Angle of a One-Mass-Spring System with Damping

Figure A-5. Modulus and Phase of the Impedance (from Coerman, Ref. A-2)

It can be shown that this impedance function is simply related to the transmissibility as in Eqs. A-3 and A-4.

$$\text{Impedance} = M_b s\left(\frac{a_{z_s}}{a_{z_p}}\right) = \frac{M_b s(B_b s + K_b)}{M_b s^2 + B_b s + K_b} \tag{A-3}$$

$$= \frac{B_b s[s + \gamma_b]}{[s^2 + 2\zeta_b \omega_b s + \omega_b{}^2]} \tag{A-4}$$

where

$$\gamma_b = K_b/B_b = 2\pi(11) = 69.1$$
$$\zeta_b = 1/2\ B_b(K_b M_b)^{-1/2} = 0.285$$
$$\omega_b = (K_b/M_b)^{1/2} = 2\pi(6.3) = 39.6$$

In Fig. A-2 the shoulder motion that results from vertical platform vibration drives the linkage, L_1, L_2, which connects to the top of the center stick.

For low frequency vibration the model mass, M_b, moves essentially in phase with the platform and there is very little vibration input into the stick. For frequencies at and above resonance the mass lags the platform, causing the shoulder to top of stick distance to change, resulting in vibration feedthrough into the stick and thence into the tracking loop.

Not shown in Fig. A-2 are the muscles which torque links L_1 and L_2 about the shoulder and elbow. For simplicity we shall analyze the data as if the muscles were tense enough so that the shoulder-to-top-of-stick distance (L_T in Fig. A-2) were constant — thus when the shoulder lags an upward moving platform the stick is pushed forward. This quasi-rigid link assumption simplifies the problem considerably. However we shall formulate the link kinematics for the general case so as to evaluate the rigid link assumption.

The equation for the instantaneous velocity at the top of the stick is as follows (every term in Eq. A-5 is a vector):

$$\dot{Z}_p + \omega_c \times L_c = \dot{Z}_s + \omega_1 \times L_1 + \omega_2 \times L_2 \tag{A-5}$$

where

ω_c = angular velocity of stick (positive into the paper)

ω_1, ω_2 are the angular velocities of links 1 and 2 (both assumed positive in the counterclockwise direction)

Separately evaluating the horizontal and vertical components yields the scalar equations:

$$\dot{c} = [L_1 \cos \theta_1] \omega_1 + [L_2 \sin (\theta_2 - \theta_1 - \tfrac{\pi}{2})] \omega_2 \quad \text{(A-6)}$$

$$\dot{Z}_p = \dot{Z}_s + [L_1 \sin \theta_1] \omega_1 + [L_2 \cos (\theta_2 - \theta_1 - \tfrac{\pi}{2})] \omega_2 \quad \text{(A-7)}$$

where $(\theta_2 - \theta_1 - \frac{\pi}{2})$ is the angle of L_2 from the horizontal. For small perturbations about an operating point all the terms in square brackets in Eqs. A-6 and A-7 are constants. Therefore differentiating both sides of Eqs. A-6 and A-7 and eliminating terms involving $\dot{\omega}_2$ yields:

$$\ddot{c} = [\tan (\theta_2 - \theta_1 - \tfrac{\pi}{2})](a_{z_p} - a_{z_s}) + \left[L_1 \frac{\sin \theta_2}{\sin(\theta_2 - \theta_1)}\right] \omega_1 \quad \text{(A-8)}$$

Stick motion depends on the difference between platform and shoulder $(a_{z_p} - a_{z_s})$ as well as upper arm angular motion (ω_1).

For the rigid link assumption L_1, L_2, and L_T rotate together (i.e., $\omega_2 \equiv \omega_1$); thus Eqs. A-6 and A-7 could be rewritten in terms of L_T and its angle as:

$$\dot{c} = [L_T \cos (\theta_1 + \theta_3)] \omega_1 \quad \text{(A-9)}$$

$$\dot{Z}_p = \dot{Z}_s + [L_T \sin (\theta_1 + \theta_3)] \omega_1 \quad \text{(A-10)}$$

Differentiating both sides of Eqs. A-9 and A-10 and eliminating ω_1 yields

$$\ddot{c} = [\operatorname{ctn} (\theta_1 + \theta_3)](a_{z_p} - a_{z_s}) \quad \text{(A-11)}$$

which depends only on the differential body motion between platform and shoulder. Finally, a more convenient form of Eq. A-11 is to solve for the stick-deflection-to-platform acceleration transfer function:

$$\frac{c}{a_{z_p}} = [\text{ctn}\,(\theta_1 + \theta_3)] \left[\frac{1 - (a_{z_s}/a_{z_p})}{s^2} \right] \qquad \text{(A-12)}$$

Thus the rigid link assumption has led to Eq. A-12 which describes the vertical feedthrough dynamics, Y_{vz}, of Fig. 2 in Section II. This model shows that the pitch control feedthrough due to vertical vibration is determined by the vertical platform-to-shoulder transmissibility and is scaled by the cotangent of $(\theta_1 + \theta_3)$. These angles are given in Fig. A-1 for each of the subjects.

The rigid link assumption can be evaluated by inserting data measurements of (a_{z_s}/a_{z_p}) into Eq. A-12 and comparing with direct (c/a_{z_p}) measurements. A similar check is to curve fit spring-mass, damper values to fit (a_{z_s}/a_{z_p}), and insert them into the "model" equation:

$$\frac{c}{a_{z_p}} = \frac{\text{ctn}\,(\theta_1 + \theta_3)}{s^2 + (B_b/M_b)s + (K_b/M_b)} \qquad \text{(A-13)}$$

C. DATA INTERPRETATION WITH RIGID LINK MODEL

The frequency measurements obtained in the vertical study used sine wave platform vibrations of 0.4 g zero-to-peak from 2 to 10 Hz. Stick position as well as head, shoulder and elbow accelerations were recorded. Figures A-4 and A-5 are representative traces at 4 Hz for subject BB, from which (a_{z_s}/a_{z_p}) and $c/a_{z_p})$ data were evaluated.

Points worth noting from Figs. A-4 and A-5 are:

- Shoulder and elbow vertical motions are closely in phase, justifying the quasi-rigid link assumption. This occurs at most frequencies up to 7-8 Hz.

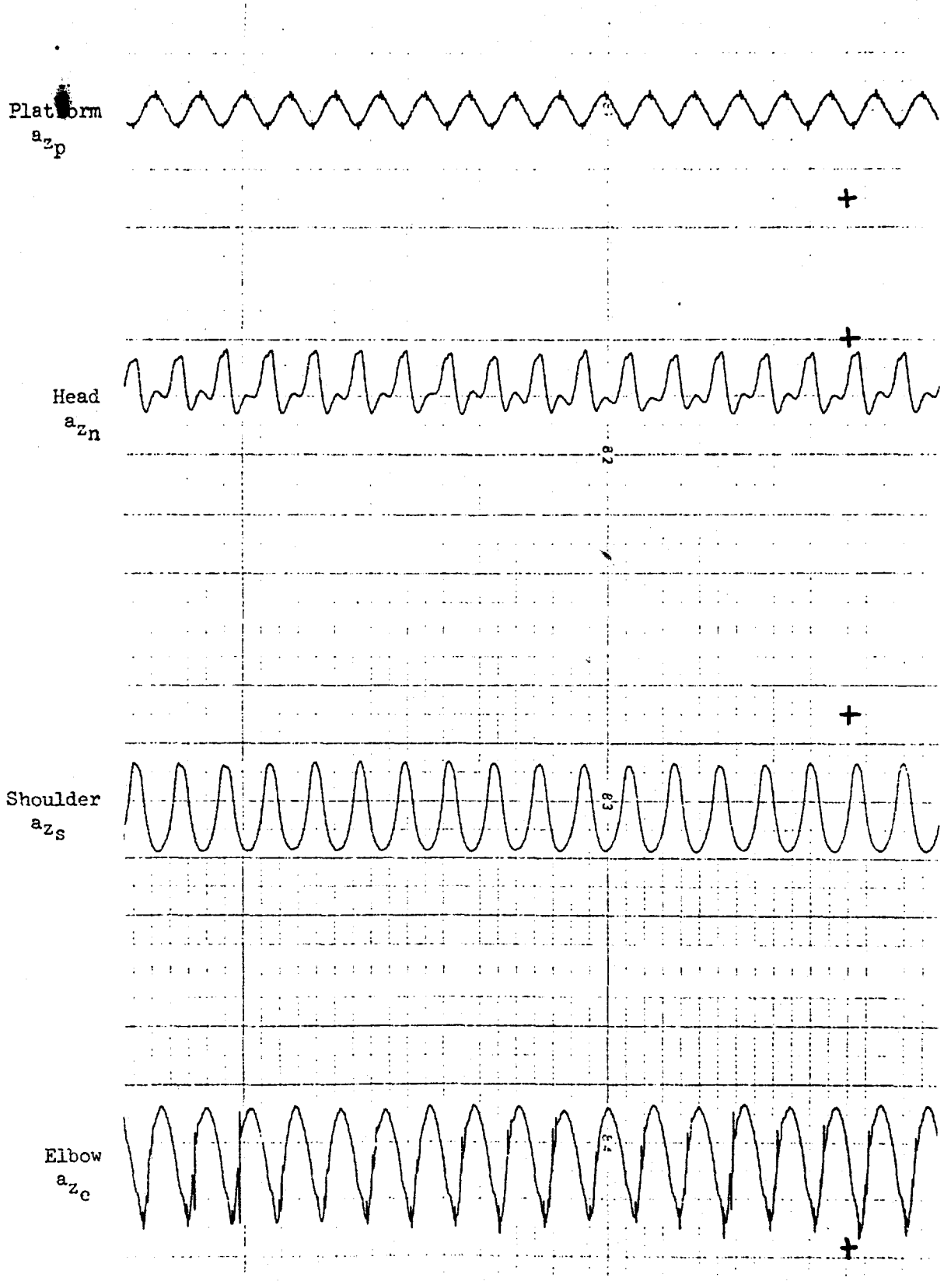

Figure A-4. Typical Acceleration Traces at 4 Hz, Subject BB.

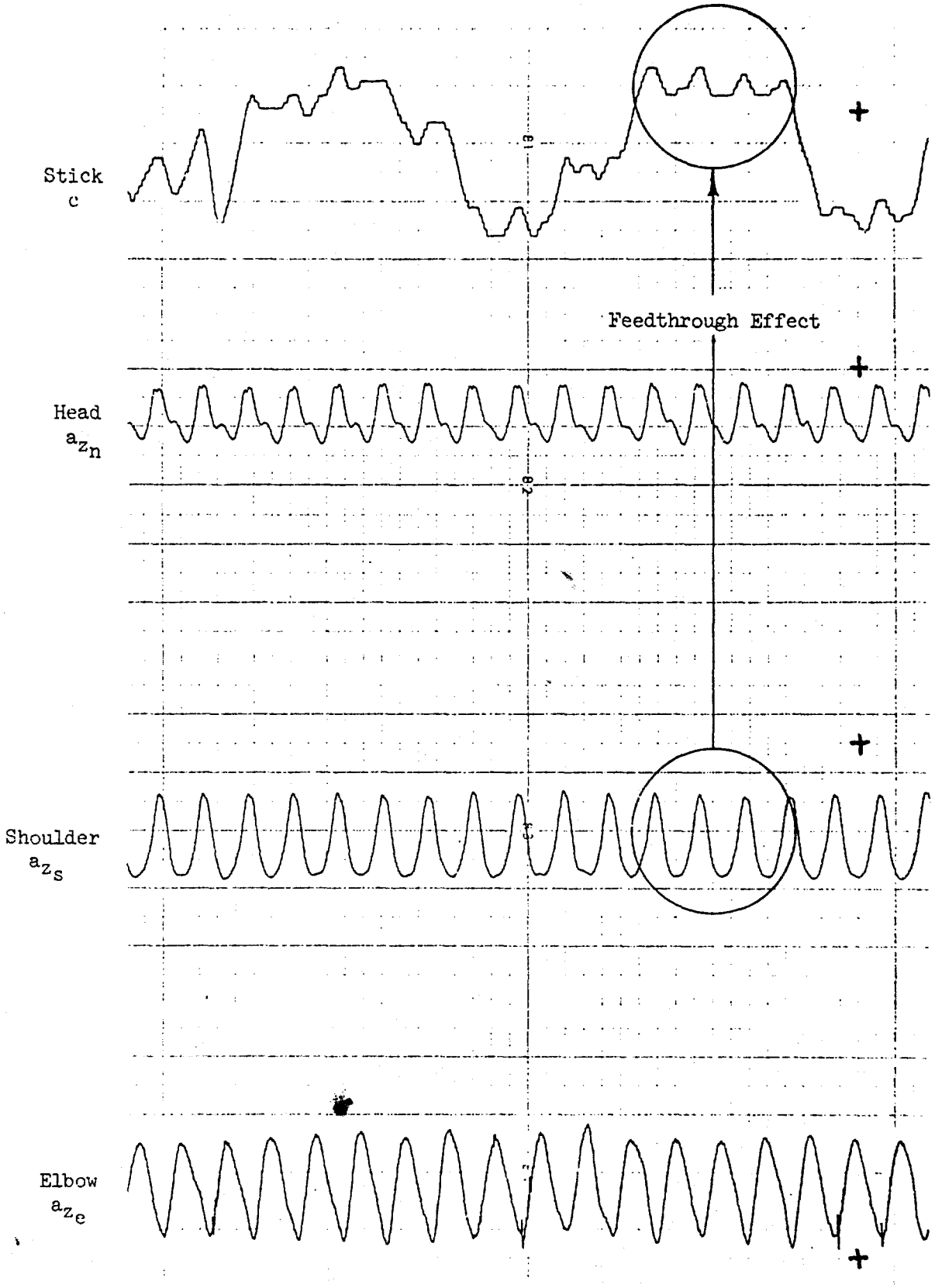

Figure A-5. Acceleration and Stick Traces at 4 Hz, Subject BB

- Stick feedthrough motion actually leads the shoulder acceleration somewhat, because the stick motion depends on the difference between platform and shoulder motions.

- Although the feedthrough frequency is apparent in the control stick trace, it tends to be masked somewhat by additional tracking control components.

Figure A-6 shows the vertical transmissibility data for the two most extreme subjects; BB whose hand and arm was extended, and JS who had the most rearward elbow position (Fig. A-1). Also shown in Fig. A-6 is a curve fit to the data using the platform to shoulder model form in Fig. A-2 and Eq. A-2. BB's data is very closely fit by the model, while JS's data is closely fit up to the resonant peak then falls under, just above the peak, and finally returns to the curve at 10 Hz. JS's data relative to the model curve is quite similar to that in Fig. A-3 for the Sitting Erect case measurements versus the spring-mass-damper model. However there is evidence from his time traces and via observations that he occasionally changed position between runs (i.e., between frequencies).

BB's data has a flat spot near 8-10 Hz which resembles that in Fig. A-7 for Shoulder/Seat. The implication is that this effect reflects a head-on-shoulder mode — however this is a second order effect and the simple model fits the basic data trend in both amplitude and phase very well.

Figure A-7 compares the measured feedthrough dynamics (Y_{vz}) with that predicted by the quasi-rigid linkage model (Eq. A-12) using the subject's measured transmissibility dynamics. Also shown is the predicted feedthrough dynamics using the transmissibility model fit from Fig. A-6 in Eq. A-14. The measured and predicted feedthrough dynamics agree quite well for subject BB. The predicted amplitude ratio is about 2.5 dB or 30% high in the region of the resonant peak and the phase data agree closely beyond 4 Hz. The phase shifts at 3 Hz and below were hard to measure from the strip chart records and are not very reliable. The feedthrough predictions for subject JS are not in as good agreement with the measurements as for subject BB, with differences on the order of 6 dB (a factor of 2) in the region of the resonant peak. JS had greater elbow flexon than BB, however, and the rigid link model may be a poorer approximation for this case.

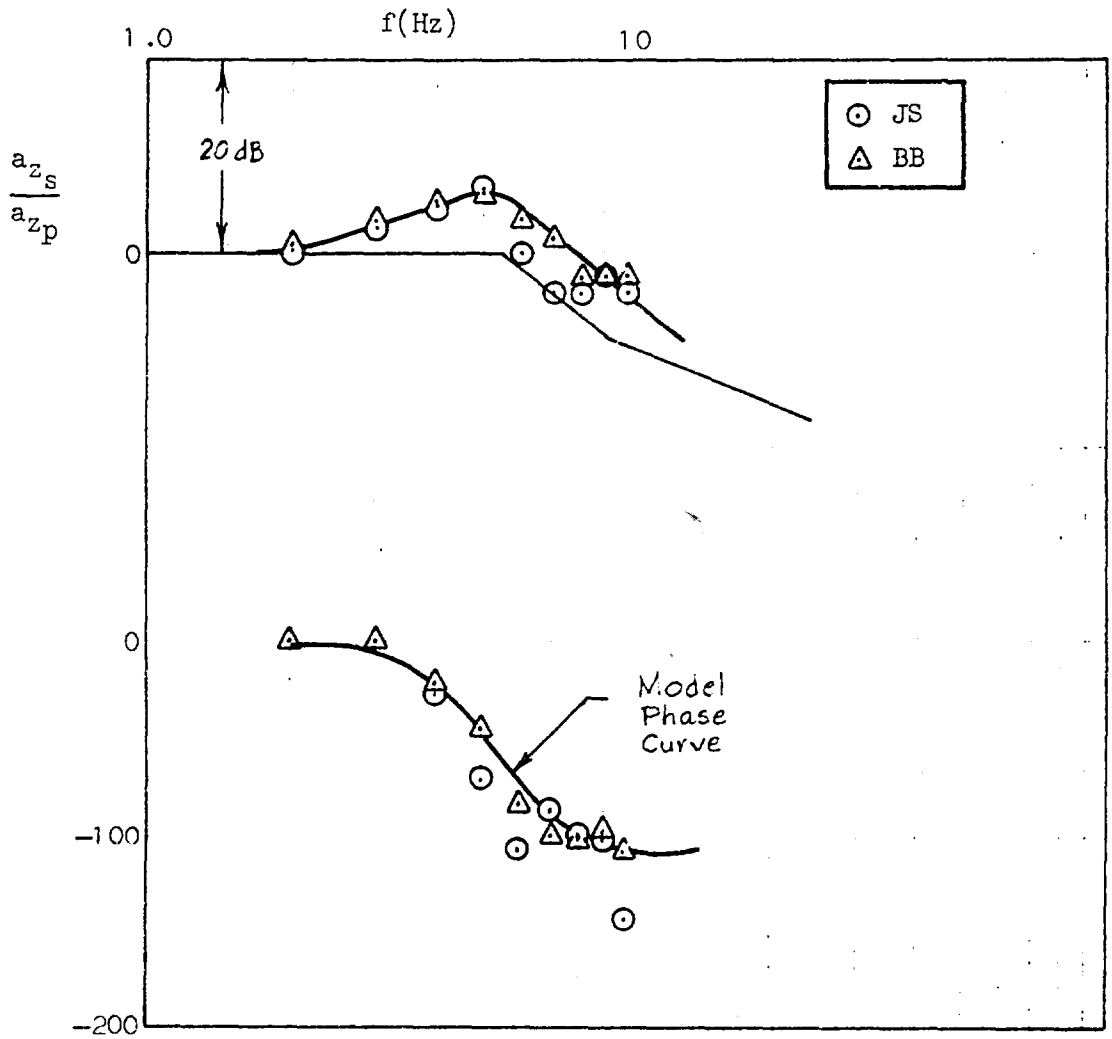

Model Curve Fit

$$\frac{[1 + (s/57.8)]}{[1 + 2(0.3)(s/34.5) + (s/34.5)^2]}$$

$$s = (2\pi f)j$$

Figure A-6. Transmissibility Data and Model Fit (Lightly Spring Restrained Stick)

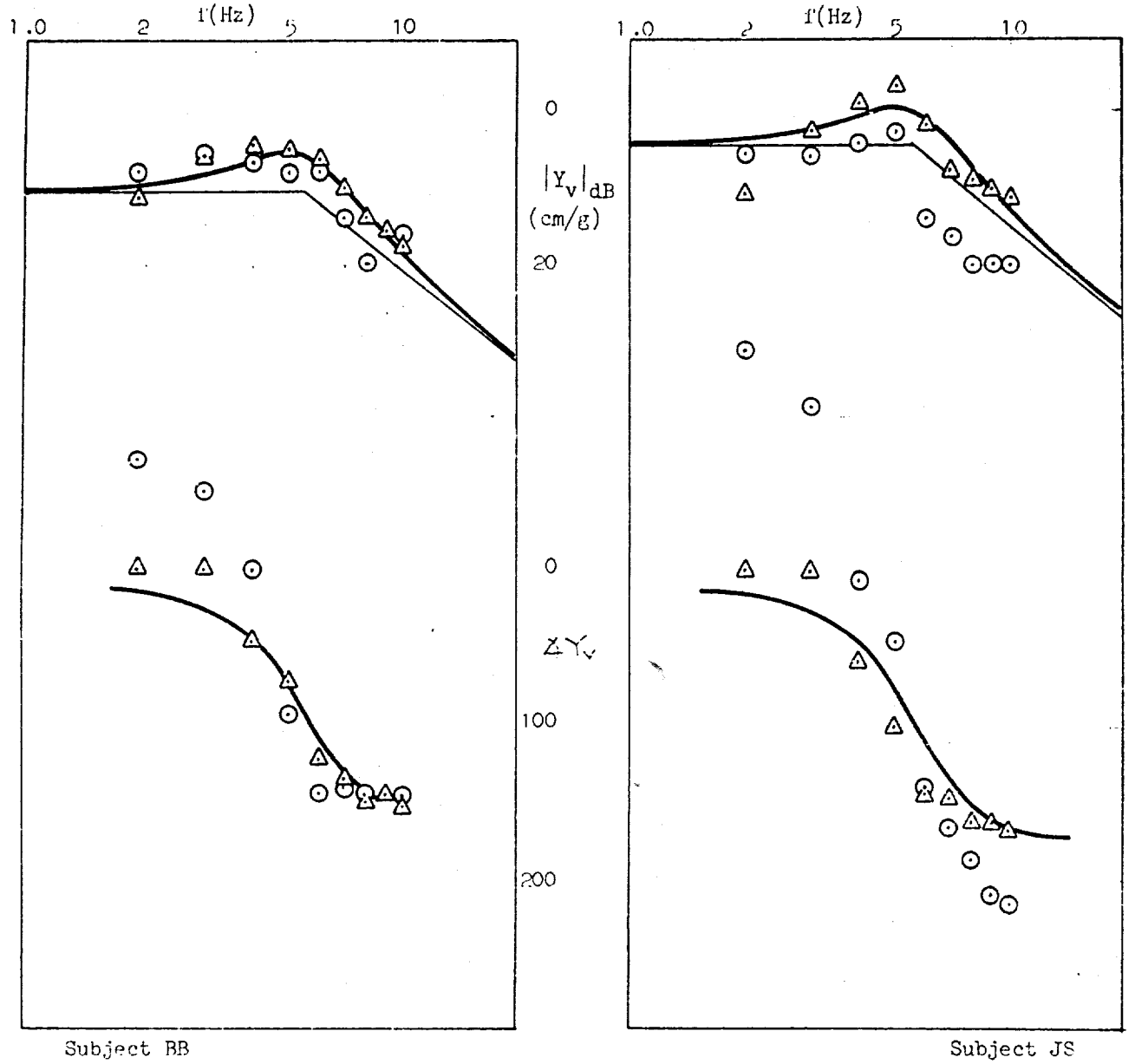

○ Measured Y_v

$\angle$ Y_v Predicted from Transmissibility Measurements

—— Y_v Predicted from Model Fit to Transmissibility

$$981\,(c/a_{zp})$$

$$[981 \text{ ctn } (\theta_1 + \theta_3]\left(\frac{1 - \frac{a_{z_s}}{a_{z_p}}(s)}{s^2}\right)_{s\,=\,2\pi fj}$$

$$\frac{981 \text{ ctn } (\theta_1 + \theta_3)}{\left(s^2 + 2(0.3)(34.5)s + (34.5)^2\right)_{s\,=\,2\pi fj}}$$

Figure A-7. Vibration Feedthrough Frequency Response Data

Given the crude testing and measurement methods, however, the simple feedthrough model developed here is surprisingly good in the following respects:

- It predicts the resonant second order nature of the feedthrough dynamics.
- The feedthrough resonant peak is closely matched.
- The order of magnitude of the feedthrough effect is correct, with one subject's data matching within 30%.

In addition the model is quite simple and is based on transmissibility dynamics which have been measured extensively by several investigators and are well understood.

REFERENCES FOR APPENDIX A

A-1. von Gierke, H. E., "Biodynamic Response of the Human Body," Applied Mechanics Reviews, Vol. 17, Dec. 1964.

A-2. Coermann, Rolf R., The Mechanical Impedance of the Human Body in Sitting and Standing Position at Low Frequencies, ASD Tech. Rept. 61-492, Sept. 1961.

A-3. von Gierke, H. E., "Response of the Body to Mechanical Forces — An Overview," paper presented at the Conference on Prevention of and Protection against Accidental Explosion of Munitions, Fuels and Other Hazardous Mixtures, New York Academy of Sciences, New York, 10-13 Oct. 1966.

A-4. Schubert, Dale W., Jerome S. Pepi, and Frank E. Roman, Investigation of the Vibration Isolation of Commercial Jet Transport Pilots during Turbulent Air Penetration, NASA CR-1560, July 1970.

A-5. Weis, Edmund B., Neville P. Clarke, James W. Erinkley, et al., "Mechanical Impedance as a Tool on Human Response to Acceleration," Aerospace Medicine, Vol. 35, No. 10, Oct. 1964, pp. 945-950.

A-6. Lee, Richard A., and Fred Pradko, Analytical Analysis of Human Vibration, SAE Paper No. 680091, Jan. 1968.

A-7. Pradko, Fred, Theodore R. Orr, and Richard A. Lee, Human Vibration Analysis, SAE Paper No. 650426, May 1965.

APPENDIX B

DERIVATION OF LATERAL VIBRATION TRANSMISSIBILITY AND FEEDTHROUGH MODELS AND DATA COMPARISON

Body, limb, and control response due to lateral vibration is much more complicated than the vertical situation analyzed in Appendix A, because various components of the human/control stick system undergo rotational as well as translational motion. In this appendix we will develop equations of motion for the various components which combine to give control response due to vibration feedthrough (i.e., seat to shoulder transmissibility, limb/muscle dynamics, hand to stick interface dynamics and control stick dynamics). These components are combined into a matrix which allows computing transfer functions between vibration input (platform or seat acceleration) and various output responses such as shoulder motion (i.e., transmissibility, Y_{T_y}) and control response (i.e., lateral vibration control feedthrough, Y_{V_y}). Model response is compared with experimental data, and simplified models are presented to given insight into the lateral vibration feedthrough phenomenon. The experimental setup and techniques for obtaining validation data were similar to those described in Appendix A and Section III and are not repeated here.

A. GENERAL CONTROL STRUCTURE AND BIOMECHANICAL CONSIDERATIONS

A general manual control system structure for a single loop compensatory control task is shown in Fig. B-1. Here the operator commands his neuromuscular system (NMS) based on the state of the error signal. The NMS then moves the limb which in turn actuates the control stick. The neuromuscular, limb, and control stick dynamics are coupled and thus are not shown as separate blocks. Inputs from a motion environment enter the loop by acting directly on the control stick, and by causing limb motions due to shoulder motions transmitted through the operator's torso.

The biomechanical process causing motion induced control responses for lateral vibration are more clearly illustrated in Fig. B-2. Here major mechanical elements and assumptions for our lateral motion feedthrough

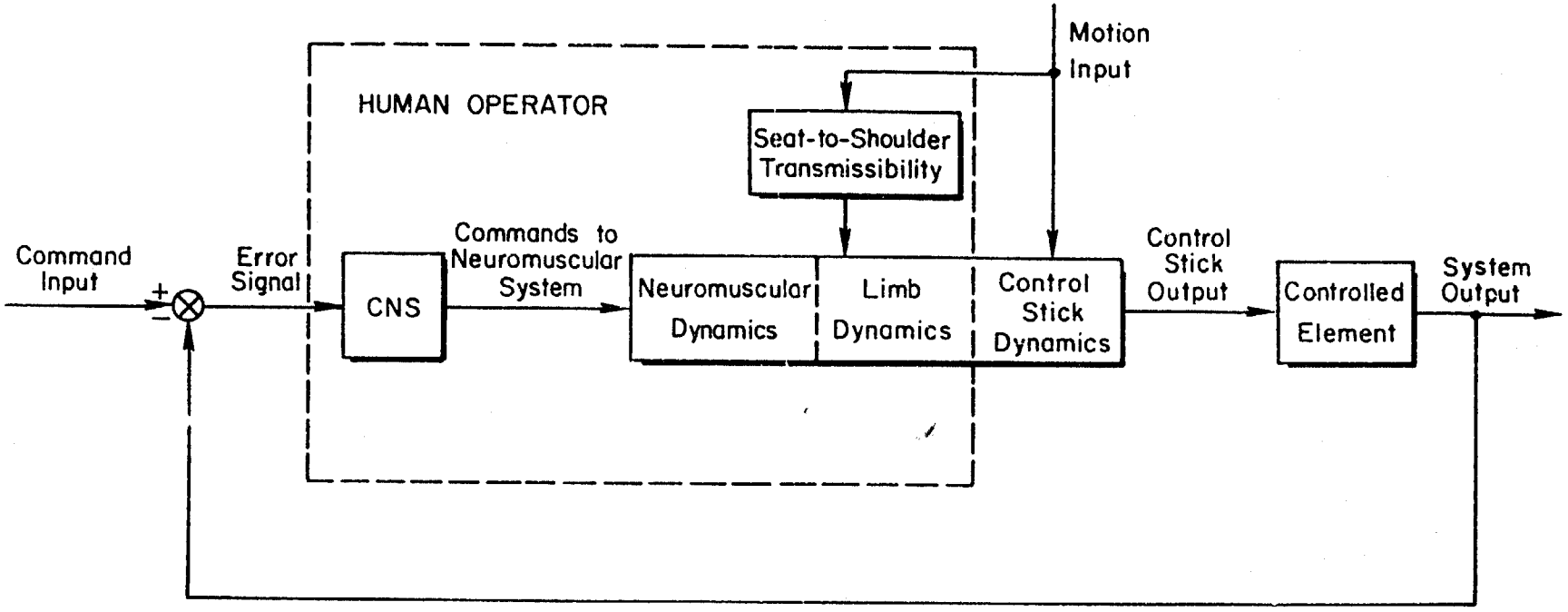

Figure B-1. Compensatory Manual Control System Structure

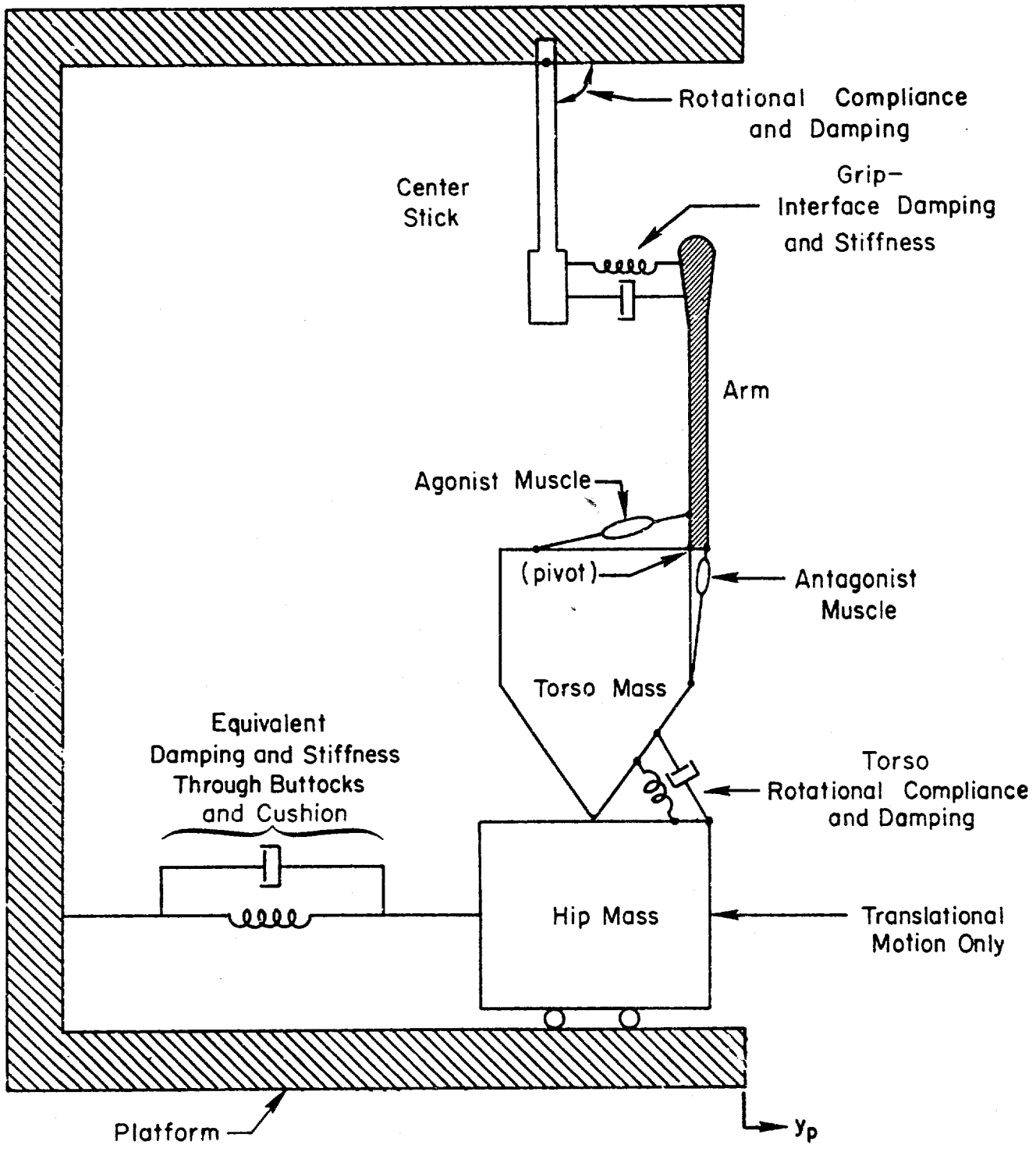

Figure B-2. Equivalent Mechanical System Model for Control Feedthrough Response Due to Vibration

model are illustrated for the subject seating position shown in Fig. 4 of the main text (Section III). The elements for the vertically positioned stick as well as upper torso plus hip body segments have been "folded flat" into the plane of lateral arm motions. The arm pivots about the shoulder and connects to the top of the center stick through interface damping and compliance. The arm is modeled by a simple solid inertial segment as independent motion at the elbow is not considered important based on observations during the experiment. The control stick has distributed mass and is restrained by rotational compliance and damping.

The arm is driven, relative to the shoulder, by agonist/antagonist muscle pairs for which our model will use one net muscle pair (Refs. B-2,-3). The torso is assumed to pivot as a solid body about the hip complex, and is restrained by rotational compliance and damping. The hip complex is shown undergoing pure translation only*, being restrained by compliance and damping provided by the subject using his legs to brace himself as well as by flesh movement at the seat cushion interface.

B. EQUATIONS OF MOTION

For y axis table inputs all the major mechanical elements in Fig. B-2 undergo small perturbation translations and possibly rotations about their respective c.g.'s. For this specialized case of planar motion we have used an equivalent two-degree-of-freedom translational equation set for each solid body (assuming small displacements). Thus instead of equations describing rotation about the c.g. and its translation, we are interested in the linear translations of two points on the body such as each end of the arm or the pivot point and hip attachment point for the torso in Fig. B-2. These are the interface points between the major segments that are involved in vibration feedthrough to the stick.

The equivalent two-degree-of-freedom equations of motion for a solid body (as adapted from Ref. B-1) are given below for the example in Fig. B-3.

---

*In the following subsection the equations of motion are derived assuming both translation and rotation. Rotational stiffness is then assumed large to fit the observation that hip translation was the dominant motion.

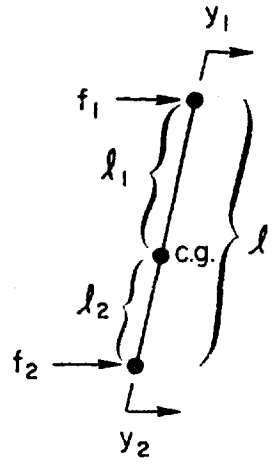

Figure B-3. Solid Body Undergoing Small Perturbation Linear Translation and Rotation

$$M_1\ddot{y}_1 + M_m\ddot{y}_2 = f_1$$

$$M_m\ddot{y}_1 + M_2\ddot{y}_2 = f_2 \qquad \text{(B-1)}$$

where

$$M_1 \triangleq M\left(\frac{\ell_2^2 + h^2}{\ell^2}\right) = \frac{J_1}{\ell^2}\text{, effective mass for end 1 (with end 2 fixed)}$$

$$M_2 \triangleq M\left(\frac{\ell_1^2 + h^2}{\ell^2}\right) = \frac{J_2}{\ell^2}\text{, effective mass for end 2 (with end 1 fixed)}$$

$$M_m \triangleq M\left(\frac{\ell_1\ell_2 - h^2}{\ell^2}\right)\text{, mutual mass}$$

where

h = radius of gyration about c.g.

M = mass of the body = $M_1 + 2M_m + M_2$

In this case forces and displacements of the body are defined as positive to the right. We've assumed that the c.g. is near the line connecting Points 1 and 2, and further that this line is nearly perpendicular to the y_1 and y_2 displacements. Equation Set B-1 describes the body response to

forces f_1 and f_2 in terms of the displacements y_1 and y_2 and the mass descriptors defined above. The mutual mass provides coupling between the y_1 and y_2 coordinate motions. M_1 and M_2 are equivalent translational masses as seen at their respective ends if the other end is constrained to act as a pivot. However the equations hold even if both ends are moving in space. Thus equation set B-1 gives a convenient description of the forces and displacements at the interfaces allowing simple coupling or uncoupling to other bodies. These equations will now be used to couple the rotating and translating masses of the torso, arm, and control stick in order to obtain an overall control feedthrough model.

1. Stick Dynamics

Applying Eq. B-1 to the center stick descriptors given in Fig. B-4 yields*

$$M_F s^2 c_i + M_{m_F} s^2 y_p = f_{c_a} - f_r \qquad \text{(B-2)}$$

$$M_{m_F} s^2 c_i + M_{F_1} s^2 y_p = f_p + f_r \qquad \text{(B-3)}$$

where

f_{c_a} = interface force applied by the hand to the top of the stick

c_i = inertial displacement of top of stick

y_p = inertial table displacement

f_p = platform force on the bottom of the stick

f_r = equivalent restraint forces = $(B_F s + K_F)(c_i - y_p)$

M_F = self mass at top of stick

M_{F_1} = self mass at bottom of stick

M_{m_F} = mutual mass

---

*All ensuing equations will be expressed in Laplace transform notation where s is a complex operator.

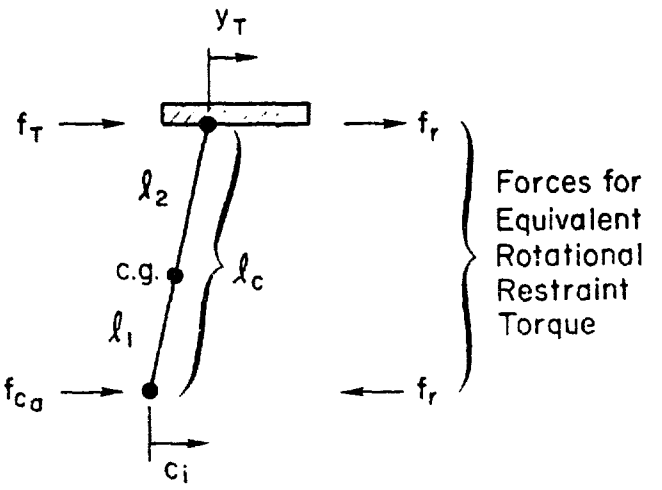

Figure B-4. Center Stick Forces and Displacements

Equation B-3 is not needed so long as we regard table position as the input and are not interested in the force, f_T, of the platform on the stick. Thus using the expression $c = c_i - y_T$ to eliminate the inertial stick position, c_i, allows Eq. B-2 to be written in terms of the relative stick displacement as

$$\left(s^2 + \frac{B_F s}{M_F} + \frac{K_F}{M_F}\right)c = \frac{f_{c_a}}{M_F} - L_F a_{y_p} \qquad \text{(B-4)}$$

where

c = $c_i - y_p$, the relative stick displacement that is the input to the controlled element (Fig. B-1)

$$L_F = \frac{M_F + M_{mF}}{M_F} = \frac{(\ell_2)(\ell_c)}{\ell_2^2 + h_c^2}$$

h_c = radius of gyration about stick c.g.

Note the L_F defined above is a "kinematic gain" which reflects the fact that the output signal depends on the physical locations of the c.g. and the point considered as the output signal as well as the mass distribution. For example, consider the case where the stick mass is concentrated at the top of the stick ($\ell_2 = \ell_c$, $h_c = 0$), then $L_F = 1$ and the high frequency response of Eq. B-4 indicates

$$\frac{s^2 c}{a_{y_p}} = -L_F = -1$$

Thus a step input of acceleration produces initially an equal and opposite acceleration of c; in this case because the mass at the top of the stick doesn't move initially when the bottom does. The polarity reverses if the c.g. is below the pivot point (i.e., "mass-overbalanced").

2. Seat-to-Shoulder Transmissibility

Figure B-5 details the forces and displacements in the simplified model for torso and hip dynamics that affect the arm pivot point (Fig. B-2). Here we have general rotational restraints, f_{B_r} on torso and f_L on hip. The latter restraint will later be assumed very stiff, however, such that the hip has only translation at the seat interface. We also assume that there is shearing in the cushion and buttocks, which allows hip translation relative to the seat, with attendant compliance, K_a, and damping, B_a.

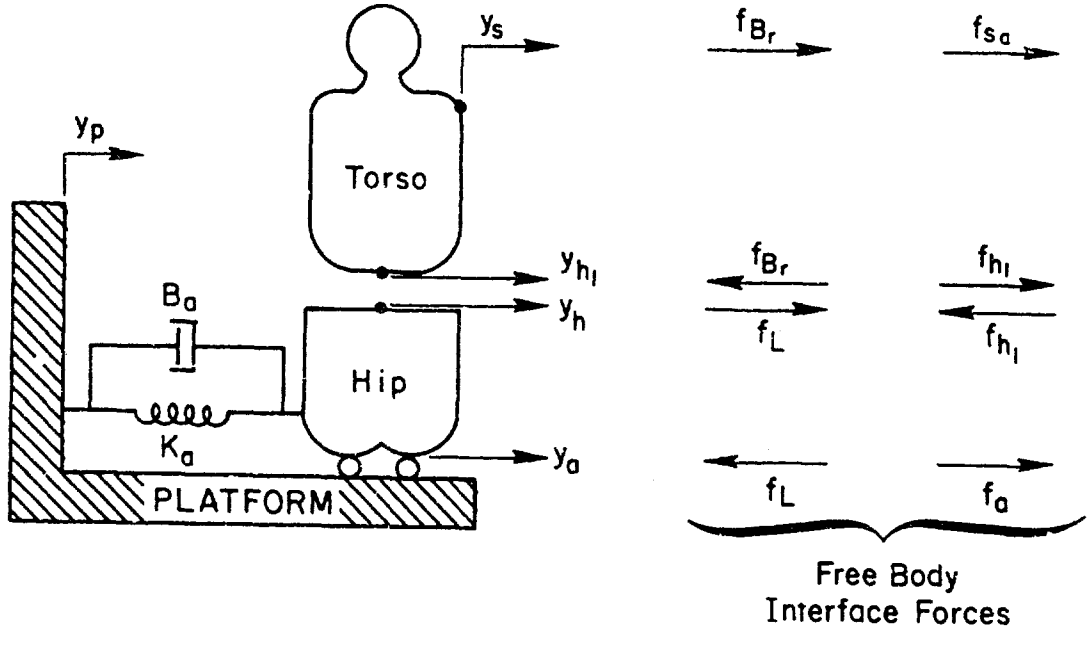

Figure B-5. Torso and Hip Forces, Displacements, and Restraints

Applying equation set B-1 separately to the torso and hip bodies yields

Torso:

$$M_{B_1}s^2y_s + M_{BM}s^2y_{h_1} = f_{s_a} + f_{B_r} \quad \text{(B-5)}$$

$$M_{B_m}s^2y_s + M_{B_2}s^2y_{h_1} = f_{h_1} - f_{B_r} \quad \text{(B-6)}$$

Hip:

$$M_{L_1}s^2y_h + M_{L_m}s^2y_a = -f_{h_1} + f_L \quad \text{(B-7)}$$

$$M_{L_m}s^2y_h + M_{L_2}s^2y_a = -f_L + f_a \quad \text{(B-8)}$$

where

f_{s_a} = interface force the arm imparts to the shoulder

f_{B_r} = $(B_Bs + K_B)(y_s - y_{h_1})$, the torsional restraint force on the torso

f_{h_1} = force across the torso/hip interface

f_L = $-(B_Ls + K_L)(y_h - y_a)$, the torsional restraint force of the hip

f_a = $-(B_as + K_a)(y_a - y_p)$

Equations B-5 to B-8 can be simplified by noting that $y_{h_1} = y_h$, and then eliminating the forces f_{h_1} and f_L between Eqs. B-6, B-7, and B-8 which results in one equation. Further, if the equivalent rotational restraints, B_L and K_L, are assumed infinitely large, then the lack of rotation of the hip segment implies that displacements at the top and bottom of the hip segment are identical, e.g., $y_h = y_a$. All the above steps then yield

$$M_{B_1}s^2y_s + M_{B_m}s^2y_a = f_{sa} + f_{B_r} \quad \text{(B-9)}$$

$$M_{B_m}s^2y_s + (M_L + M_{B_2})s^2y_a = f_a - f_{B_r} \quad \text{(B-10)}$$

where

M_L = $(M_{L_1} + 2M_{L_m} + M_{L_2})$, the mass of the hip segment

Finally, Eq. B-10 can be modified by adding Eq. B-9 and using the following substitutions to describe shoulder and hip motion variables relative to platform motion

$$y_{s_p} = y_s - y_p \tag{B-11}$$

$$y_{a_p} = y_a - y_p \tag{B-12}$$

Thus we obtain the two equations describing relative shoulder and hip translation

$$(M_{B_1}s^2 + B_Bs + K_B)y_{s_p} + \underbrace{(M_{B_m}s^2 - B_Bs - K_B)}_{(L_{B_1} - 1)M_{B_1}}y_{a_p} = f_{s_a} - L_{B_1}M_{B_1}a_{y_p} \tag{B-13}$$

$$\underbrace{(M_{B_1} + M_{B_m})}_{L_{B_1}M_{B_1}}s^2y_{s_p} + \underbrace{[(M_L + M_{B_2} + M_{B_m})}_{M_T - L_{B_1}M_{B_1}}s^2 + B_as + K_a]y_{a_p} = f_{s_a} - M_Ta_{y_p} \tag{B-14}$$

where

$L_{B_1} = \dfrac{M_{B_1} + M_{B_m}}{M_{B_1}}$, the "kinematic gain" of the torso motion about the hip pivot

and

$M_T = M_L + M_B$, the total mass of the hip and torso segments

These two equations describe shoulder and hip motions in response to table acceleration and the force at the shoulder/arm interface. Shoulder motion couples into arm motions via f_{s_a}, the force across the interface.

3. Arm Dynamics Including Simplified Neuromuscular Restraints and Hand/Stick Interface Coupling

Under lateral vibration the operator's arm will experience both translational and rotational motions. A simple mechanical model for representing this effect is shown in Fig. B-6. Arm rotation is restrained relative to the shoulder by effective neuromuscular elements representing the closed loop effects. The limb/neuromuscular system (NMS) has been extensively

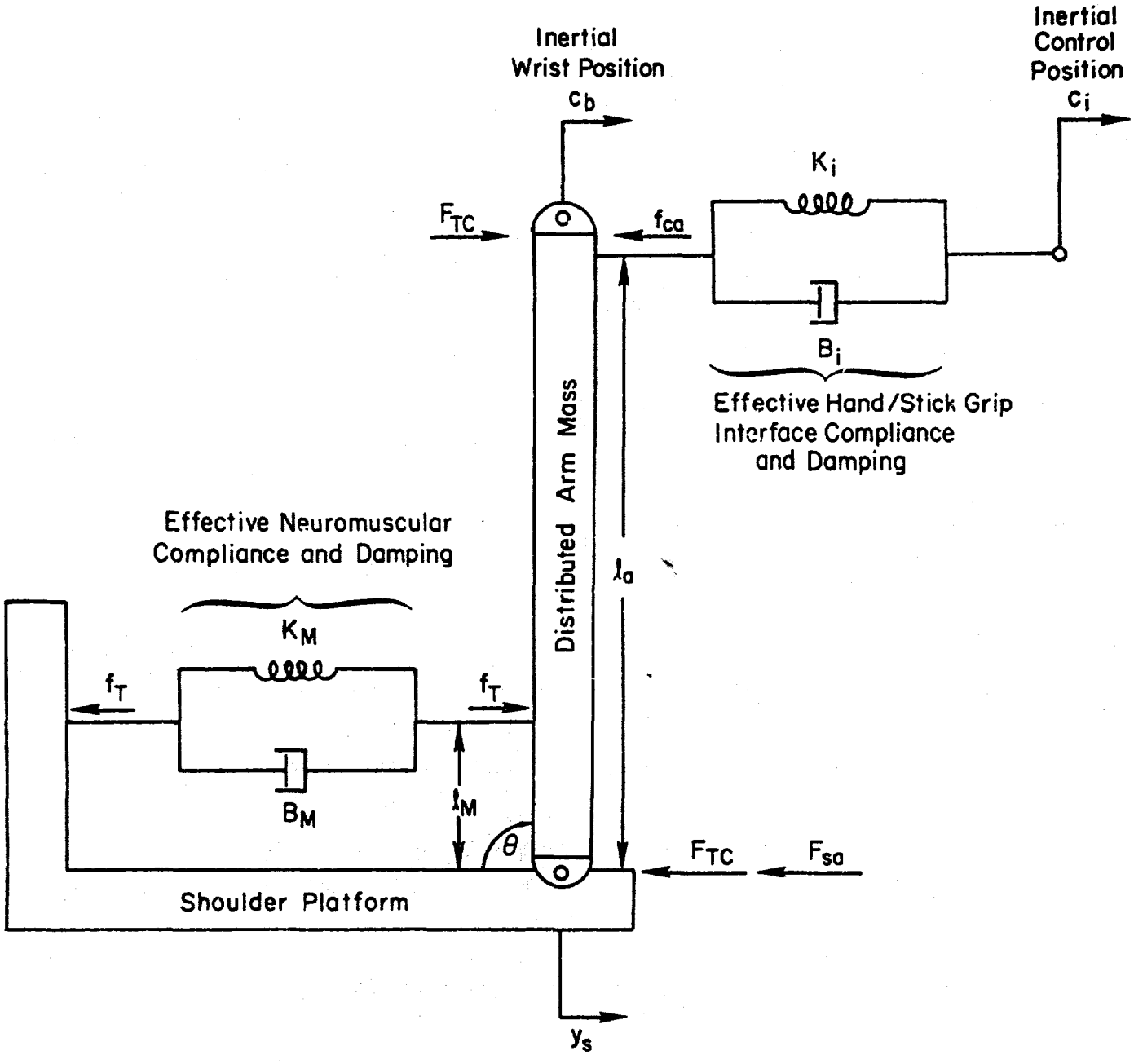

Figure B-6. Mechanical Model for Arm Motion with Neuromuscular Restraints and Interface Dynamics

measured and modeled (Refs. B-2, B-3) in terms of its response to commands from the CNS (Fig. B-1). In the present case we are concerned with the effects of NMS restraints on arm motion relative to the operator's shoulder in response to motion inputs. Based on Refs. B-2 and B-3, the simple compliance and damping shown in Fig. B-6 are assumed to represent the basic NMS effects as a low frequency approximation. At the hand the arm is restrained by the control stick, and here we assume that there are additional coupling dynamics contributed by flesh characteristics and small amounts of finger and wrist flexion which are modeled as an equivalent compliance and damping as shown in Fig. B-6.

Applying equation set B-1 to the arm model in Fig. B-6 yields

$$M_2 s^2 c_b + M_m s^2 y_s = F_{T_c} - f_{c_a} \qquad \text{(B-15)}$$

$$M_m s^2 c_b + M_1 s^2 y_s = -F_{T_c} - f_{s_a}$$

where

f_{c_a} = interface force applied by the top of the stick on the hand

f_{s_a} = interface force applied by the shoulder to the top of the arm

F_{T_c} = effective force at the hand and shoulder due to the neuromuscular force, f_T, where $F_{T_c} = (\ell_m/\ell_a) f_T$

M_2, M_m, and M_1 are defined as in equation set B-1

The interface force, f_{c_a}, and effective neuromuscular force, f_T, are given by

$$f_{c_a} = (K_i + B_i s)(c_b - c_i) \qquad \text{(B-17)}$$

$$f_T = (K_m + B_m s)(\ell_m \theta) = F_{T_c}(\ell_a/\ell_m) \qquad \text{(B-18)}$$

where

$$\theta = \frac{c_b - y_s}{\ell_a}$$

In terms of displacements relative to the table platform, Eqs. B-15 to B-18 become

$$M_2 s^2 c + M_m s^2 y_{s_p} = F_{T_c} - f_{c_a} - (M_2 + M_m) a_{y_p} \quad \text{(B-19)}$$

$$M_m s^2 c + M_1 s^2 y_{s_p} = -F_{T_c} - f_{s_a} - (M_1 + M_m) a_{y_p} \quad \text{(B-20)}$$

$$F_{T_c} = -(K_m + B_m s)(\ell_m/\ell_a)^2 (c_{b_p} - y_{s_p}) \quad \text{(B-21)}$$

$$f_{c_a} = (K_i + B_i s)(c_{b_p} - c) \quad \text{(B-22)}$$

where

$c = c_i - y_p$

$c_{b_p} = c_b - y_p$

ℓ_m/ℓ_a = the lever arm ratio

For simplicity we shall lump the square of the lever arm ratio into K_m and B_m, the effective NM system dynamics.

4. Matrix of Equations

The matrix of equations given in Table B-1 summarizes the equations of motion (note the text equation numbers). The left hand side matrix variables are mostly platform referenced rather than inertial referenced since this simplified the equation forms. The exception is y_s, the inertial shoulder position which is used to calculate transmissibility as $a_{y_S}/a_{yP} = y_S/y_P$, while stick feedthrough is c/a_{y_p}.

Table B-2 gives the values for the Feel System, Arm, Torso and Hip Dynamics that were either measured, derived or obtained by curve fitting. Obviously some of these parameters will change with subject size and geometry. However, this parameter set will suffice to illustrate various model features (in following subsections).

TABLE B-1. MATRIX OF EQUATIONS (LATERAL VIBRATION INPUT)

Component Equations:	c	y_{s_p}	f_{s_a}	f_{c_a}	f_{r_c}	c_{b_p}	y_{a_p}	y_s	=	y_p	a_{y_p}
Stick (Eq. B-4)	$s^2 + \frac{B_F}{M_F} s + K_F/M_F$			$\frac{-1}{M_F}$						$-L_F s^2$	$-L_F$
Torso (Eq. B-13)		$s^2 + \frac{B_B}{M_{B_1}} s + K_B/M_{B_1}$	$\frac{-1}{M_{B_1}}$				$(L_{B_1} - 1)s^2 \frac{-B_B}{M_{B_1}} s - \frac{K_B}{M_{B_1}}$			$-L_{B_1} s^2$	$-L_{B_1}$
Shoulder End of Arm (Eq. B-20)	$M_m s^2$	$M_1 s^2$	1		1					$-(M_1 + M_m)s^2$	$-(M_1 + M_m)$
Hand End of Arm (Eq. B-19)	$M_2 s^2$	$M_m s^2$		1	-1					$-(M_2 + M_m)s^2$	$-(M_2 + M_m)$
Effective MM System (Eq. B-21)		$-(B_M s + K_M)$			1	$(B_M s + K_M)$					
Hand/Stick Interface (Eq. B-22)	$-(B_i s + K_i)$			-1		$(B_i s + K_i)$					
Hip (Eq. B-14)		$L_{B_1} s^2$	$\frac{-1}{M_{B_1}}$				$\left(\frac{M_T}{M_{B_1}} - L_{B_1}\right)s^2 + B_a s + K_a$			$-(M_T/M_{B_1})s^2$	$-(M_T/M_{B_1})$
Inertial Shoulder Position		-1						1		1	

TABLE B-2. FEEL SYSTEM, ARM, TORSO AND HIP DYNAMICS

Feel System Dynamics

	SPRING STICK	STIFF STICK
ω_F	25 rad/sec	207 rad/sec
ζ_F	0.3	0.0138
K_F	197 N/m	13,500 N/m
B_F	4.73 N sec/m	1.8 N sec/m
M_F	0.315 kg	
L_F	1.61	

Arm Dynamics

$M_1 = M_2 = 1.23$ kg

$M_m = 0.745$ kg

$L_A = 1.61$

} Derived from cadaver data (Ref. B-4)

Torso and Hip Dynamics

$M_T = 40.6$ kg

$M_{B_1} = 32.5$ kg

$L_{B_1} = 0.788$

$B_{B_1} = 30.45$ N sec/m

$K_{B_1} = 9130$ N/m

$B_a = 20.02$ N sec/m

$K_a = 110.9$ N/m

} Determined by curve fit to Shoulder Transmissibility data

C. MODEL FITS TO EXPERIMENTAL DATA AND DERIVATION OF SIMPLIFIED MODELS

In this section we briefly compare shoulder transmissibility data and model curve fits. This leads to a simplified model for stick feedthrough which is both analytically tractable and accurate in the most important frequency ranges.

1. Shoulder Transmissibility

Figure B-7 compares shoulder transmissibility, a_{y_S}/a_{y_T}, for the model and example data for one of the subjects (both for hand off the stick). The model fits the major trend of the data, viz., that up to about 15 rad/sec the shoulder is following the table whereas at high frequency it is attenuated.

The measured data when the pilot's hand was gripping the stick (both nontracking and tracking) fell near the hand-off data in Fig. B-7. Generally the model curve was also insensitive to hand on the stick. This is a reasonable result since the ratio of torso to arm inertias is about 25:1 (Table B-2). Thus the muscle forces required for tracking will move the arm and stick rather than torso and hips. The model fits the basic data features; that is, at low frequency the shoulder moves with the table (thereby feeding table motion into the limb) while it attenuates at high frequency (thereby making the limb root nearly inertially fixed). This observation will be used to derive a simplified model for stick feedthrough.

2. Simplified Models and Example Data Fits for Stick Feedthrough

To develop a simple model to fit basic data effects in the force and spring stick vibration feedthrough we shall start with the translational equivalent mobility diagram (Fig. B-8) that summarizes the diagrams in Figs. B-4, B-5, and B-6 and incorporates the distributed mass modeling technique from Fig. B-3 and Eq. B-1 (adapted from Ref. B-1). Note that in Fig. B-8 torso dynamics are used to represent the torso plus hip dynamics from Fig. B-5. The torso only model is based on Eqs. B-5 and B-6 as if they described all the vibration feedthrough from table to shoulder. This simple model cannot roll off as steeply as the full model results (Fig. B-7);

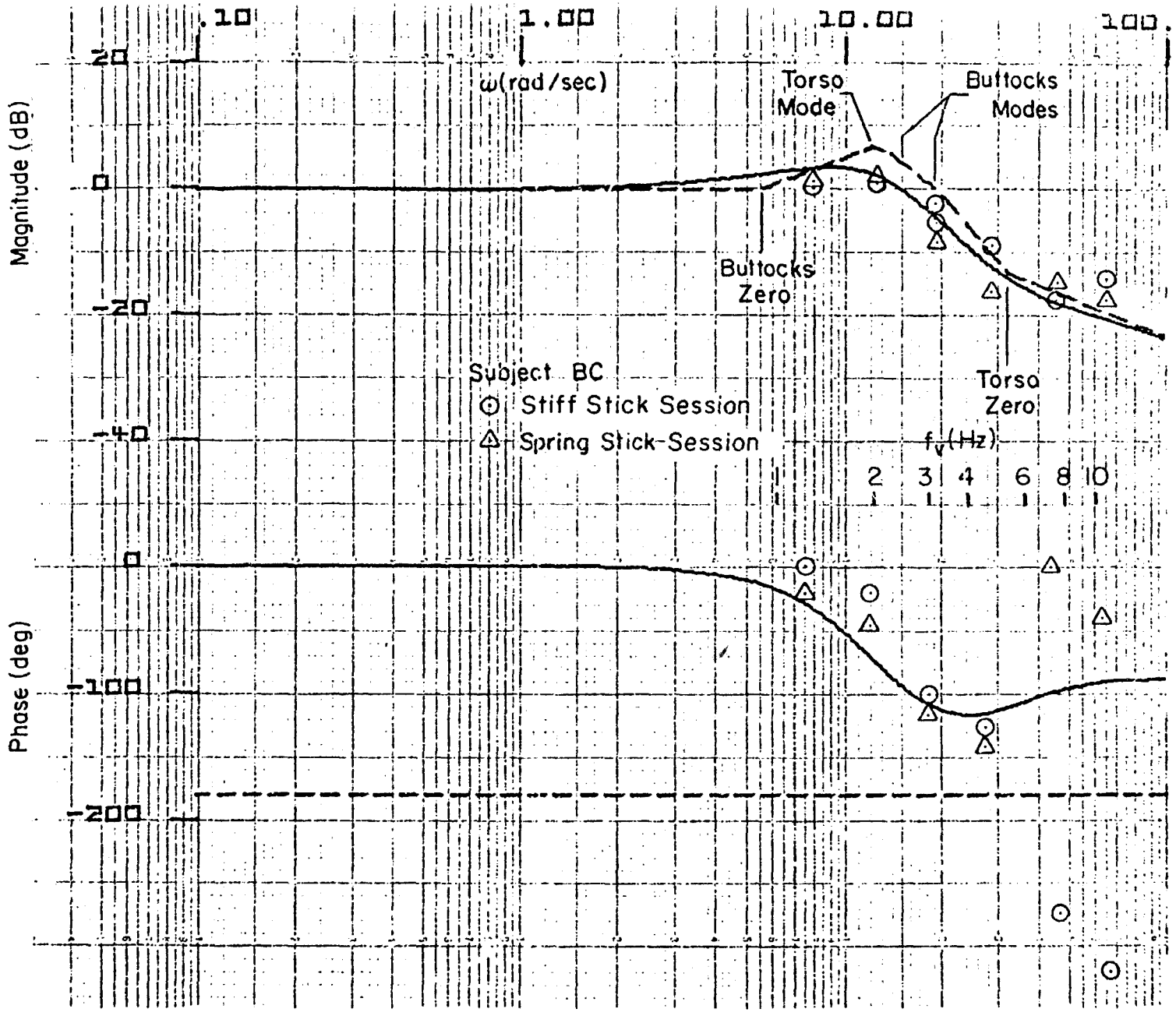

Figure B-7. Transmissibility Dynamics Between Lateral Platform and Shoulder Motions (Hand off the Stick)

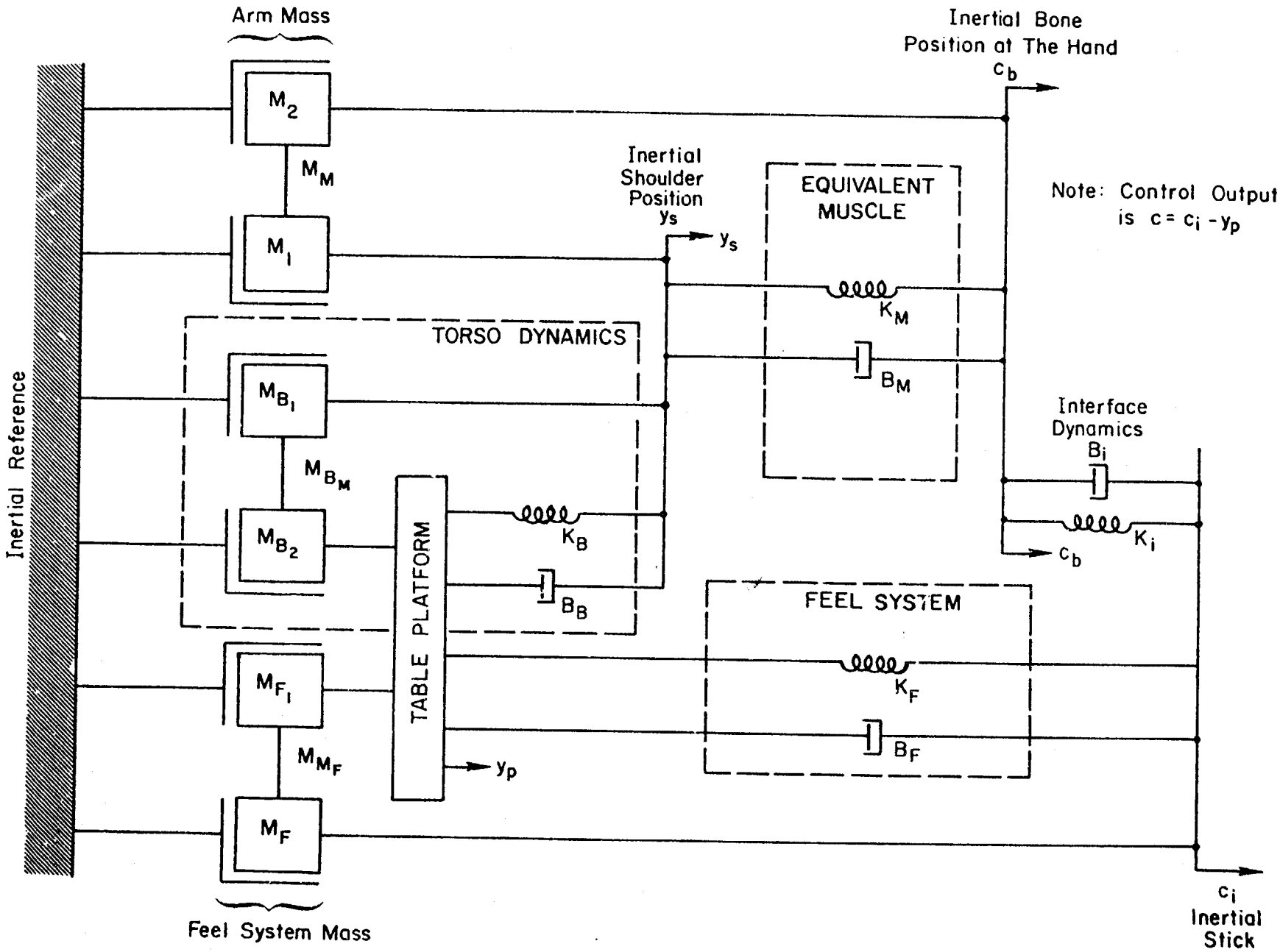

Figure B-8. Mobility Diagram Using Simplified Body Dynamics

however, it is used in Fig. B-8 to illustrate the basic feature that at low frequency the spring forces (K_B) are larger than inertia forces (M_{B_1}), and thus the shoulder moves in synchrony with the table platform thus driving the arm. At high frequencies the inertia forces dominate, and the shoulder response is attenuated and lags the table; thus the shoulder tends to revert to inertial reference. The feel system mass model follows that of Eqs. B-2 and B-3, whereas the arm mass model follows that of Eqs. B-15 and B-16.

As indicated earlier, the effects of shoulder transmissibility on vibration feedthrough to the stick was at high frequency. Thus we can further simplify Fig. B-8 by assuming that the torso spring (K_B) is very large such that the shoulder moves with the table at all frequencies. This results in Fig. B-9, where the stick and arm masses are changed to table reference and the kinematic gains, L_A and L_F, account for this change as well as containing the effects of the mutual mass descriptors, M_m and M_{m_F}.

The equations of motion for Fig. B-9 are

$$[M_F s^2 + (B_i + B_F)s + K_i + K_F]c - (B_i s + K_i)c_{b_p} = L_F M_F(-a_{y_p}) \qquad \text{(B-23)}$$

$$-(B_i s + K_i)c + [M_A s^2 + (B_i + B_M)s + K_i + K_M]c_{b_p} = L_A M_A(-a_{y_p}) \qquad \text{(B-24)}$$

Solving for the vibration feedthrough yields the general expression for either stiff or spring stick feedthrough dynamics as

$$\frac{c}{-a_{y_p}} = \frac{(B_i s + K_i)(L_F M_F + L_A M_A) + (M_A s^2 + B_M s + K_M)\,\vert\, L_F M_F}{(B_i s + K_i)[(M_F + M_A)s^2 + (B_F + B_M)s + K_F + K_M] + (M_A s^2 + B_M s + K_M)\,\vert\,(M_F s^2 + B_F s + K_F)} \qquad \text{(B-25)}$$

where the terms have been grouped so that various limiting cases can be readily seen. For example, with the hand off the stick ($K_i = B_i = 0$), only the terms to the right of the dashed line remain, which yields

Stick Alone

$$\frac{c}{-a_{y_p}} = \frac{L_F M_F}{M_F s^2 + B_F s + K_F} \; ; \; \frac{m}{m/sec^2} \qquad \text{(B-26)}$$

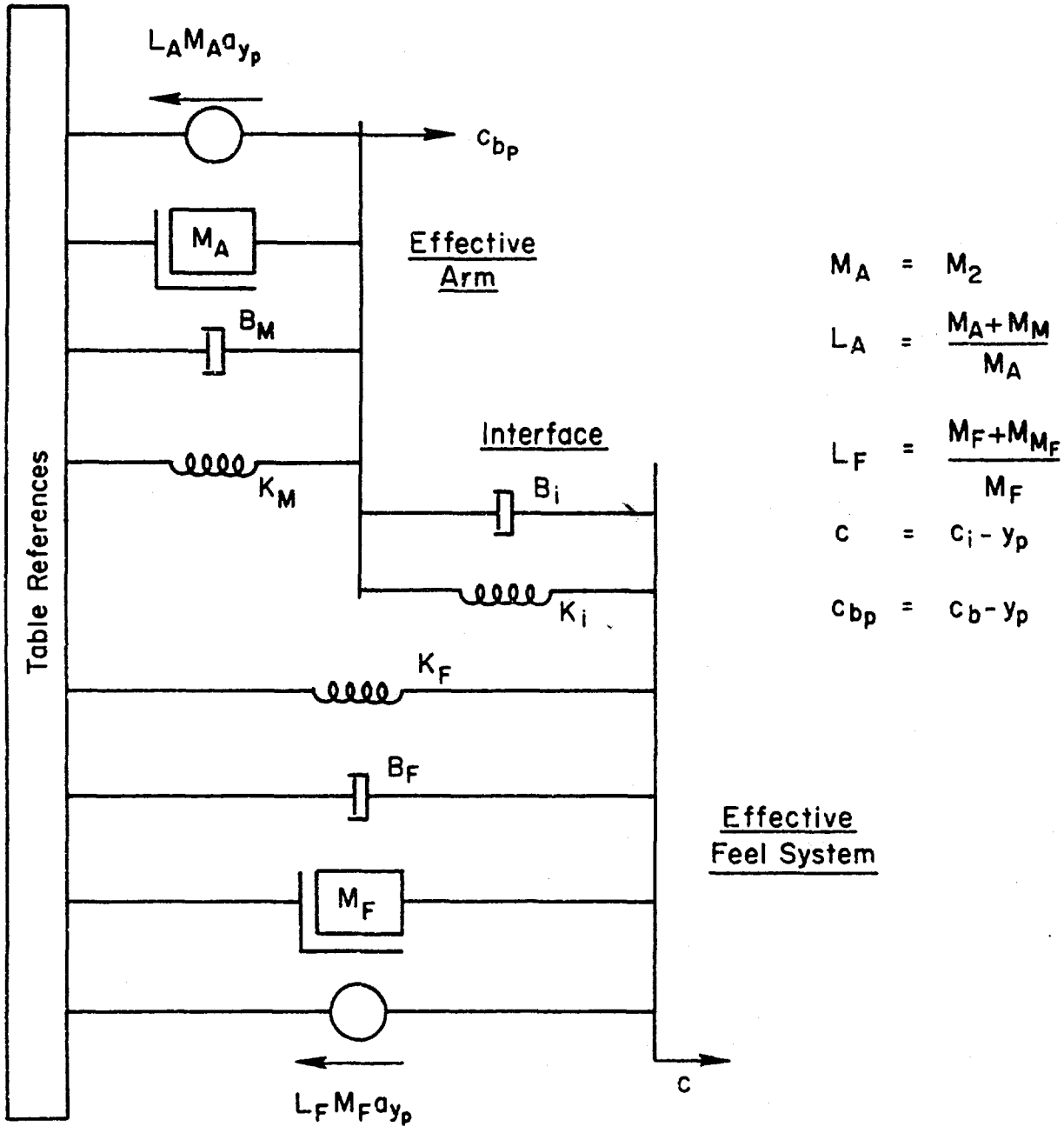

Figure B-9. Simplified Mobility Diagram for Lateral Stick Feedthrough

and below the break frequency the stick position response is sensing table acceleration through the "bobweight gain", $L_F M_F / K_F$.

The bobweight gain expressions for the tracking situations can be found by evaluating Eq. B-25 at zero frequency ($s \rightarrow 0$):

Stiff Stick

$$\left.\frac{K_F c}{-a_{y_p}}\right|_{s=0} = \frac{9.8 L_F M_F G [1 + K_M/GK_i]}{[1 + K_M/K_i + \underbrace{K_M/K_F}_{\doteq 0}]} \; ; \; \frac{N}{g} \qquad \text{(B-27)}$$

Spring Stick

$$\left.\frac{c}{-a_{y_p}}\right|_{s=0} = \frac{980 L_F M_F G [1 + K_M/GK_i]}{K_F [1 + K_M/K_i + K_M/K_F]} \; ; \; \frac{c_m}{g} \qquad \text{(B-28)}$$

where

G = Increase in "Bobweight gain" for no muscle forces

$= 1 + L_A M_A / L_F M_F = 4.9$ (from Table B-2)

Thus putting the hand on the stick increases its bobweight gain by nearly 5:1 [in the absence of muscle forces ($K_M = 0$)].

The general expression (Eq. B-25) can be further simplified using the approximations for each stick shown below

Stiff Stick (assuming $K_F \gg$ other elements)

$$\frac{K_F c}{-a_{y_p}} \doteq 9.8 L_F M_F G \left[\frac{(K_i + K_M/G) + (B_i + B_M/G)s + (M_A/G)s^2}{(K_i + K_M) + (B_i + B_M)s + M_A s^2}\right] \; ; \; \frac{N}{g} \qquad \text{(B-29)}$$

Spring Stick (assuming K_i, $B_i \gg$ other elements)

$$\frac{c}{-a_{y_p}} \doteq \frac{980 L_F M_F G}{(K_F + K_M) + (B_F + B_M)s + (M_F + M_A)s^2} \; ; \; \frac{c_m}{g} \qquad \text{(B-30)}$$

The following set of interface and effective muscle parameters were used for both the stiff and spring stick model fits (Fig. B-10) to the open-visual-loop experimental data for two subjects.

$$K_i = 354 \text{ N/m}$$

$$B_i = 30.5 \text{ N sec/m}$$

$$K_M = 138 \text{ N/m}$$

$$B_M = 8.85 \text{ N sec/m}$$

The two subjects selected illustrate that vibration feedthrough is quite similar at low and high frequencies yet differs at 28 rad/sec (4.5 Hz), particularly in the phase. The other subject's data clustered around and between that in Fig. B-10.

In Fig. B-10 the stick alone curves show the vibration feedthrough exciting stick properties per Eq. 26 (for the stiff stick the natural frequency is at 207 rad/sec). The increase in Bobweight gain (4.9 or 13.8 dB) for arm plus stick, but no muscle forces, is the same for both sticks. Finally, the approximate simplified model curves for the stiff stick in Fig. B-10 were obtained from Eq. B-29 and Eq. B-30 for spring stick dynamics but using the zero frequency gain expression (Eq. B-28). The amplitude fits are generally quite good at low frequencies and are at least consistent with the high frequency data trends. The phase fits follow the general data trends at all frequencies.

While not shown in Fig. B-10, we compared the approximate simplified model curve fits (from Eqs. B-29 and B-30) with those obtained from the general formula (Eq. B-25). Except for the spring stick zero frequency gain these were within a "line width" of the approximate results; thus the approximate formulas (Eqs. B-29 and B-30) are very good descriptors for the Simplified Model for Stiff and Spring stick vibration feedthrough. However, the simplified model is also an approximation relying on the assumption that the shoulder (limb root point) always follows the platform, as discussed earlier under Shoulder Transmissibility (Section B-2). An examination of the full matrix and evaluation of limiting conditions at high frequency indicated that as the shoulder motion changes from platform

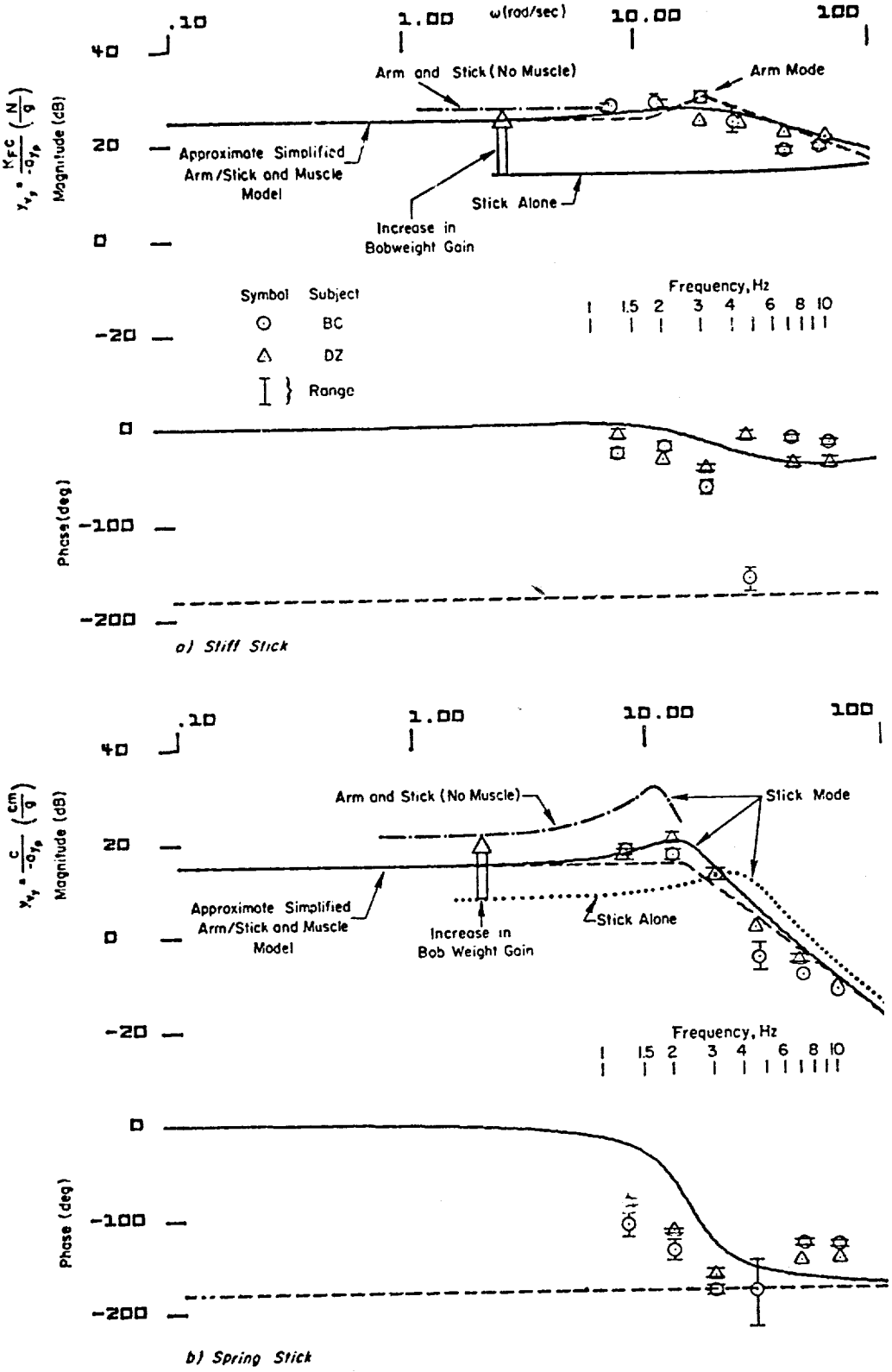

Figure B-10. Comparison of Simplified Model and Data for Open-Loop Feedthrough Dynamics (Lateral Vibration, Shoulder Assumed at Table Reference)

following at moderate frequency (below 2.5 Hz) to inertially stationary at high frequency (above 5 Hz) the major effect was to change the expression for G, the increase in bobweight gain, to

$$G' = 1 + \frac{L_A' M_A}{L_F M_F} \qquad \text{(B-31)}$$

where

$$L_A' = \begin{cases} L_A \text{ at moderate frequency (below 2.5 Hz)} \\ 1. \text{ at high frequency (above 5 Hz)} \end{cases}$$

with a gradual transition between these limits. The interpretation of this change in the kinematic gain is that at moderate frequency, table motion drives the shoulder which then drives the hand end of the arm in much the same way that table motion at the bottom of the stick drives the top of the stick (Fig. B-2). When the shoulder reverts to inertial reference at high frequency, then the effective mass of the arm as seen from the hand end, M_A, acts as if it were concentrated at the top of the stick (see discussion following Eq. B-4). In Fig. B-10 this change in G will lower the curve fit by about 3 dB above 30 rad/sec (4+ Hz) which would generally improve the fit.

D. CONCLUDING REMARKS

The model results suggest that lateral stick vibration feedthrough is primarily caused by the "bobweight" effect of arm on the stick but can be reduced by increased neuromuscular stiffness. Limb root motion due to shoulder transmissibility has minor effects only above 2 Hz.

A useful set of approximate factors for stick feedthrough was derived. The bobweight gain effect of hand on stick plus effective closed loop neuromuscular dynamics as well as effective interface dynamics were used to give excellent fits to the amplitude ratio. While the phase fit is not as good, neither is it as important, as the amplitude is what provides task disturbance. Since the vibration is uncorrelated with the task following command, the phase has relatively less importance. However, the phase effects can provide clues to model refinement for both subject to subject differences

as well as allowing extrapolation to other situations (gripping technique, other spring gradients, etc.).

This model can, and should be, extended to cover related lateral feedthrough situations such as sidestick, resting the arm on the seat or leg, etc. It also makes a good starting point for an axial feedthrough model (fore-aft vibration) in which the bobweight effect of arm on the stick will be dominant and arm and torso effects are present.

REFERENCES FOR APPENDIX B

B-1. Gardner, Murray F., and John L. Barnes, Transients in Linear Systems, Vol. I, New York, John Wiley, 1942.

B-2. Magdaleno, R. E., and D. T. McRuer, Experimental Validation and Analytical Elaboration for Models of the Pilot's Neuromuscular Subsystem in Tracking Tasks, NASA CR-1757, April 1971.

B-3. Magdaleno, Raymond E. Magdaleno, Duane T. McRuer, and George P. Moore, Small Perturbation Dynamics of the Neuromuscular System in Tracking Tasks, NASA CR-1212, Dec. 1968.

B-4. Braune, W., O. Fischer, et al., Human Mechanics - Four Monographs Abridged, AMRL-TDR-63-123, Dec. 1963.

☆U.S.Government Printing Office: 1973 — 758-429/327